6

Radiative Forcing of Climate Change

Co-ordinating Lead Author
V. Ramaswamy

Lead Authors
O. Boucher, J. Haigh, D. Hauglustaine, J. Haywood, G. Myhre, T. Nakajima, G.Y. Shi, S. Solomon

Contributing Authors
R. Betts, R. Charlson, C. Chuang, J.S. Daniel, A. Del Genio, R. van Dorland, J. Feichter, J. Fuglestvedt,
P.M. de F. Forster, S.J. Ghan, A. Jones, J.T. Kiehl, D. Koch, C. Land, J. Lean, U. Lohmann,
K. Minschwaner, J.E. Penner, D.L. Roberts, H. Rodhe, G.J. Roelofs, L.D. Rotstayn, T.L. Schneider,
U. Schumann, S.E. Schwartz, M.D. Schwarzkopf, K.P. Shine, S. Smith, D.S. Stevenson, F. Stordal,
I. Tegen, Y. Zhang

Review Editors
F. Joos, J. Srinivasan

Contents

Executive Summary

- Radiative forcing continues to be a useful tool to estimate, to a first order, the relative climate impacts (viz., relative global mean surface temperature responses) due to radiatively induced perturbations. The practical appeal of the radiative forcing concept is due, in the main, to the assumption that there exists a general relationship between the global mean forcing and the global mean equilibrium surface temperature response (i.e., the global mean climate sensitivity parameter, λ) which is similar for all the different types of forcings. Model investigations of responses to many of the relevant forcings indicate an approximate near invariance of λ (to about 25%). There is some evidence from model studies, however, that λ can be substantially different for certain forcing types. Reiterating the IPCC WGI Second Assessment Report (IPCC, 1996a) (hereafter SAR), the global mean forcing estimates are not necessarily indicators of the detailed aspects of the potential climate responses (e.g., regional climate change).

- The simple formulae used by the IPCC to calculate the radiative forcing due to well-mixed greenhouse gases have been improved, leading to a slight change in the forcing estimates. Compared to the use of the earlier expressions, the improved formulae, for fixed changes in gas concentrations, decrease the carbon dioxide (CO_2) and nitrous oxide (N_2O) radiative forcing by 15%, increase the CFC-11 and CFC-12 radiative forcing by 10 to 15%, while yielding no change in the case of methane (CH_4). Using the new expressions, the radiative forcing due to the increases in the well-mixed greenhouse gases from the pre-industrial (1750) to present time (1998) is now estimated to be +2.43 Wm^{-2} (comprising CO_2 (1.46 Wm^{-2}), CH_4 (0.48 Wm^{-2}), N_2O (0.15 Wm^{-2}) and halocarbons (halogen-containing compounds) (0.34 Wm^{-2})), with an uncertainty[1] of 10% and a high level of scientific understanding (LOSU).

- The forcing due to the loss of stratospheric ozone (O_3) between 1979 and 1997 is estimated to be −0.15 Wm^{-2} (range: −0.05 to −0.25 Wm^{-2}). The magnitude is slightly larger than in the SAR owing to the longer period now considered. Incomplete knowledge of the O_3 losses near the tropopause continues to be the main source of uncertainty. The LOSU of this forcing is assigned a medium rank.

- The global average radiative forcing due to increases in tropospheric O_3 since pre-industrial times is estimated to be +0.35 ± 0.15 Wm^{-2}. This estimate is consistent with the SAR estimate, but is based on a much wider range of model studies and a single analysis that is constrained by observations; there are uncertainties because of the inter-model

differences, the limited information on pre-industrial O_3 distributions, and the limited data that are available to evaluate the model trends for modern (post-1960) conditions. A rank of medium is assigned for the LOSU of this forcing.

- The changes in tropospheric O_3 are mainly driven by increased emissions of CH_4, carbon monoxide (CO), non-methane hydrocarbons (NMHCs) and nitrogen oxides (NO_x), but the specific contributions of each are not yet well quantified. Tropospheric and stratospheric photochemical processes lead to other indirect radiative forcings through, for instance, changes in the hydroxyl radical (OH) distribution and increase in stratospheric water vapour concentrations.

- Models have been used to estimate the direct radiative forcing for five distinct aerosol species of anthropogenic origin. The global, annual mean radiative forcing is estimated as −0.4 Wm^{-2} (−0.2 to −0.8 Wm^{-2}) for sulphate aerosols; −0.2 Wm^{-2} (−0.07 to −0.6 Wm^{-2}) for biomass burning aerosols; −0.10 Wm^{-2} (−0.03 to −0.30 Wm^{-2}) for fossil fuel organic carbon aerosols; +0.2 Wm^{-2} (+0.1 to +0.4 Wm^{-2}) for fossil fuel black carbon aerosols; and in the range −0.6 to +0.4 Wm^{-2} for mineral dust aerosols. The LOSU for sulphate aerosols is low while for biomass burning, fossil fuel organic carbon, fossil fuel black carbon, and mineral dust aerosols the LOSU is very low.

- Models have been used to estimate the "first" indirect effect of anthropogenic sulphate and carbonaceous aerosols (namely, a reduction in the cloud droplet size at constant liquid water content) as applicable in the context of liquid clouds, yielding global mean radiative forcings ranging from −0.3 to −1.8 Wm^{-2}. Because of the large uncertainties in aerosol and cloud processes and their parametrizations in general circulation models (GCMs), the potentially incomplete knowledge of the radiative effect of black carbon in clouds, and the possibility that the forcings for individual aerosol types may not be additive, a range of radiative forcing from 0 to −2 Wm^{-2} is adopted considering all aerosol types, with no best estimate. The LOSU for this forcing is very low.

- The "second" indirect effect of aerosols (a decrease in the precipitation efficiency, increase in cloud water content and cloud lifetime) is another potentially important mechanism for climate change. It is difficult to define and quantify in the context of current radiative forcing of climate change evaluations and current model simulations. No estimate is therefore given. Nevertheless, present GCM calculations suggest that the radiative flux perturbation associated with the second aerosol indirect effect is of the same sign and could be of similar magnitude compared to the first effect.

- Aerosol levels in the stratosphere have now fallen to well below the peak values seen in 1991 to 1993 in the wake of the Mt. Pinatubo eruption, and are comparable to the low values seen in about 1979, a quiescent period for volcanic activity. Although episodic in nature and transient in duration, stratospheric

---

[1] The "uncertainty range" for the global mean estimates of the various forcings in this chapter is guided, for the most part, by the spread in the published estimates. It is not statistically based and differs in this respect from the manner "uncertainty range" is treated elsewhere in this document.

aerosols from explosive volcanic eruptions can exert a significant influence on the time history of radiative forcing of climate.

- Owing to an increase in land-surface albedo during snow cover in deforested mid-latitude areas, changes in land use are estimated to yield a forcing of -0.2 Wm^{-2} (range: 0 to -0.4 Wm^{-2}). However, the LOSU is very low and there have been much less intensive investigations compared with other anthropogenic forcings.

- Radiative forcing due to changes in total solar irradiance (TSI) is estimated to be $+0.3 \pm 0.2$ Wm^{-2} for the period 1750 to the present. The wide range given, and the very low LOSU, are largely due to uncertainties in past values of TSI. Satellite observations, which now extend for two decades, are of sufficient precision to show variations in TSI over the solar 11-year activity cycle of about 0.08%. Variations over longer periods may have been larger but the techniques used to reconstruct historical values of TSI from proxy observations (e.g., sunspots) have not been adequately verified. Solar radiation varies more substantially in the ultraviolet region and GCM studies suggest that inclusion of spectrally resolved solar irradiance variations and solar-induced stratospheric O_3 changes may improve the realism of model simulations of the impact of solar variability on climate. Other mechanisms for the amplification of solar effects on climate, such as enhancement of the Earth's electric field causing electrofreezing of cloud particles, may exist but do not yet have a rigorous theoretical or observational basis.

- Radiative forcings and Global Warming Potentials (GWPs) are presented for an expanded set of gases. New categories of gases in the radiative forcing set include fluorinated organic molecules, many of which are ethers that may be considered as halocarbon substitutes. Some of the GWPs have larger uncertainties than others, particularly for those gases where detailed laboratory data on lifetimes are not yet available. The direct GWPs have been calculated relative to CO_2 using an improved calculation of the CO_2 radiative forcing, the SAR response function for a CO_2 pulse, and new estimates for the radiative forcing and lifetimes for a number of gases. As a consequence of changes in the radiative forcing for CO_2 and CFC-11, the revised GWPs are typically 20% higher than listed in the SAR. Indirect GWPs are also discussed for some new gases, including CO. The direct GWPs for those species whose lifetimes are well characterised are estimated to be accurate (relative to one another) to within $\pm 35\%$, but the indirect GWPs are less certain.

- The geographical distributions of each of the forcing mechanisms vary considerably. While well-mixed greenhouse gases exert a significant radiative forcing everywhere on the globe, the forcings due to the short-lived species (e.g., direct and indirect aerosol effects, tropospheric and stratospheric O_3) are not global in extent and can be highly spatially inhomogeneous. Furthermore, different radiative forcing mechanisms lead to differences in the partitioning of the perturbation between the atmosphere and surface. While the Northern to Southern Hemisphere ratio of the solar and well-mixed greenhouse gas forcings is very nearly 1, that for the fossil fuel generated sulphate and carbonaceous aerosols and tropospheric O_3 is substantially greater than 1 (i.e., primarily in the Northern Hemisphere), and that for stratospheric O_3 and biomass burning aerosol is less than 1 (i.e., primarily in the Southern Hemisphere).

- The global mean radiative forcing evolution comprises of a steadily increasing contribution due to the well-mixed greenhouse gases. Other greenhouse gas contributions are due to stratospheric O_3 from the late 1970s to the present, and tropospheric O_3 whose precise evolution over the past century is uncertain. The evolution of the direct aerosol forcing due to sulphates parallels approximately the secular changes in the sulphur emissions, but it is more difficult to estimate the temporal evolution due to the other aerosol components, while estimates for the indirect forcings are even more problematic. The temporal evolution estimates indicate that the net natural forcing (solar plus stratospheric aerosols from volcanic eruptions) has been negative over the past two and possibly even the past four decades. In contrast, the positive forcing by well-mixed greenhouse gases has increased rapidly over the past four decades.

- Estimates of the global mean radiative forcing due to different future scenarios (up to 2100) of the emissions of trace gases and aerosols have been performed (Nakićenović *et al.*, 2000; see also Chapters 3, 4 and 5). Although there is a large variation in the estimates from the different scenarios, the results indicate that the forcing (evaluated relative to pre-industrial times, 1750) due to the trace gases taken together is projected to increase, with the fraction of the total due to CO_2 becoming even greater than for the present day. The direct aerosol (sulphate, black and organic carbon components taken together) radiative forcing (evaluated relative to the present day, 2000) varies in sign for the different scenarios. The direct aerosol effects are estimated to be substantially smaller in magnitude than that of CO_2. No estimates are made for the spatial aspects of the future forcings. Relative to 2000, the change in the direct plus indirect aerosol radiative forcing is projected to be smaller in magnitude than that of CO_2.

6.1 Radiative Forcing

6.1.1 Definition

The term "radiative forcing" has been employed in the IPCC Assessments to denote an externally imposed perturbation in the radiative energy budget of the Earth's climate system. Such a perturbation can be brought about by secular changes in the concentrations of radiatively active species (e.g., CO_2, aerosols), changes in the solar irradiance incident upon the planet, or other changes that affect the radiative energy absorbed by the surface (e.g., changes in surface reflection properties). This imbalance in the radiation budget has the potential to lead to changes in climate parameters and thus result in a new equilibrium state of the climate system. In particular, IPCC (1990, 1992, 1994) and the Second Assessment Report (IPCC, 1996) (hereafter SAR) used the following definition for the radiative forcing of the climate system: "The radiative forcing of the surface-troposphere system due to the perturbation in or the introduction of an agent (say, a change in greenhouse gas concentrations) is the change in net (down minus up) irradiance (solar plus long-wave; in Wm^{-2}) at the tropopause AFTER allowing for stratospheric temperatures to readjust to radiative equilibrium, but with surface and tropospheric temperatures and state held fixed at the unperturbed values". In the context of climate change, the term forcing is restricted to changes in the radiation balance of the surface-troposphere system imposed by external factors, with no changes in stratospheric dynamics, without any surface and tropospheric feedbacks in operation (i.e., no secondary effects induced because of changes in tropospheric motions or its thermodynamic state), and with no dynamically-induced changes in the amount and distribution of atmospheric water (vapour, liquid, and solid forms). Note that one potential forcing type, the second indirect effect of aerosols (Chapter 5 and Section 6.8), comprises microphysically-induced changes in the water substance. The IPCC usage of the "global mean" forcing refers to the globally and annually averaged estimate of the forcing.

The prior IPCC Assessments as well as other recent studies (notably the SAR; see also Hansen *et al.* (1997a) and Shine and Forster (1999)) have discussed the rationale for this definition and its application to the issue of forcing of climate change. The salient elements of the radiative forcing concept that characterise its eventual applicability as a tool are summarised in Appendix 6.1 (see also WMO, 1986; SAR). Defined in the above manner, radiative forcing of climate change is a modelling concept that constitutes a simple but important means of estimating the relative impacts due to different natural and anthropogenic radiative causes upon the surface-troposphere system (see Section 6.2.1). The IPCC Assessments have, in particular, focused on the forcings between pre-industrial times (taken here to be 1750) and the present (1990s, and approaching 2000). Another period of interest in recent literature has been the 1980 to 2000 period, which corresponds to a time frame when a global coverage of the climate system from satellites has become possible.

We find no reason to alter our view of any aspect of the basis, concept, formulation, and application of radiative forcing, as laid down in the IPCC Assessments to date and as applicable to the forcing of climate change. Indeed, we reiterate the view of previous IPCC reports and recommend a continued usage of the forcing concept to gauge the relative strengths of various perturbation agents, but, as discussed below in Section 6.2, urge that the constraints on the interpretation of the forcing estimates and the limitations in its utility be noted.

6.1.2 Evolution of Knowledge on Forcing Agents

The first IPCC Assessment (IPCC, 1990) recognised the existence of a host of agents that can cause climate change including greenhouse gases, tropospheric aerosols, land-use change, solar irradiance and stratospheric aerosols from volcanic eruptions, and provided firm quantitative estimates of the well-mixed greenhouse gas forcing since pre-industrial times. Since that Assessment, the number of agents identified as potential climate changing entities has increased, along with knowledge on the space-time aspects of their operation and magnitudes. This has prompted the radiative forcing concept to be extended, and the evaluation to be performed for spatial scales less than global, and for seasonal time-scales.

IPCC (1992) recognised the importance of the forcing due to anthropogenic sulphate aerosols and assessed quantitative estimates for the first time. IPCC (1992) also recognised the forcing due to the observed loss of stratospheric O_3 and that due to an increase in tropospheric O_3. Subsequent assessments (IPCC, 1994; SAR) have performed better evaluations of the estimates of the forcings due to agents having a space-time dependence such as aerosols and O_3, besides strengthening further the confidence in the well-mixed greenhouse gas forcing estimates. More information on changes in solar irradiance have also become available since 1990. The status of knowledge on forcing arising due to changes in land use has remained somewhat shallow.

For the well-mixed greenhouse gases (CO_2, CH_4, N_2O and halocarbons), their long lifetimes and near uniform spatial distributions imply that a few observations coupled with a good knowledge of their radiative properties will suffice to yield a reasonably accurate estimate of the radiative forcing, accompanied by a high degree of confidence (SAR; Shine and Forster, 1999). But, in the case of short-lived species, notably aerosols, observations of the concentrations over wide spatial regions and over long time periods are needed. Such global observations are not yet in place. Thus, estimates are drawn from model simulations of their three-dimensional distributions. This poses an uncertainty in the computation of forcing which is sensitive to the space-time distribution of the atmospheric concentrations and chemical composition of the species.

6.2 Forcing-Response Relationship

6.2.1 Characteristics

As discussed in the SAR, the change in the net irradiance at the tropopause, as defined in Section 6.1.1, is, to a first order, a good indicator of the equilibrium global mean (understood to be

globally and annually averaged) surface temperature change. The climate sensitivity parameter (global mean surface temperature response ΔT_s to the radiative forcing ΔF) is defined as:

$$\Delta T_s / \Delta F = \lambda \qquad (6.1)$$

(Dickinson, 1982; WMO, 1986; Cess *et al.*, 1993). Equation (6.1) is defined for the transition of the surface-troposphere system from one equilibrium state to another in response to an externally imposed radiative perturbation. In the one-dimensional radiative-convective models, wherein the concept was first initiated, λ is a nearly invariant parameter (typically, about 0.5 K/(Wm^{-2}); Ramanathan *et al.*, 1985) for a variety of radiative forcings, thus introducing the notion of a possible universality of the relationship between forcing and response. It is this feature which has enabled the radiative forcing to be perceived as a useful tool for obtaining first-order estimates of the relative climate impacts of different imposed radiative perturbations. Although the value of the parameter "λ" can vary from one model to another, within each model it is found to be remarkably constant for a wide range of radiative perturbations (WMO, 1986). The invariance of λ has made the radiative forcing concept appealing as a convenient measure to estimate the global, annual mean surface temperature response, without taking the recourse to actually run and analyse, say, a three-dimensional atmosphere-ocean general circulation model (AOGCM) simulation.

In the context of the three-dimensional AOGCMs, too, the applicability of a general global mean climate sensitivity parameter (i.e., global mean surface temperature response to global mean radiative forcing) has been explored. The GCM investigations include studies of (i) the responses to short-wave forcing such as a change in the solar constant or cloud albedo or doubling of CO_2, both forcing types being approximately spatially homogeneous (e.g., Manabe and Wetherald, 1980; Hansen *et al.*, 1984, 1997a; Chen and Ramaswamy, 1996a; Le Treut *et al.*, 1998), (ii) responses due to different considered mixtures of greenhouse gases, with the forcings again being globally homogeneous (Wang *et al.*, 1991, 1992), (iii) responses to the spatially homogeneous greenhouse gas and the spatially inhomogeneous sulphate aerosol direct forcings (Cox *et al.*, 1995), (iv) responses to different assumed profiles of spatially inhomogeneous species, e.g., aerosols and O_3 (Hansen *et al.*, 1997a), and (v) present-day versus palaeoclimate (e.g., last glacial maximum) simulations (Manabe and Broccoli, 1985; Rind *et al.*, 1989; Berger *et al.*, 1993; Hewitt and Mitchell, 1997).

Overall, the three-dimensional AOGCM experiments performed thus far show that the radiative forcing continues to serve as a good estimator for the global mean surface temperature response but not to a quantitatively rigorous extent as in the case of the one-dimensional radiative-convective models. Several GCM studies suggest a similar global mean climate sensitivity for the spatially homogeneous and for many but not all of the spatially inhomogeneous forcings of relevance for climate change in the industrial era (Wang *et al.*, 1992; Roeckner *et al.*, 1994; Taylor and Penner, 1994; Cox *et al.*, 1995; Hansen *et al.*, 1997a). Paleoclimate simulations (Manabe and Broccoli, 1985; Rind *et al.*, 1989) also suggest the idea of similarities in climate sensitivity for

a spatially homogeneous and an inhomogeneous forcing (arising due to the presence of continental ice sheets at mid- to high northern latitudes during the last glacial maximum). However, different values of climate sensitivity can result from the different GCMs which, in turn, are different from the λ values obtained with the radiative-convective models. Hansen *et al.* (1997a) show that the variation in λ for most of the globally distributed forcings suspected of influencing climate over the past century is typically within about 20%. Extending considerations to some of the spatially confined forcings yields a range of about 25 to 30% around a central estimate (see also Forster *et al.*, 2001). This is to be contrasted with the variation of 15% obtained in a smaller number of experiments (all with fixed clouds) by Ramaswamy and Chen (1997b). However, in a general sense and considering arbitrary forcing types, the variation in λ could be substantially higher (50% or more) and the climate response much more complex (Hansen *et al.*, 1997a). It is noted that the climate sensitivity for some of the forcings that have potentially occurred in the industrial era have yet to be comprehensively investigated.

While the total climate feedback for the spatially homogeneous and the considered inhomogeneous forcings does not differ significantly, leading to a near-invariant climate sensitivity, the individual feedback mechanisms (water vapour, ice albedo, lapse rate, clouds) can have different strengths (Chen and Ramaswamy, 1996a,b). The feedback effects can be of considerably larger magnitude than the initial forcing and govern the magnitude of the global mean response (Ramanathan, 1981; Wetherald and Manabe, 1988; Hansen *et al.*, 1997a). For different types of perturbations, the relative magnitudes of the feedbacks can vary substantially.

For spatially homogeneous forcings of opposite signs, the responses are somewhat similar in magnitude, although the ice albedo feedback mechanism can yield an asymmetry in the high latitude response with respect to the sign of the forcing (Chen and Ramaswamy, 1996a). Even if the forcings are spatially homogeneous, there could be changes in land surface energy budgets that depend on the manner of the perturbation (Chen and Ramaswamy, 1996a). Furthermore, for the same global mean forcing, dynamic feedbacks involving changes in convective heating and precipitation can be initiated in the spatially inhomogeneous perturbation cases that differ from those in the spatially homogeneous perturbation cases.

The nature of the response and the forcing-response relation (Equation 6.1) could depend critically on the vertical structure of the forcing (see WMO, 1999). A case in point is O_3 changes, since this initiates a vertically inhomogeneous forcing owing to differing characteristics of the solar and long-wave components (WMO, 1992). Another type of forcing is that due to absorbing aerosols in the troposphere (Kondratyev, 1999). In this instance, the surface experiences a deficit while the atmosphere gains short-wave radiative energy. Hansen *et al.* (1997a) show that, for both these special types of forcing, if the perturbation occurs close to the surface, complex feedbacks involving lapse rate and cloudiness could alter the climate sensitivity substantially from that prevailing for a similar magnitude of perturbation imposed at other altitudes. A different kind of example is illustrated by model experiments indicating that the climate sensitivity is considerably different for

O_3 losses occurring in the upper rather than lower stratosphere (Hansen *et al*., 1997a; Christiansen, 1999). Yet another example is stratospheric aerosols in the aftermath of volcanic eruptions. In this case, the lower stratosphere is radiatively warmed while the surface-troposphere cools (Stenchikov *et al*., 1998) so that the climate sensitivity parameter does not convey a complete picture of the climatic perturbations. Note that this contrasts with the effects due to CO_2 increases, wherein the surface-troposphere experiences a radiative heating and the stratosphere a cooling. The vertical partitioning of forcing between atmosphere and surface could also affect the manner of changes of parameters other than surface temperature, e.g., evaporation, soil moisture.

Zonal mean and regional scale responses for spatially inhomogeneous forcings can differ considerably from those for homogeneous forcings. Cox *et al.* (1995) and Taylor and Penner (1994) conclude that the spatially inhomogeneous sulphate aerosol direct forcing in the northern mid-latitudes tends to yield a significant response there that is absent in the spatially homogeneous case. Using a series of idealised perturbations, Ramaswamy and Chen (1997b) show that the gradient of the equator-to-pole surface temperature response to spatially homogeneous and inhomogeneous forcings is significantly different when scaled with respect to the global mean forcing, indicating that the more spatially confined the forcing, the greater the meridional gradient of the temperature response. In the context of the additive nature of the regional temperature change signature, Penner *et al.* (1997) suggest that there may be some limit to the magnitude of the forcings that yield a linear signal.

A related issue is whether responses to individual forcings can be linearly added to obtain the total response to the sum of the forcings. Indications from experiments that have attempted a very limited number of combinations are that the forcings can indeed be added (Cox *et al.*, 1995; Roeckner *et al.*, 1994; Taylor and Penner, 1994). These investigations have been carried out in the context of equilibrium simulations and have essentially dealt with the CO_2 and sulphate aerosol direct forcing. There tends to be a linear additivity not only for the global mean temperature, but also for the zonal mean temperature and precipitation (Ramaswamy and Chen, 1997a). Haywood *et al.* (1997c) have extended the study to transient simulations involving greenhouse gases and sulphate aerosol forcings in a GCM. They find the linear additivity to approximately hold for both the surface temperature and precipitation, even on regional scales. Parameters other than surface temperature and precipitation have not been tested extensively. Owing to the limited sets of forcings examined thus far, it is not possible as yet to generalise to all natural and anthropogenic forcings discussed in subsequent sections of this chapter.

One caveat that needs to be reiterated (see IPCC, 1994 and SAR) regarding forcing-response relationships is that, even if there is a cancellation in the global mean forcing due to forcings that are of opposite signs and distributed spatially in a different manner, and even if the responses are linearly additive, there could be spatial aspects of the responses that are not necessarily null. In particular, circulation changes could result in a distinct regional response even under conditions of a null global mean forcing and a null global mean surface temperature response (Ramaswamy and Chen, 1997a). Sinha and Harries (1997) suggest that there can be characteristic vertical responses even if the net radiative forcing is zero.

6.2.2 Strengths and Limitations of the Forcing Concept

Radiative forcing continues to be a useful concept, providing a convenient first-order measure of the relative climatic importance of different agents (SAR; Shine and Forster, 1999). It is computationally much more efficient than a GCM calculation of the climate response to a specific forcing; the simplicity of the calculation allows for sophisticated, highly accurate radiation schemes, yielding accurate forcing estimates; the simplicity also allows for a relative ease in conducting model intercomparisons; it yields a first-order perspective that can then be used as a basis for more elaborate GCM investigations; it potentially bypasses the complex tasks of running and analysing equilibrium-response GCM integrations; it is useful for isolating errors and uncertainties due to radiative aspects of the problem.

In gauging the relative climatic significance of different forcings, an important question is whether they have similar climate sensitivities. As discussed in Section 6.2.1, while models indicate a reasonable similarity of climate sensitivities for spatially homogeneous forcings (e.g., CO_2 changes, solar irradiance changes), it is not possible as yet to make a generalisation applicable to all the spatially inhomogeneous forcing types. In some cases, the climate sensitivity differs significantly from that for CO_2 changes while, for some other cases, detailed studies have yet to be conducted. A related question is whether the linear additivity concept mentioned above can be extended to include all of the relevant forcings, such that the sum of the responses to the individual forcings yields the correct total climate response. As stated above, such tests have been conducted only for limited subsets of the relevant forcings.

Another important limitation of the concept is that there are parameters other than global mean surface temperature that need to be determined, and that are as important from a climate and societal impacts perspective; the forcing concept cannot provide estimates for such climate parameters as directly as for the global mean surface temperature response. There has been considerably less research on the relationship of the equilibrium response in such parameters as precipitation, ice extent, sea level, etc., to the imposed radiative forcing.

Although the radiative forcing concept was originally formulated for the global, annual mean climate system, over the past decade, it has been extended to smaller spatial domains (zonal mean), and smaller time-averaging periods (seasons) in order to deal with short-lived species that have a distinct geographical and seasonal character, e.g., aerosols and O_3 (see also the SAR). The global, annual average forcing estimate for these species masks the inhomogeneity in the problem such that the anticipated global mean response (via Equation 6.1) may not be adequate for gauging the spatial pattern of the actual climate change. For these classes of radiative perturbations, it is incorrect to assume that the characteristics of the responses would be necessarily co-located with the forcing, or that the magnitudes would follow the forcing patterns exactly (e.g., Cox *et al.*, 1995; Ramaswamy and Chen, 1997b).

6.3 Well-mixed Greenhouse Gases

The well-mixed greenhouse gases have lifetimes long enough to be relatively homogeneously mixed in the troposphere. In contrast, O_3 (Section 6.5) and the NMHCs (Section 6.6) are gases with relatively short lifetimes and are therefore not homogeneously distributed in the troposphere.

Spectroscopic data on the gaseous species have been improved with successive versions of the HITRAN (Rothman *et al.*, 1992, 1998) and GEISA databases (Jacquinet-Husson *et al.*, 1999). Pinnock and Shine (1998) investigated the effect of the additional hundred thousands of new lines in the 1996 edition of the HITRAN database (relative to the 1986 and the 1992 editions) on the infrared radiative forcing due to CO_2, CH_4, N_2O and O_3. They found a rather small effect due to the additional lines, less than a 5% effect for the radiative forcing of the cited gases and less than 1.5% for a doubling of CO_2. For the chlorofluorocarbons (CFCs) and their replacements, the uncertainties in the spectroscopic data are much larger than for CO_2, CH_4, N_2O and O_3, and differ more among the various laboratory studies. Christidis *et al.* (1997) found a range of 20% between ten different spectroscopic studies of CFC-11. Ballard *et al.* (2000) performed an intercomparison of laboratory data from five groups and found the range in the measured absorption cross-section of HCFC-22 to be about 10%.

Several previous studies of radiative forcing due to well-mixed greenhouse gases have been performed using single, mostly global mean, vertical profiles. Myhre and Stordal (1997) investigated the effects of spatial and temporal averaging on the globally and annually averaged radiative forcing due to the well-mixed greenhouse gases. The use of a single global mean vertical profile to represent the global domain, instead of the more rigorous latitudinally varying profiles, can lead to errors of about 5 to 10%; errors arising due to the temporal averaging process are much less (~1%). Freckleton *et al.* (1998) found similar effects and suggested three vertical profiles which could represent global atmospheric conditions satisfactorily in radiative transfer calculations. In the above two studies as well as in Forster *et al.* (1997), it is the dependence of the radiative forcing on the tropopause height and thereby also the vertical temperature profile, that constitutes the main reason for the need of a latitudinal resolution in radiative forcing calculations. The radiative forcing due to halocarbons depends on the tropopause height more than is the case for CO_2 (Forster *et al.*, 1997; Myhre and Stordal, 1997).

Not all greenhouse gases are well mixed vertically and horizontally in the troposphere. Freckleton *et al.* (1998) have investigated the effects of inhomogeneities in the concentrations of the greenhouse gases on the radiative forcing. For CH_4 (a well-mixed greenhouse gas), the assumption that it is well-mixed horizontally in the troposphere introduces an error much less than 1% relative to a calculation in which a chemistry-transport model predicted distribution of CH_4 was used. For most halocarbons, and to a lesser extent for CH_4 and N_2O, the mixing ratio decays with altitude in the stratosphere. For CH_4 and N_2O, this implies a reduction in the radiative forcing of up to about 3% (Freckleton *et al.*, 1998; Myhre *et al.*, 1998b). For most halocarbons, this implies a reduction in the radiative forcing up to about 10%

(Christidis *et al.*, 1997; Hansen *et al.*, 1997a; Minschwaner *et al.*, 1998; Myhre *et al.*, 1998b) while it is found to be up to 40% for a short-lived component found in Jain *et al.* (2000).

Trapping of the long-wave radiation due to the presence of clouds reduces the radiative forcing of the greenhouse gases compared to the clear-sky forcing. However, the magnitude of the effect due to clouds varies for different greenhouse gases. Relative to clear skies, clouds reduce the global mean radiative forcing due to CO_2 by about 15% (Pinnock *et al.*, 1995; Myhre and Stordal, 1997), that due to CH_4 and N_2O is reduced by about 20% (derived from Myhre *et al.*, 1998b), and that due to the halocarbons is reduced by up to 30% (Pinnock *et al.*, 1995; Christidis *et al.*, 1997; Myhre *et al.*, 1998b).

The effect of stratospheric temperature adjustment also differs between the various well-mixed greenhouse gases, owing to different gas optical depths, spectral overlap with other gases, and the vertical profiles in the stratosphere. The stratospheric temperature adjustment reduces the radiative forcing due to CO_2 by about 15% (Hansen *et al.*, 1997a). CH_4 and N_2O estimates are slightly modified by the stratospheric temperature adjustment, whereas the radiative forcing due to halocarbons can increase by up to 10% depending on the spectral overlap with O_3 (IPCC, 1994).

Radiative transfer calculations are performed with different types of radiative transfer schemes ranging from line-by-line models to band models (IPCC, 1994). Evans and Puckrin (1999) have performed surface measurements of downward spectral radiances which reveal the optical characteristics of individual greenhouse gases. These measurements are compared with line-by-line calculations. The agreement between the surface measurements and the line-by-line model is within 10% for the most important of the greenhouse gases: CO_2, CH_4, N_2O, CFC-11 and CFC-12. This is not a direct test of the irradiance change at the tropopause and thus of the radiative forcing, but the good agreement does offer verification of fundamental radiative transfer knowledge as represented by the line-by-line (LBL) model. This aspect concerning the LBL calculation is reassuring as several radiative forcing determinations which employ coarser spectral resolution models use the LBL as a benchmark tool (Freckleton *et al.*, 1996; Christidis *et al.*, 1997; Minschwaner *et al.*, 1998; Myhre *et al.*, 1998b; Shira *et al.*, 2001). Satellite observations can also be useful in estimates of radiative forcing and in the intercomparison of radiative transfer codes (Chazette *et al.*, 1998).

6.3.1 Carbon Dioxide

IPCC (1990) and the SAR used a radiative forcing of 4.37 Wm^{-2} for a doubling of CO_2 calculated with a simplified expression. Since then several studies, including some using GCMs (Mitchell and Johns, 1997; Ramaswamy and Chen, 1997b; Hansen *et al.*, 1998), have calculated a lower radiative forcing due to CO_2 (Pinnock *et al.*, 1995; Roehl *et al.*, 1995; Myhre and Stordal, 1997; Myhre *et al.*, 1998b; Jain *et al.*, 2000). The newer estimates of radiative forcing due to a doubling of CO_2 are between 3.5 and 4.1 Wm^{-2} with the relevant species and various overlaps between greenhouse gases included. The lower forcing in the cited newer

studies is due to an accounting of the stratospheric temperature adjustment which was not properly taken into account in the simplified expression used in IPCC (1990) and the SAR (Myhre *et al.*, 1998b). In Myhre *et al.* (1998b) and Jain *et al.* (2000), the short-wave forcing due to CO_2 is also included, an effect not taken into account in the SAR. The short-wave effect results in a negative forcing contribution for the surface-troposphere system owing to the extra absorption due to CO_2 in the stratosphere; however, this effect is relatively small compared to the total radiative forcing (< 5%).

The new best estimate based on the published results for the radiative forcing due to a doubling of CO_2 is 3.7 Wm^{-2}, which is a reduction of 15% compared to the SAR. The forcing since pre-industrial times in the SAR was estimated to be 1.56 Wm^{-2}; this is now altered to 1.46 Wm^{-2} in accordance with the discussion above. The overall decrease of about 6% (from 1.56 to 1.46) accounts for the above effect and also accounts for the increase in CO_2 concentration since the time period considered in the SAR (the latter effect, by itself, yields an increase in the forcing of about 10%).

While an updating of the simplified expressions to account for the stratospheric adjustment becomes necessary for radiative forcing estimates, it is noted that GCM simulations of CO_2-induced climate effects already account for this physical effect implicitly (see also Chapter 9). In some climate studies, the sum of the non-CO_2 well-mixed greenhouse gases forcing is represented by that due to an equivalent amount of CO_2. Because the CO_2 forcing in the SAR was higher than the new estimate, the use of the equivalent CO_2 concept would underestimate the impact of the non-CO_2 well-mixed gases, if the IPCC values of radiative forcing were used in the scaling operation.

6.3.2 Methane and Nitrous Oxide

The SAR reported that several studies found a higher forcing due to CH_4 than IPCC (1990), up to 20%; however the recommendation was to use the same value as in IPCC (1990). The higher radiative forcing estimates were obtained using band models. Recent calculations using LBL and band models confirm these results (Lelieveld *et al.*, 1998; Minschwaner *et al.*, 1998; Jain *et al.*, 2000). Using two band models, Myhre *et al.* (1998b) found the computed radiative forcing to differ by almost 10%. This was attributed to difficulties in the treatment of CH_4 in band models since, given its present abundance, the CH_4 absorption lies between the weak line and the strong line limits (Ramanathan *et al.*, 1987). After updating for a small increase in concentration since the SAR, the radiative forcing due to CH_4 is 0.48 Wm^{-2} since pre-industrial times. This estimate for forcing due to CH_4 is only for the direct effect of CH_4; for radiative forcing of the indirect effect of CH_4, see Sections 6.5 and 6.6.

The problem mentioned above with the band models for CH_4 does not occur to the same degree in the case of N_2O, given the latter's present concentrations. Three recent studies, Myhre *et al.* (1998b) (two models), Minschwaner *et al.* (1998) (one model), and Jain *et al.* (2000) (one model), calculated lower radiative forcing for N_2O than reported in previous IPCC assessments, viz., 0.13, 0.12, 0.11, and 0.12 Wm^{-2}, respectively, compared to 0.14 Wm^{-2} in the SAR. For N_2O, effects of change in spectroscopic data, stratospheric adjustment, and decay of the mixing ratio in the stratosphere are all found to be small effects. However, effects of clouds and different radiation schemes are potential sources for the difference between the newer estimates and the SAR. A value of 0.15 Wm^{-2} is now suggested for the radiative forcing due to N_2O, taking into account an increase in the concentration since the SAR, together with a smaller pre-industrial concentration than assumed in IPCC (1996a; Table 2.2) (see Chapter 4).

6.3.3 Halocarbons

The SAR referred to Pinnock *et al.* (1995), who obtained a higher radiative forcing for CFC-11 than used in previous IPCC reports, but refrained from changing the recommended value pending further investigations. Since then several papers have investigated CFC-11, confirming the higher forcing value (Christidis *et al.*, 1997; Hansen *et al.*, 1997a; Myhre and Stordal, 1997; Good *et al.*, 1998; Myhre *et al.*, 1998b; Jain *et al.*, 2000) with a range from 0.24 to 0.29 Wm^{-2} $ppbv^{-1}$. As mentioned above, Christidis *et al.* (1997) found a large discrepancy in the absorption data for CFC-11 in the literature. Other causes for the difference in the radiative forcing are different treatments of the decrease in mixing ratio in the stratosphere and the fact that some estimates are performed with a single global mean column atmospheric profile. Taking these effects into account, a radiative efficiency due to CFC-11 of 0.25 Wm^{-2} $ppbv^{-1}$ is used, the same value as in WMO (1999). For the present concentration of CFC-11, this yields a forcing of 0.07 Wm^{-2} since pre-industrial times. In previous IPCC reports, radiative forcing due to CFCs and their replacements have been given relative to CFC-11. CFC-11 is now revised and this introduces a complicating factor since the radiative forcing for the CFCs and CFC replacements are given as absolute values in some studies, but relative to CFC-11 in others. WMO (1999) updated several of the halocarbons giving radiative forcing in absolute values (in Wm^{-2} $ppbv^{-1}$).

CFC-12 is investigated in Hansen *et al.* (1997a), Myhre *et al.* (1998b), Minschwaner *et al.* (1998), Good *et al.* (1998) and Jain *et al.* (2000). The difference in the results is up to 20% which is due to differing impact of clouds, absorption cross-section data, and the vertical profile of decay of the mixing ratio in the stratosphere. The radiative forcing due to CFC-12 of 0.32 Wm^{-2} $ppbv^{-1}$ used in WMO (1999) is retained, which is slightly higher than the SAR value. The present radiative forcing due to CFC-12 is therefore 0.17 Wm^{-2}, which is the third highest forcing among the well-mixed greenhouse gases.

Radiative forcing values for well-mixed greenhouse gases with non-negligible contributions at present are included in Table 6.1. Several recent studies have investigated various CFC replacements (Imasu *et al.*, 1995; Gierczak *et al.*, 1996; Barry *et al.*, 1997; Christidis *et al.*, 1997; Grossman *et al.*, 1997; Papasavva *et al.*, 1997; Good *et al.*, 1998; Heathfield *et al.*, 1998b; Highwood and Shine, 2000; Ko *et al.*, 1999; Myhre *et al.*, 1999; Jain *et al.*, 2000; Li *et al.*, 2000; Naik *et al.*, 2000; Shira *et al.*, 2001). For some CFC replacements not included in Table 6.1, the radiative forcings are shown in Tables 6.7 and 6.8 (Section 6.12).

Table 6.1: *Pre-industrial (1750) and present (1998) abundances of well-mixed greenhouse gases and the radiative forcing due to the change in abundance. Volume mixing ratios for CO_2 are in ppm, for CH_4 and N_2O in ppb, and for the rest in ppt.*

Gas	Abundance (Year 1750)	Abundance (Year 1998)	Radiative forcing (Wm^{-2})
Gases relevant to radiative forcing only			
CO_2	278	365	1.46
CH_4	700	1745	0.48
N_2O	270	314	0.15
CF_4	40	80	0.003
C_2F_6	0	3	0.001
SF_6	0	4.2	0.002
HFC-23	0	14	0.002
HFC-134a	0	7.5	0.001
HFC-152a	0	0.5	0.000
Gases relevant to radiative forcing and ozone depletion			
CFC-11	0	268	0.07
CFC-12	0	533	0.17
CFC-13	0	4	0.001
CFC-113	0	84	0.03
CFC-114	0	15	0.005
CFC-115	0	7	0.001
CCl_4	0	102	0.01
CH_3CCl_3	0	69	0.004
HCFC-22	0	132	0.03
HCFC-141b	0	10	0.001
HCFC-142b	0	11	0.002
Halon-1211	0	3.8	0.001
Halon-1301	0	2.5	0.001

Table 6.2: *Simplified expressions for calculation of radiative forcing due to CO_2, CH_4, N_2O, and halocarbons. The first row for CO_2 lists an expression with a form similar to IPCC (1990) but with newer values of the constants. The second row for CO_2 is a more complete and updated expression similar in form to that of Shi (1992). The third row expression for CO_2 is from WMO (1999), based in turn on Hansen et al. (1988).*

Trace gas	Simplified expression Radiative forcing, ΔF (Wm^{-2})	Constants
CO_2	$\Delta F = \alpha \ln(C/C_0)$ $\Delta F = \alpha \ln(C/C_0) + \beta(\sqrt{C} - \sqrt{C_0})$ $\Delta F = \alpha(g(C) - g(C_0))$ where $g(C) = \ln(1 + 1.2C + 0.005C^2 + 1.4 \times 10^{-6}C^3)$	$\alpha = 5.35$ $\alpha = 4.841$, $\beta = 0.0906$ $\alpha = 3.35$
CH_4	$\Delta F = \alpha(\sqrt{M} - \sqrt{M_0}) - (f(M,N_0) - f(M_0,N_0))$	$\alpha = 0.036$
N_2O	$\Delta F = \alpha(\sqrt{N} - \sqrt{N_0}) - (f(M_0,N) - f(M_0,N_0))$	$\alpha = 0.12$
CFC-11[a]	$\Delta F = \alpha(X - X_0)$	$\alpha = 0.25$
CFC-12	$\Delta F = \alpha(X - X_0)$	$\alpha = 0.32$

$f(M,N) = 0.47 \ln[1 + 2.01 \times 10^{-5} (MN)^{0.75} + 5.31 \times 10^{-15} M(MN)^{1.52}]$

C is CO_2 in ppm

M is CH_4 in ppb

N is N_2O in ppb

X is CFC in ppb

The constant in the simplified expression for CO_2 for the first row is based on radiative transfer calculations with three-dimensional climatological meteorological input data (Myhre *et al.*, 1998b). For the second and third rows, constants are derived with radiative transfer calculations using one-dimensional global average meteorological input data from Shi (1992) and Hansen *et al.* (1988), respectively.

The subscript 0 denotes the unperturbed concentration.

[a] The same expression is used for all CFCs and CFC replacements, but with different values for α (i.e., the radiative efficiencies in Table 6.7).

The values of CFC-115 and CCl_4 have been substantially revised since the IPCC (1994) report, with a lower and higher radiative forcing estimate, respectively. Highwood and Shine (2000) calculated a radiative forcing due to chloroform ($CHCl_3$) which is much stronger than the SAR value. They suggest that this is due to the neglect of bands outside 800 to 1,200 cm^{-1} in previous studies of chloroform. Highwood and Shine (2000) found a radiative forcing due to HFC-23 which is substantially lower than the value given in the SAR.

6.3.4 Total Well-Mixed Greenhouse Gas Forcing Estimate

The radiative forcing due to all well-mixed greenhouse gases since pre-industrial times was estimated to be 2.45 Wm^{-2} in the SAR with an uncertainty of 15%. This is now altered to a radiative forcing of 2.43 Wm^{-2} with an uncertainty of 10%, based on the range of model results and the discussion of factors leading to uncertainties in the radiative forcing due to these greenhouse gases. The uncertainty in the radiative forcing due to CO_2 is estimated to be smaller than for the other well-mixed greenhouse gases; less than 10% (Section 6.3.1). For the CH_4 forcing the main uncertainty is connected to the radiative transfer code itself and is estimated to be about 15% (Section 6.3.2). The uncertainty in N_2O (Section 6.3.2) is similar to that for CO_2, whereas the main uncertainties for halocarbons arise from the spectroscopic data. The estimated uncertainty for halocarbons is 10 to 15% for the most frequently studied species, but higher for some of the less investigated molecules (Section 6.3.3). A small increase in the concentrations of the well-mixed greenhouse gases since the SAR has compensated for the reduction in radiative forcing resulting from improved radiative transfer calculations. The rate of increase in the well-mixed greenhouse gas concentrations, and thereby the radiative forcing, has been smaller over the first half of the 1990s compared to previous decades (see also Hansen *et al.*, 1998). This is mainly a result of reduced growth in CO_2 and CH_4 concentrations and smaller increase or even reduction in the concentration of some of the halocarbons.

6.3.5 Simplified Expressions

IPCC (1990) used simplified analytical expressions for the well-mixed greenhouse gases based in part on Hansen *et al.* (1988). With updates of the radiative forcing, the simplified expressions

need to be reconsidered, especially for CO_2 and N_2O. Shi (1992) investigated simplified expressions for the well-mixed greenhouse gases and Hansen *et al.* (1988, 1998) presented a simplified expression for CO_2. Myhre *et al.* (1998b) used the previous IPCC expressions with new constants, finding good agreement (within 5%) with high spectral resolution radiative transfer calculations. The already well established and simple functional forms of the expressions used in IPCC (1990), and their excellent agreement with explicit radiative transfer calculations, are strong bases for their continued usage, albeit with revised values of the constants, as listed in Table 6.2. Shi (1992) has suggested more physically based and accurate expressions which account for (i) additional absorption bands that could yield a separate functional form besides the one in IPCC (1990), and (ii) a better treatment of the overlap between gases. WMO (1999) used a simplified expression for CO_2 based on Hansen *et al.* (1988) and this simplified expression is used in the calculations of GWP in Section 6.12. For CO_2 the simplified expressions from Shi (1992) and Hansen *et al.* (1988) are also listed alongside the IPCC (1990)-like expression for CO_2 in Table 6.2. Compared to IPCC (1990) and the SAR and for similar changes in the concentrations of well-mixed greenhouse gases, the improved simplified expressions result in a 15% decrease in the estimate of the radiative forcing by CO_2 (first row in Table 6.2), a 15% decrease in the case of N_2O, an increase of 10 to 15% in the case of CFC-11 and CFC-12, and no change in the case of CH_4.

6.4 Stratospheric Ozone

6.4.1 Introduction

The observed stratospheric O_3 losses over the past two decades have caused a negative forcing of the surface-troposphere system (IPCC, 1992, 1994; SAR). In general, the sign and magnitude of the forcing due to stratospheric O_3 loss are governed by the vertical profile of the O_3 loss from the lower through to the upper stratosphere (WMO, 1999). Ozone depletion in the lower stratosphere, which occurs mainly in the mid- to high latitudes is the principal component of the forcing. It causes an increase in the solar forcing of the surface-troposphere system. However, the long-wave effects consist of a reduction of the emission from the stratosphere to the troposphere. This comes about due to the O_3 loss, coupled with a cooling of the stratospheric temperatures in the stratospheric adjustment process, with a colder stratosphere emitting less radiation. The long-wave effects, after adjustment of the stratospheric temperatures to the imposed perturbation, overwhelm the solar effect i.e., the negative long-wave forcing prevails over the positive solar to lead to a net negative radiative forcing of the surface-troposphere system (IPCC, 1992). The magnitude of the forcing is dependent on the loss in the lower stratosphere, with the estimates subject to some uncertainties in view of the fact that detailed observations on the vertical profile in this region of the atmosphere are difficult to obtain.

Typically, model-based estimates involve a local (i.e., over the grid box of the model) adjustment of the stratosphere (Section 6.1) assuming the dynamical heating to be fixed (FDH approximation; see also Appendix 6.1). An improved version of this scheme is the so-called seasonally evolving fixed dynamical heating (SEFDH; Forster *et al.*, 1997; Kiehl *et al.*, 1999). The adjustment of the stratosphere to a new thermal equilibrium state is a critical element for estimating the sign and magnitude of the forcing due to stratospheric O_3 loss (WMO, 1992, 1995). While the computational procedures are well established for the FDH and SEFDH approximations in the context of the surface-troposphere forcing, one test of the approximations lies in the comparison of the computed with observed temperature changes, since it is this factor that plays a large role in the estimate of the forcing. While the temperature changes going into the determination of the forcing are broadly consistent with the observations, there are challenges in comparing quantitatively the actual temperature changes (which undoubtedly are affected by other influences and may even contain feedbacks due to O_3 and other forcings) with the FDH or SEFDH model simulations (which necessarily do not contain feedback effects other than the stratospheric temperature response due to the essentially radiative adjustment process).

We reiterate both the concept of the forcing for stratospheric O_3 changes and the fact that this has led to a negative radiative forcing since the late 1970s. Further, the model-based estimates that necessarily rely on satellite observations of O_3 losses are likely the most reliable means to derive the forcing, notwithstanding the uncertainty in the vertical profile of loss in the vicinity of the tropopause. Since several model estimates have employed the Total Ozone Mapping Spectrometer (TOMS) observations as one of the inputs for the calculations, there is the likelihood of a small tropospheric O_3 change component contaminating the stratospheric O_3 loss amounts, especially for the lowermost regions of the lower stratosphere (Hansen *et al.*, 1997a; Shine and Forster, 1999). Both the estimates derived in the earlier IPCC assessments and the studies since the SAR show that the forcing pattern increases from the mid- to high latitudes consistent with the O_3 loss amounts. Seasonally, the winter/springtime forcings are the largest, again consistent with the temporal nature of the observed O_3 depletion.

It is logical to enquire into the realism of the computed coolings with the available observations using models more realistic than FDH/SEFDH, namely GCMs. Furthermore, comparison of the FDH and SEFDH derived temperature changes with those from a GCM constitutes another test of the approximations. WMO (1999) concluded, on the basis of intercomparisons of the temperature records as measured by different instruments, that there has been a distinct cooling of the global mean temperature of the lower stratosphere over the past two decades, with a value of about 0.5°C/decade. Model simulations from GCMs using the observed O_3 losses yield global mean temperature changes that are approximately consistent with the observations. Such a cooling is also much larger than that due to the well-mixed greenhouse gases taken together over the same time period. Although the possibility of other trace species also contributing to this cooling cannot be ruled out, the consistency between observations and model simulations enhances the general principle of an O_3-induced cooling of the lower stratosphere, and thus the negativity of the radiative forcing due to the O_3 loss. Going from global, annual mean to zonal, seasonal mean

changes in the lower stratosphere, the agreement between models and observations tends to be less strong than for the global mean values, but the suggestion of an O_3-induced signal exists. Note though that water vapour changes could also be contributing (see Section 6.6.4; Forster and Shine, 1999), complicating the quantitative attribution of the cooling solely due to O_3. As far as the FDH models that have been employed to derive the forcing are concerned, their temperature changes are broadly consistent with the GCMs and the observed cooling. However, the mid- to high latitude cooling in FDH tends to be stronger than in the GCMs and is more than that observed. The SEFDH approximation tends to do better than the FDH calculation when compared against observations (Forster *et al.*, 1997).

6.4.2 Forcing Estimates

Earlier IPCC reports had quoted a value of about -0.1 Wm^{-2}/decade with a factor of two uncertainty. There have been revisions in this estimate based on new data available on the O_3 trends (Harris *et al.*, 1998; WMO, 1999), and an extension of the period over which the forcing is computed. Models using observed O_3 changes but with varied methods to derive the temperature changes in the stratosphere have obtained -0.05 to -0.19 Wm^{-2}/decade (WMO, 1999).

Hansen *et al.* (1997a) have extended the calculations to include the O_3 loss up to the mid-1990s and performed a variety of O_3 loss experiments to investigate the forcing and response. In particular, they obtained forcings of -0.2 and -0.28 Wm^{-2} for the period 1979 to 1994 using SAGE/TOMS and SAGE/SBUV satellite data, respectively. Hansen *et al.* (1998) updated their forcing to -0.2 Wm^{-2} with an uncertainty of 0.1 Wm^{-2} for the period 1970 to present. Forster and Shine (1997) obtained forcings of -0.17 Wm^{-2} and -0.22 Wm^{-2} for the period 1979 to 1996 using SAGE and SBUV observations, respectively. The WMO (1999) assessment gave a value of -0.2 Wm^{-2} with an uncertainty of ± 0.15 Wm^{-2} for the period from late 1970s to mid-1990s. Forster and Shine (1997) have also extended the computations back to 1964 using O_3 changes deduced from surface-based observations; combining these with an assumption that the decadal rate of change of forcing from 1979 to 1991 was sustained to the mid-1990s yielded a total stratospheric O_3 forcing of about -0.23 Wm^{-2}. Shine and Forster (1999) have revised this value to -0.15 Wm^{-2} for the period 1979 to 1997, choosing not to include the values prior to 1979 in view of the lack of knowledge on the vertical profile which makes the sign of the change also uncertain. They also revised the uncertainty to ± 0.12 Wm^{-2} around the central estimate. A more recent estimate by Forster (1999) yields -0.10 ± 0.02 Wm^{-2} for the 1979 to 1997 period using the SPARC O_3 profile (Harris *et al.*, 1998).

There have been attempts to use satellite-observed O_3 and temperature changes to gauge the forcing. Thus, Zhong *et al.* (1996, 1998) obtained a small value of -0.02 Wm^{-2}/decade; and with inclusion of the 14 micron band, a value of -0.05 Wm^{-2}/decade. It has been noted that the poor vertical resolution of the satellite temperature retrievals makes it difficult to estimate the forcing; in fact, a similar calculation using radiosonde-based temperatures yields a value of -0.1 Wm^{-2}/decade (Shine *et al.*,

1998). The main difficulty is that the temperature change in the vicinity of the lower stratosphere critically affects the emission from the stratosphere into the troposphere. Thus any uncertainty in the MSU satellite retrieval induced by the broad altitude weighting function (see WMO, 1999) becomes an important factor in the estimation of the forcing. Further, the degree of response of the climate system, embedded in the observed temperature change (i.e., feedbacks), is not resolved in an easy manner. This makes it difficult to distinguish quantitatively the part of temperature change that is a consequence of the stratospheric adjustment process (which would be, by definition, a legitimate component of the forcing estimate) and that which is due to mechanisms other than O_3 loss. Thus, using observed temperatures to estimate the forcing may be more uncertain than the model-based estimates. It must be noted though that both methods share the difficulty of quantifying the vertical and geographical distributions of the O_3 changes near the tropopause, and the rigorous association of this to the observed temperature changes. In an overall sense, it is a difficult task to verify the radiative forcing in cases where the stratospheric adjustment yields a dramatically different result than the instantaneous forcing i.e., where the species changes affect stratospheric temperatures and alter substantially the long-wave radiative effects at the tropopause. A related point is the possible upward movement of the tropopause which could explain in part the observed negative trends in O_3 and temperature (Fortuin and Kelder, 1996).

Kiehl *et al.* (1999) obtained a radiative forcing of -0.187 Wm^{-2} using the O_3 profile data set describing changes since the late 1970s due to stratospheric depletion alone, consistent with the range of other models (see Shine *et al.*, 1995). Kiehl *et al.* (1999) also present results using a very different set of O_3 change profiles deduced from satellite-derived total column O_3 and satellite-inferred tropospheric O_3 measurements to arrive at an implied O_3 forcing, considering changes at and above the tropopause, of -0.01 Wm^{-2}. The reason for the considerably weaker estimate reflects the increased O_3 in the tropopause region that is believed to have occurred since pre-industrial times (largely before 1970) in many polluted areas. How the changes in O_3 at the tropopause are prescribed is hence an important factor for the difference between this calculation and those from the other estimates.

Clearly, since WMO (1992), this forcing has been investigated in an intensive manner using different approaches, and the observational evidence of the O_3 losses, including the spatial and seasonal characteristics, are now on a firmer footing. In arriving at a best estimate for the forcing, we rely essentially on the studies that have made use of stratospheric O_3 observations directly. Based on this consideration, we adopt here a forcing of -0.15 ± 0.1 Wm^{-2} for the 1979 to 1997 period. However, it is cautioned that the small values obtained by the two specific studies mentioned above inhibit the placement of a high confidence in the estimate quoted.

In general, the reliability of the estimates above is affected by the fact that the O_3 changes in the lower stratosphere, tropopause, and upper troposphere are all poorly quantified, around the globe in general, such that the entire global domain

from 200 to 50 hPa becomes crucial for the temperature change and the adjusted forcing. Forster and Shine (1997) note that the sensitivity of forcing to percentage of O_3 loss near the tropopause is more than when the changes occur lower in the atmosphere.

Myhre *et al.* (1998a) derived O_3 changes using a chemical model in contrast to observations. As the loss of O_3 in the upper stratosphere in the simulations was large, a positive forcing of 0.02 Wm^{-2}/decade was obtained (see Ramanathan and Dickinson (1979) for an explanation of the change of sign for a O_3 loss in the lower stratosphere versus the upper stratosphere). While there are difficulties in modelling the O_3 depletion in the global strato-sphere (WMO, 1999), this study reiterates the need to be cognisant of the role played by the vertical profile of O_3 loss amounts in the entire stratosphere, i.e., middle and upper strato-sphere as well, besides the lower stratosphere.

An important issue is whether the actual surface temperature responses to the forcing by stratospheric O_3 has the same relationship with forcing as obtained for, say, CO_2 or solar constant changes. Hansen *et al.* (1997a) and Christiansen (1999) have performed a host of GCM experiments to test this concept. The forcing by lower stratospheric O_3 is an unusual one in that it has a positive short-wave and a negative long-wave radiative forcing. Moreover, it has a unique vertical structure owing to the fact that the short-wave effects are felt at the surface while the long-wave is felt only initially at the upper troposphere (Ramanathan and Dickinson, 1979; WMO, 1992). Compared to, say, CO_2 change, the stratospheric O_3 forcing is not global in extent, being very small in the tropics and increasing from mid- to high latitudes; the O_3 forcing also differs in its vertical structure, since the radiative forcings for CO_2 change in both the troposphere and surface are of the same sign (WMO, 1986). The relationship between the global mean forcing and response differs by less than 20% for O_3 profiles, resembling somewhat the actual losses (Hansen *et al.*, 1997a). However, serious departures occur if the O_3 changes are introduced near surface layers when the lapse rate change, together with cloud feedbacks, make the climate sensitivity quite different from the nominal values. There also occur substantial differences in the climate sensitivity parameter for O_3 losses in the upper stratosphere. This is further substantiated by Christiansen (1999) who shows that the higher climate sensitivity for upper stratospheric O_3 losses relative to lower stratospheric depletion is related to the vertical partitioning of the forcing, in particular the relative roles of short-wave and long-wave radiation in the surface-troposphere system. It is encouraging that the global mean climate sensitivity parameter for cases involving lower stratospheric O_3 changes and that for CO_2 changes (viz., doubling) are reasonably similar in Christiansen (1999) while being within about 25% of a central value in Hansen *et al.* (1997a). An energy balance model study (Bintanja *et al.*, 1997) suggests a stronger albedo feedback for O_3 changes than for CO_2 perturbations (see also WMO, 1999).

The evolution of the forcing due to stratospheric O_3 loss hinges on the rate of recovery of the ozone layer, with special regards to the spatial structure of such a recovery in the mid- to high latitudes. If the O_3 losses are at their maximum or will reach a maximum within the next decade, then the forcing may not become much more negative (i.e., it was −0.1 Wm^{-2} for just the 1980s; inclusion of the 1990s increases the magnitude by about 50%). And, as the O_3 layer recovers, the forcing may remain static, eventually tending to become less negative. At this time, there will be a lesser offset of the positive greenhouse effects of the halocarbons and the other well-mixed greenhouse gases (WMO, 1999). Solomon and Daniel (1996) point out that the global mean stratospheric O_3 forcing can be expected to scale down substantially in importance relative to the well-mixed greenhouse gases, in view of the former's decline and the latter's sustained increase in concentrations. Note, however, that the evolution of the negativity of the stratospheric O_3 forcing may vary considerably with latitude and season i.e., the recovery may not occur at all locations and seasons at the same rate. Thus, the spatial and seasonal evolution of forcing in the future requires as much scrutiny as the global mean estimate.

6.5 Radiative Forcing by Tropospheric Ozone

6.5.1 Introduction

Human activities have long been known to influence tropospheric O_3, not only in urban areas where O_3 is a major component of 'smog', but also in the remote atmosphere (e.g., IPCC, l990, l994; the SAR and references therein). The current state of scientific understanding of tropospheric O_3 chemistry and trends is reviewed in Chapter 4 of this report, where it is emphasised that tropospheric O_3 has an average lifetime of the order of weeks. This relatively short lifetime implies that the distribution of tropospheric O_3, as well as the trends in that distribution (which in turn lead to radiative forcing) are highly variable in space and time. Studies relating to the evaluation of radiative forcing due to estimated tropospheric O_3 increases since pre-industrial times are discussed here. While there are a number of sites where high quality surface measurements of O_3 have been obtained for a few decades, there are fewer locations where ozonesonde data allow study of the vertical distribution of the trends, and fewer still with records prior to about l970. A limited number of surface measure-ments in Europe date back to the late l9th century. These suggest that O_3 has more than tripled in the 20th century there (Marenco *et al.*, l994). The lack of global information on pre-industrial tropospheric O_3 distributions is, however, a major uncertainty in the evaluation of the forcing of this key gas (see Chapter 4).

Biomass burning plays a significant role in tropospheric O_3 production and hence in tropical radiative forcing over large spatial scales, particularly in the tropical Atlantic west of the coast of Africa (e.g., Fishman, l99l; Fishman and Brackett, l997; Portmann *et al.*, l997; Hudson and Thompson, l998) and in Indonesia (Hauglustaine *et al.*, l999). Export of industrial pollution to the Arctic can lead to increased O_3 over a highly reflective snow or ice surface, and correspondingly large local radiative forcings (Hauglustaine *et al.*, 1998; Mickley *et al.*, 1999).

Chapter 4 and Sections 6.6.2 and 6.6.3 discuss the chemistry responsible for the tropospheric O_3 forcing; here we emphasise that the tropospheric O_3 forcing is driven by and broadly attribut-able to emissions of other gases. The observed regional variability of O_3 trends is related to the transport of key precur-

sors, particularly reactive nitrogen, CO, and NMHCs (see Chapter 4). However, the chemistry of O_3 production can be non-linear, so that increased emissions of, for example, the nitric oxide precursor do not necessarily lead to linear responses in O_3 concentrations over all ranges of likely values (e.g, Kleinman, l994; Klonecki and Levy, l997). Further, the relationship of precursor emissions to O_3 trends may also vary in time. One study suggests that the O_3 production efficiency per mole of nitrogen oxide emitted has decreased globally by a factor of two since pre-industrial times (Wang and Jacob, 1998). Because of these complex and poorly understood interactions, the forcing due to tropospheric O_3 trends cannot be reliably and uniquely attributed in a quantitative fashion to the emissions of specific precursors.

For the purposes of this report, several evaluations of the global radiative forcing due to tropospheric O_3 changes since pre-industrial times have been intercompared. It will be shown that the uncertainties in radiative forcing can be better understood when both the absolute radiative forcing (Wm^{-2}) and normalised forcing (Wm^{-2} per Dobson Unit of tropospheric O_3 change) are considered. The results of this intercomparison and the availability of numerous models using different approaches suggest reduced uncertainties in the radiative forcing estimates compared to those of the SAR. Furthermore, recent work has shown that the dependence of the forcing on the altitude where the O_3 changes occur within the troposphere is less pronounced than previously thought, providing improved scientific understanding. Finally, some estimates of the likely magnitude of future tropospheric O_3 radiative forcing are presented and discussed.

6.5.2 Estimates of Tropospheric Ozone Radiative Forcing since Pre-Industrial Times

6.5.2.1 Ozone radiative forcing: process studies

The dependence of surface temperature response on the height of an imposed constant change in O_3 amount (often 10 Dobson Units, or DU) can be estimated using radiative convective models (e.g., Wang *et al.*, l980; Lacis *et al.*, 1990; Forster and Shine, l997). Figure 6.1a shows the results of such a calculation. This figure suggests that surface temperature is particularly sensitive to O_3 trends near 8 to 15 km, in the vicinity of the tropopause. However, Forster and Shine (l997) made the important point that since there is far less O_3 in the troposphere than near the tropopause and in the stratosphere, the use of a constant pertur-bation is unlikely to provide a realistic measure of the sensitivity profile. For example, 10 DU corresponds to roughly a 400% increase in mid-tropospheric O_3, but much less at higher levels. Figure 6.1b shows how a 10% (rather than 10 DU) local O_3 perturbation affects the calculated surface temperature as a function of the altitude where the O_3 change is imposed (from Forster and Shine, l997). This figure suggests that the sensitivity of surface temperature to the altitude of O_3 perturbations is considerably smaller than suggested by earlier studies that employed constant absolute changes to probe these effects. While the study of Forster and Shine (l997) employed a simple radiative/convective model, Hansen *et al.* (l997a) carried out similar calculations using a GCM. Their study suggests that cloud feedbacks could further lower the altitude at which surface temperature is most sensitive to O_3 perturbations (Hansen *et al.*, l997a; WMO, l999), but this work employed perturbations of 10
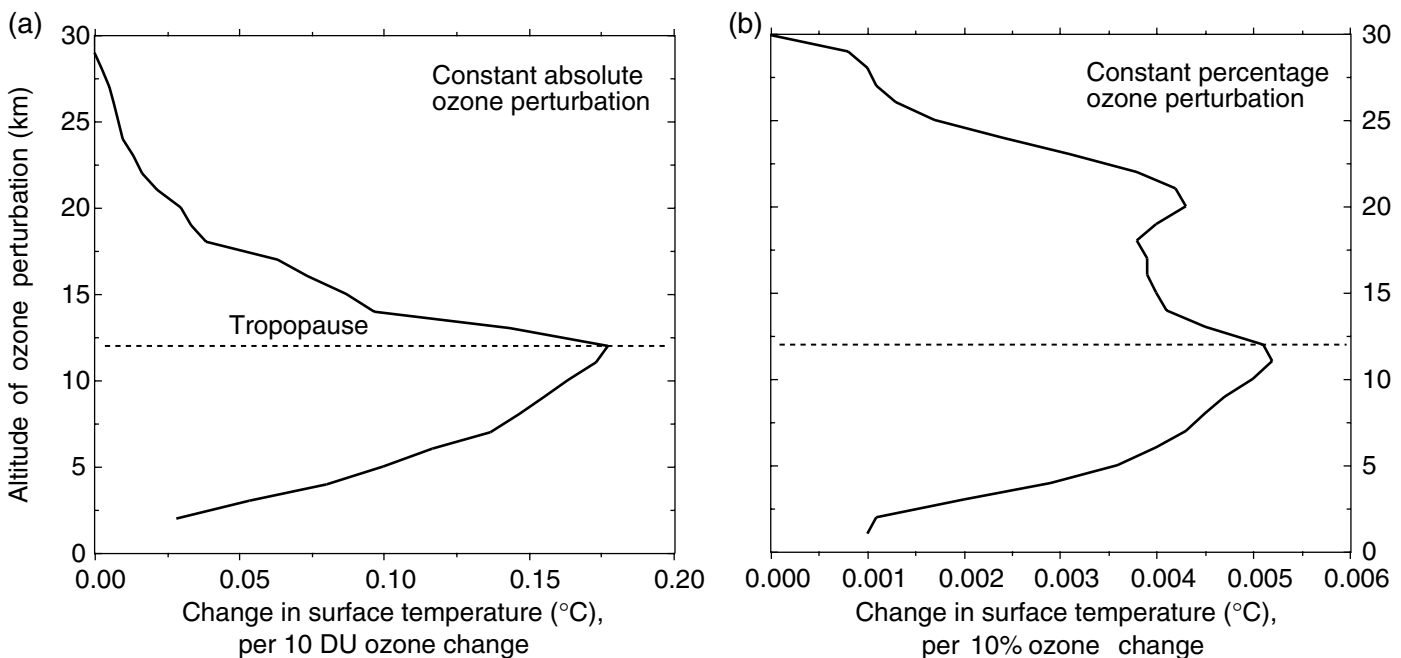

Figure 6.1: Dependence of the surface temperature response on the height and type of O_3 perturbation; (a) shows the sensitivity to a constant absolute change (10 DU), while (b) shows the sensitivity to a constant percentage change (10%). The model tropopause is at 12 km. From Forster and Shine (1997).

DU in each layer (which is necessary to obtain a significant signal in the GCM but is, as noted above, an unrealistically large value for the tropospheric levels in particular).

Portmann *et al.* (1997) and Kiehl *et al.* (1999) combined an O_3 climatology based upon satellite measurements of the tropospheric column content (from Fishman and Brackett, 1997) with a model calculation to derive estimates of the O_3 radiative forcing for the tropics and for the globe, respectively. They showed that the dependence of the normalised O_3 forcing (Wm^{-2} per DU of integrated O_3 column change) upon uncertainties in the vertical distribution of the perturbation was less than previously thought, about 0.03 to 0.06 Wm^{-2} per DU based upon their radiative code and considering a range of profile shapes. This rather limited sensitivity to the altitude distribution of the imposed perturbation is broadly consistent with the work of Forster and Shine (1997) highlighted above and in Figure 6.1.

6.5.2.2 Model estimates

Table 6.3 presents a comparison of estimates of globally averaged O_3 change since pre-industrial times and its corresponding radiative forcing based on published literature and including stratospheric temperature adjustment. Results from several studies are presented, one constrained by the climatology derived from observations discussed in the previous section, and ten from global chemistry/transport models. Results are presented for both clear sky and for total sky conditions, providing an indication of the role of clouds, and long-wave and short-wave contributions are shown separately. In addition, the globally averaged integrated tropospheric O_3 change (DU) is also indicated, to give a sense of the range in published model estimates of this key factor. Finally, the normalised O_3 forcings are also presented (Wm^{-2} per DU).

Table 6.3 summarises the ranges obtained in these model studies. For total sky conditions, the range in globally and annual averaged tropospheric O_3 forcing from all of these models is from 0.28 to 0.43 Wm^{-2}, while the normalised forcing is 0.033 to 0.056 Wm^{-2} per DU. The tropospheric O_3 forcing constrained by the observational climatology is 0.32 Wm^{-2} for globally averaged, total sky conditions. These estimates are comparable in magnitude (and qualitatively similar in pattern, see Section 6.14) but opposite in sign to that believed to be due to the direct effect of sulphate aerosols.

Figure 6.2 presents the latitudinal distributions of absolute and normalised forcings for both January and July, from several chemistry/transport models and from the observationally constrained evaluation. The figure shows that the tropics and northern mid-latitude regions account for the bulk of the global forcing. The contribution from northern mid-latitudes is particularly large in summer, when it can reach as much as 1 Wm^{-2} locally near 40 to 50°N. These latitudinal gradients and seasonal changes in the zonally-averaged forcing are likely to be reflected at least in part in patterns of response (Hansen *et al.*, 1997a) and hence are a needed element in the detection and attribution of climate change.

Figure 6.2 shows that the large seasonal and inter-model ranges in absolute forcings compress somewhat when normalised forcings are considered. At 40°N for example, the absolute forcing differs over all models and seasons by more than a factor of 5 (Figure 6.2a), while the differences in normalised forcings are about a factor of 2.5 (Figure 6.2b). Mickley *et al.* (1999)

Table 6.3: *Tropospheric O_3 change (ΔO_3) in Dobson Units (DU) since pre-industrial times, and the accompanying short-wave (SW), long-wave (LW), and net (SW plus LW) radiative forcings (Wm^{-2}), after accounting for stratospheric temperature adjustment (using the Fixed Dynamical Heating method). Estimates are taken from the published literature. Normalised forcings (norm.) refer to radiative forcing per O_3 change (Wm^{-2} per DU).*

| Reference		Clear sky conditions					Total sky conditions			
	ΔO_3	LW	SW	SW (norm.)	Net	Net (norm.)	LW	SW	Net	Net (norm.)
Berntsen *et al.* (1997) – [Reading model]	7.600	0.260	0.050	0.007	0.310	0.041	0.210	0.070	0.280	0.037
Stevenson *et al.* (1998)	8.700	0.326	0.065	0.007	0.391	0.045	0.201	0.088	0.289	0.033
Berntsen *et al.* (1997) – [Oslo model]	7.600	0.330	0.060	0.008	0.390	0.051	0.230	0.080	0.310	0.041
Haywood *et al.* (1998a)	7.900	0.330	0.050	0.006	0.380	0.048	0.230	0.080	0.310	0.039
Kiehl *et al.* (1999)	8.400	0.316	0.063	0.008	0.379	0.045	0.251	0.069	0.320	0.038
Berntsen *et al.* (2000)	9.600	0.357	0.071	0.007	0.428	0.045	0.246	0.096	0.342	0.036
Brasseur *et al.* (1998)	–	–	–	–	–	–	–	–	0.370	–
van Dorland *et al.* (1997)	8.070	0.390	0.054	0.007	0.443	0.055	0.304	0.076	0.380	0.047
Roelofs *et al.* (1997)	7.200	0.350	0.047	0.007	0.397	0.055	0.287	0.117	0.404	0.056
Lelieveld and Dentener (2000)	–	–	–	–	–	–	–	–	0.420	–
Hauglustaine *et al.* (1998)	8.940	0.448	0.063	0.007	0.511	0.057	0.338	0.088	0.426	0.048
Mean	8.224	0.345	0.058	0.007	0.403	0.049	0.255	0.085	0.343	0.042
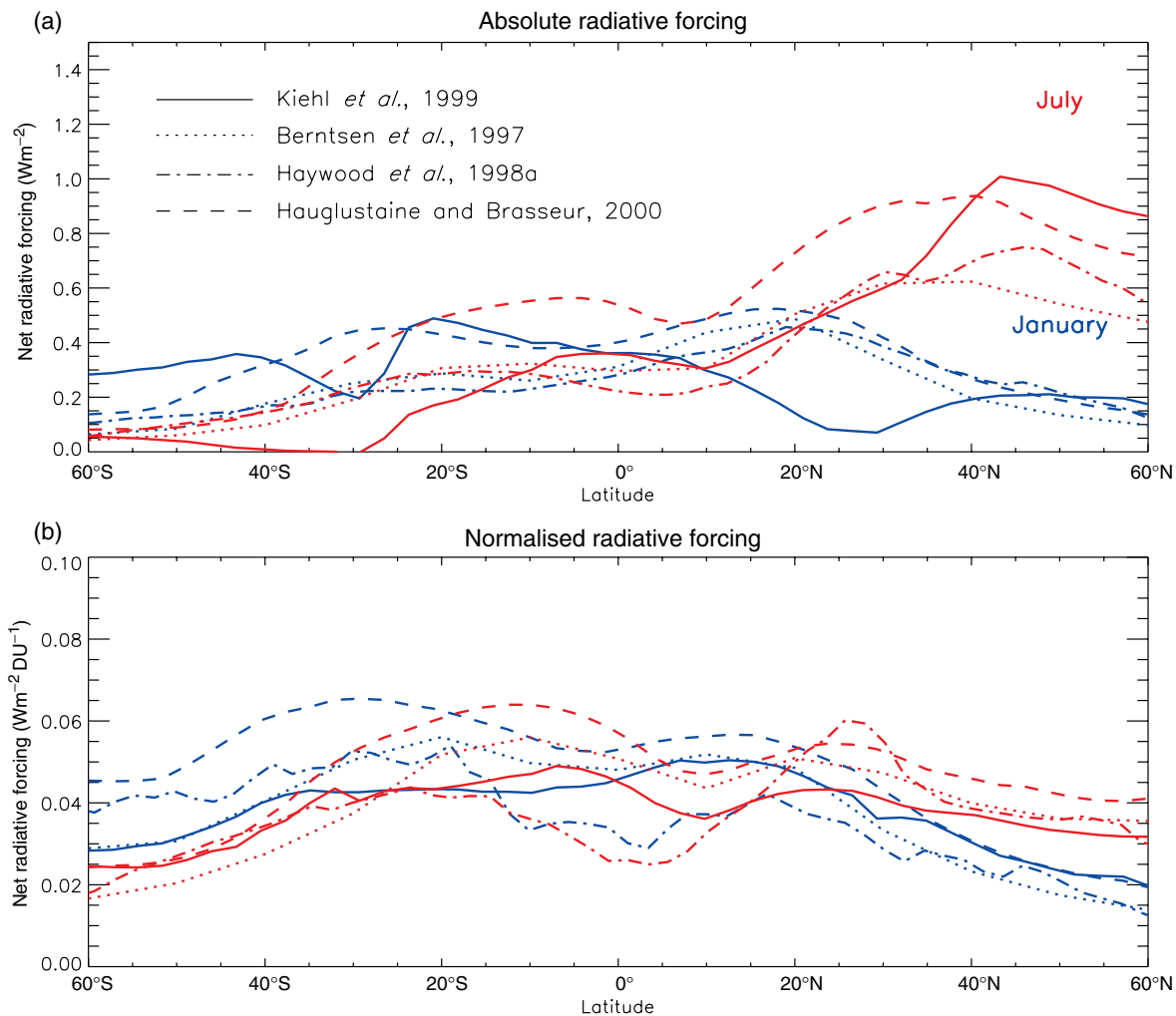
Figure 6.2: Latitudinal distribution of absolute (Wm^{-2}) and normalised (Wm^{-2} DU^{-1}) tropospheric O$_3$ radiative forcing for summer and winter conditions calculated by several models.

demonstrate that the normalised forcing at extra-tropical latitudes is largely determined by the temperature difference between the tropopause and the Earth's surface, while cloud cover plays a dominant role in the tropics. This suggests that the differences in physical climatology between models, and their comparison to the real atmosphere, may be a key factor in improving understanding of the normalised forcing. The difference between the normalised tropical and mid-latitude forcings also emphasises the need to quantify both the O$_3$ produced by biomass burning (and other tropical processes), and that produced by industrial practices, especially in the northern hemisphere. Some of the studies in Figure 6.2 suggest, for example, that a model producing larger O$_3$ changes in the tropics could produce a greater globally averaged tropospheric O$_3$ forcing than one producing larger changes in northern mid-latitudes, even if the globally averaged O$_3$ increases in the two studies were identical. Overall, this Figure suggests that the differences between model estimates of tropospheric O$_3$ forcing since pre-industrial times are likely to be dominated by chemistry (e.g., emission inventories, chemical processes, and transport) rather than by factors relating to radiative transfer.

6.5.3 *Future Tropospheric Ozone Forcing*

As noted in Harris *et al.* (1998) and Oltmans *et al.* (1998), the observed upward trends in surface O$_3$ in Europe and North America appear to be less steep in the past decade or two than in earlier periods (e.g., before about 1980), perhaps because of control measures designed to reduce emissions of O$_3$ precursors and mitigate urban pollution problems. Non-linear chemical feedbacks may also contribute to damping the recent past and future trends (Wang and Jacob, 1998). Theoretical studies using chemistry/transport models have attempted to prescribe likely future emissions of precursors and predict future tropospheric O$_3$ abundances. The largest future increases in O$_3$ forcings may occur in Asia in association with projected population growth and future development (van Dorland *et al.*, 1997; Brasseur *et al.*, 1998). Chalita *et al.* (1996) calculated a globally averaged radiative forcing from pre-industrial times to 2050 of 0.43 Wm^{-2}. The models of van Dorland *et al.* (1997) and Brasseur *et al.* (1998) suggest a higher globally averaged total radiative forcing from pre-industrial times to 2050 of 0.66 Wm^{-2} and 0.63 Wm^{-2}, respectively, while that of Stevenson *et al.* (1998) yields a forcing

of 0.48 Wm^{-2} in 2100. As the analysis presented above shows, these differences are likely to be due to modelled differences in the latitudinal distributions or magnitudes of the projected O_3 change due for example to different emission inventories or model processes such as transport, and much less likely to be due to differences in radiative codes.

6.6 Indirect Forcings due to Chemistry

In addition to the direct forcings caused by injection of radiatively active gases to the atmosphere, some compounds or processes can also modify the radiative balance through indirect effects relating to chemical transformation or change in the distribution of radiatively active species. As previously indicated (IPCC, 1992, 1994; SAR), the tropospheric chemical processes determining the indirect greenhouse effects are highly complex and not fully understood. The uncertainties connected with estimates of the indirect effects are larger than the uncertainties of those connected to estimates of the direct effects. Because of the central role that O_3 and OH play in tropospheric chemistry, the chemistry of CH_4, CO, NMHC, and NO_x is strongly intertwined, making the interpretation of the effects associated with emission changes rather complex. It should be noted that indirect effects involving OH feedback on the lifetime of well-mixed greenhouse gases, and tropospheric O_3 concentration changes since the pre-industrial are implicitly accounted for in Sections 6.3 and 6.5.

6.6.1 Effects of Stratospheric Ozone Changes on Radiatively Active Species

Increased penetration of ultraviolet radiation into the troposphere as a result of stratospheric ozone depletion leads to changes in the photodissociation rates of some key chemical species. One of the primary species affected by possible changes in photodissociation rates is the hydroxyl radical OH, which regulates the tropospheric lifetime of a large number of trace gases such as CH_4, CO, hydrochlorofluorocarbons (HCFCs), hydrofluorocarbons (HFCs), NO_x, and to a lesser extent, sulphur dioxide (SO_2) (see Chapter 4). The impact of stratospheric O_3 changes on the fate of tropospheric species has been discussed by Ma and van Weele (2000), Fuglestvedt *et al.* (1994), Bekki *et al.* (1994); and Fuglestvedt *et al.* (1995); on the basis of two-dimensional model simulations, and by Madronich and Granier (1994), Granier *et al.* (1996), Van Dop and Krol (1996) and Krol *et al.* (1998) using three-dimensional models. These studies and the updated calculations presented by WMO (1999) estimated that a 1% decrease in global total O_3 leads to a global increase in O_3 photolysis rate of 1.4%, resulting in a 0.7 to 0.8% increase in global OH. Changes in photolysis rates from reduced stratospheric O_3 also have the potential to alter tropospheric O_3 production and destruction rates. Based on stratospheric O_3 evolution over the period 1980 to 1996, Myhre *et al.* (2000) have calculated a reduction in tropospheric O_3 associated with increased ultraviolet penetration and a corresponding negative radiative forcing reaching -0.01 Wm^{-2} over that period of time. Another indirect impact of stratospheric O_3 depletion on

climate forcing has been proposed by Toumi *et al.* (1994, 1995). The hydroxyl radical oxidises SO_2 to gaseous sulphuric acid, which is a source of H_2SO_4 particles. Changes in H_2SO_4 formation resulting from OH changes might affect the number of particles which act as condensation nuclei. Rodhe and Crutzen (1995) challenged whether this mechanism was of importance.

6.6.2 Indirect Forcings of Methane, Carbon Monoxide and Non-Methane Hydrocarbons

CH_4 is oxidised primarily (>90%) in the troposphere through reaction with OH. Since the CH_4 oxidation cycle provides a substantial fraction of the OH loss in the troposphere, there is strong interaction between OH and CH_4. This causes the OH to decrease when CH_4 increases, leading to a further increase in CH_4. This chemical feedback is examined in Chapter 4. Lelieveld and Crutzen (1992), Brühl (1993), Lelieveld *et al.* (1993, 1998), Hauglustaine *et al.* (1994) and Fuglestvedt *et al.* (1996) estimated that this feedback added 25 to 35% to the direct CH_4 forcing depending on the initial CH_4 perturbation and the model used. These values are in line with the 30% contribution estimated by IPCC (1992) and the SAR. The tropospheric O_3 increase associated with photochemical production from the CH_4 oxidation cycle also contributes to enhancing the total CH_4 radiative forcing. The forcing from enhanced levels of tropospheric O_3 estimated by Lelieveld and Crutzen (1992), Lelieveld *et al.* (1993, 1998), Hauglustaine *et al.* (1994) and Fuglestvedt *et al.* (1996) contributes a further 30 to 40% on top of the CH_4 forcing, due directly to CH_4 emissions. IPCC (1992) estimated a lower contribution of O_3 of approximately 20%. Lelieveld *et al.* (1998) have estimated a direct radiative forcing associated with CH_4 increase since the pre-industrial era (1850 to 1992) of 0.33 Wm^{-2} and an additional forcing of 0.11 Wm^{-2} associated with OH feedback. The increased tropospheric O_3 contributes an additional 0.11 Wm^{-2} and stratospheric H_2O another 0.02 Wm^{-2}. These authors found that the total CH_4 forcing (0.57 Wm^{-2}) is higher by 73% than the direct forcing. The CH_4 radiative forcing given in Section 6.3 (0.5 Wm^{-2}) and based on recorded CH_4 concentration increase includes both the direct and OH indirect contributions. This updated forcing is higher by 14% than the 0.44 Wm^{-2} obtained by Lelieveld *et al.* (1998) on the basis of calculated present day and pre-industrial CH_4 distributions. In addition to that, oxidation of CH_4 also leads to the formation of CO_2, providing a further indirect effect.

In contrast to CH_4, the direct radiative forcing of CO is relatively small (Evans and Puckrin, 1995; Sinha and Toumi, 1996). Sinha and Toumi (1996) have estimated a clear sky radiative forcing of 0.024 Wm^{-2} for a uniform increase in CO from 25 ppbv to 100 ppbv. However, CO plays a primary role in governing OH abundances in the troposphere. As indicated by Prather (1994, 1996) and Daniel and Solomon (1998), CO emissions into the atmosphere may have a significant impact on climate forcing due to chemical impact on CH_4 lifetime, and tropospheric O_3 and CO_2 photochemical production (see Chapter 4). The contribution of these indirect effects to the GWPs based on box model calculations are presented in Section 6.12.

Similarly, NMHCs have a small direct radiative forcing. Highwood *et al.* (1999) estimated an upper limit of 0.015 Wm^{-2} (1% of the present day forcing due to other greenhouse gases) on the globally averaged direct forcing of sixteen NMHCs. As indicated by Johnson and Derwent (1996), the indirect forcing through changes in OH and tropospheric O$_3$ is also small for each NMHC taken individually but can be significant taken as a family. The indirect forcings of NMHCs are still poorly quantified and require the use of global three-dimensional chemical transport models. Accurate calculations of these effects are a notoriously difficult problem in atmospheric chemistry.

6.6.3 Indirect Forcing by NO$_x$ Emissions

Through production of tropospheric O$_3$, emissions of nitrogen oxides (NO$_x$ = NO + NO$_2$) lead to a positive radiative forcing of climate (warming), but by affecting the concentration of OH they reduce the levels of CH$_4$, providing a negative forcing (cooling) which partly offsets the O$_3$ forcing. Due to non-linearities in O$_3$ photochemical production together with differences in mixing regimes and removal processes, the O$_3$ and OH changes strongly depend on the localisation of the NO$_x$ surface emission perturbation, as calculated by Hauglustaine and Granier (1995), Johnson and Derwent (1996), Berntsen *et al.* (1996), Fuglestvedt *et al.* (1996, 1999) and Gupta *et al.* (1998). The CH$_4$ and O$_3$ forcings are similar in magnitude, but opposite in sign, as calculated by Fuglestvedt *et al.* (1999). Due to differences in CH$_4$ and O$_3$ lifetimes, the NO$_x$ perturbation on the CH$_4$ forcing acts on a global scale over a period of approximately a decade, while the O$_3$ forcing is of regional character and occurs over a period of weeks. Based on three-dimensional model results, Fuglestvedt *et al.* (1999) have calculated that the O$_3$ radiative forcing per change in NO$_x$ emission (10^{-2} Wm^{-2} per TgN/yr) is 0.35 and 0.29 for the USA and Scandinavia, respectively, and reaches 2.4 for Southeast Asia. The CH$_4$ forcing per change in NO$_x$ emission ranges from -0.37 (Scandinavia) and -0.5 (USA) to -2.3 (Southeast Asia) in the same units. Additional work is required to assess the impact of NO$_x$ on the radiative forcing of climate.

Deep convection can remove pollutants from the lower atmosphere and inject them rapidly into the middle and upper troposphere and, occasionally, into the stratosphere. Changes in convective regimes associated with climate changes have therefore the potential to significantly modify the distribution and the photochemistry of O$_3$ in a region where its impact on the radiative forcing is the largest. Based on the tropospheric O$_3$ column derived from satellite during the 1997 to 1998 El Niño, Chandra *et al.* (1998) reported a decrease in O$_3$ column of 4 to 8 Dobson Units (DU) in the eastern Pacific and an increase of 10 to 20 DU in the western Pacific, largely as a result of the eastward shift of the tropical convective activity. Lelieveld and Crutzen (1994) showed that convective transport can change the budget of O$_3$ in the troposphere. Berntsen and Isaksen (1999) have also indicated that changes in convection can modify the sensitivity of the atmosphere to anthropogenic perturbations as aircraft emissions. Their study indicates that reduced convective activity leads to a 40% increase in the O$_3$ response to aircraft NO$_x$ emissions due to modified background atmospheric

concentrations. In addition to that, lightning is a major source of NO$_x$ in the troposphere and thus contributes to the photochemical production of O$_3$ (Huntrieser *et al.*, 1998; Wang *et al.*, 1998; Hauglustaine *et al.*, 2001; Lelieveld and Dentener, 2000). In the tropical mid- and upper troposphere, modelling studies by Lamarque *et al.* (1996), Levy *et al.* (1996), Penner *et al.* (1998a), and Allen *et al.* (2000) have calculated a contribution of lightning to the NO$_x$ levels of 60 to 90% during summer. Direct observations by Solomon *et al.* (1999) of absorption of visible radiation indicate that nitrogen dioxide can lead to local instantaneous radiative forcing exceeding 1 Wm^{-2}. These enhancements of NO$_2$ absorption are likely to be due both to pollution and to production by lightning in convective clouds. Further measurements are required to bracket the direct radiative forcing by NO$_2$ under a variety of storm and pollution conditions. On the basis of two-dimensional model calculations, Toumi *et al.* (1996) calculated that for a 20% increase of lightning the global mean radiative forcing by enhanced tropospheric O$_3$ production is about 0.1 Wm^{-2}. Based on an apparent correlation between lightning strike rates and surface temperatures, Sinha and Toumi (1997) have suggested a positive climate feedback through O$_3$ production from lightning NO$_x$ in a warmer climate. Improved modelling and observations are required to confirm this hypothesis.

Aircraft emissions also have the potential to alter the composition of the atmosphere and induce a radiative forcing of climate. According to IPCC (1999), in 1992 the NO$_x$ emissions from subsonic aircraft are estimated to have increased O$_3$ concentrations at cruise altitudes in the Northern Hemisphere mid-latitude summer by about 6% compared with an atmosphere without aircraft. The associated global mean radiative forcing is 0.023 Wm^{-2}. In addition to increasing tropospheric O$_3$, aircraft NO$_x$ are expected to decrease the concentration of CH$_4$ inducing a negative radiative forcing of -0.014 Wm^{-2} for the 1992 aircraft fleet. Again, due to different O$_3$ and CH$_4$ lifetimes, the two forcings show very different spatial distribution and seasonal evolution (IPCC, 1999). The O$_3$ forcing shows a marked maximum at northern mid-latitudes, reaching 0.06 Wm^{-2}, whilst the CH$_4$ forcing exhibits a more uniform distribution, with a maximum of about -0.02 Wm^{-2} in the tropical regions. Based on IPCC (1999), the O$_3$ forcing calculated for 2050 conditions is 0.060 Wm^{-2} and the CH$_4$ forcing is -0.045 Wm^{-2}.

6.6.4 Stratospheric Water Vapour

The oxidation of CH$_4$ produces water vapour that can contribute significantly to the levels of H$_2$O in the stratosphere. Water vapour is also directly emitted by aircraft in the lower stratosphere. Lelieveld and Crutzen (1992), Lelieveld *et al.* (1993, 1998), Hauglustaine *et al.* (1994) and Fuglestvedt *et al.* (1996) have estimated a contribution of stratospheric water vapour of 2 to 5% of the total CH$_4$ forcing. Oltmans and Hofmann (1995) have reported an increase in lower stratospheric H$_2$O (18 to 20 km) measured at Boulder of 0.8% per year for the period 1981 to 1994. Measurements of stratospheric H$_2$O from the HALOE instrument on board the UARS satellite also show an increase in stratospheric H$_2$O between 30 and 60 km of 40 to 100 ppbv/year

for the period 1992 to 1997 (Evans *et al.*, 1998; Nedoluha *et al.*, 1998). A similar trend has also been reported by Randel *et al.* (1999) based on HALOE data for the period 1993 to 1997. In this study, a time variation and a flattening of the trend has been determined after 1996. This stratospheric H_2O increase is well above that expected from the rising CH_4 levels in the atmosphere. Based on these observed stratospheric H_2O trends, Forster and Shine (1999) have estimated a radiative forcing of 0.2 Wm^{-2} since 1980. Note that, just as for stratospheric O_3, there exists considerable uncertainty concerning the trend near the tropopause region globally. It should also be noted that if the changes in water vapour were a result of CH_4 oxidation, the changes in H_2O would be a forcing. However, if they result from changes in tropical tropopause temperature change or in dynamics, then they should be viewed as a feedback (as defined in Section 6.2). Additional measurements and analyses are clearly needed to explain the observed trends.

6.7 The Direct Radiative Forcing of Tropospheric Aerosols

Anthropogenic aerosols scatter and absorb short-wave and long-wave radiation, thereby perturbing the energy budget of the Earth/atmosphere system and exerting a direct radiative forcing. This section concentrates on estimates of the global mean direct effect of anthropogenic tropospheric aerosols and is necessarily dependent upon global models. Field campaigns which provide essential input parameters for the models, and satellite observational studies of the direct effect of tropospheric aerosols, which provide useful validation data for the models, are considered in detail in Chapter 5.

6.7.1 Summary of the IPCC WGI Second Assessment Report and Areas of Development

The SAR considered three anthropogenic aerosol species; sulphate, biomass burning aerosols, and fossil fuel black carbon (or soot). The SAR suggested a radiative forcing of −0.4 Wm^{-2} with a factor of two uncertainty for sulphate aerosols, −0.2 Wm^{-2} with a factor of three uncertainty for biomass burning, and +0.1 Wm^{-2} with a factor of three uncertainty for fossil fuel black carbon aerosols. The level of scientific understanding (referred to as a confidence level in the SAR, see Section 6.13) was classified as "low" for sulphate aerosol and "very low" for both fossil fuel black carbon and biomass burning aerosols. Since the SAR, there have been advances in both modelling and observational studies of the direct effect of tropospheric aerosols (see reviews by Shine and Forster (1999) and Haywood and Boucher (2000)). Global chemical transport modelling studies encompass a greater number of aerosol species and continue to improve the representation of the physical and chemical processes (see Chapters 4 and 5). Global models are more numerous and include more accurate radiative transfer codes, more sophisticated treatments of the effects of relative humidity for hygroscopic aerosols, better treatment of clouds, and better spatial and temporal resolution than some earlier studies. The present day direct radiative forcing due to aircraft emissions of sulphate and black carbon aerosol have been calculated to be insignificant (IPCC,

1999) and are not considered further. Spatial patterns of the calculated radiative forcings are not discussed in detail here but are presented in Section 6.14.

6.7.2 Sulphate Aerosol

Early one-dimensional box-model estimates of the radiative forcing (e.g., Charlson *et al.*, 1992) using simplified expressions for radiative forcing have been superseded by global calculations using prescribed aerosol concentrations from chemical transport models (CTMs). These studies use either three-dimensional observed fields of for example, clouds, relative humidity and surface reflectance (e.g., Kiehl and Briegleb, 1993; Myhre *et al.*, 1998c), or GCM generated fields (e.g., Boucher and Anderson, 1995; Haywood *et al.*, 1997a) together with the prescribed aerosol distributions from CTMs and detailed radiative transfer codes in calculating the radiative forcing. A growing number of studies perform both the chemical production, transformation, and transportation of aerosols and the radiative forcing calculations (see Chapter 5) with the advantage of correlating predicted aerosol distributions precisely with fields determining aerosol production and deposition such as clouds (e.g., Penner *et al.*, 1998b). Table 6.4 summarises estimates of the radiative forcing from global modelling studies.

The calculated global mean radiative forcing ranges from −0.26 to −0.82 Wm^{-2}, although most lie in the range −0.26 to −0.4 Wm^{-2}. The spatial distribution of the forcings is similar in the studies showing strongest radiative forcings over industrial regions of the Northern Hemisphere although the ratio of the annual mean Northern Hemisphere/Southern Hemisphere radiative forcing varies from 2.0 (Graf *et al.*, 1997) to 6.9 (Myhre *et al.*, 1998c) (see Section 6.14.2 for further details). The ratio of the annual mean radiative forcing over land to that over ocean also varies considerably, ranging from 1.3 (Kiehl *et al.*, 2000) to 3.4 (Boucher and Anderson, 1995). The direct radiative forcing (DRF) is strongest in the Northern Hemisphere summer when the insolation is the highest although different seasonal cycles of the sulphate burden from the chemical transport models result in maximum global mean radiative forcings ranging from May to August (e.g., Haywood and Ramaswamy, 1998), the ratio of the June-July-August/December-January-February radiative forcing being estimated to lie in the range less than 2 (e.g., van Dorland *et al.*, 1997) to > 5 (e.g., Penner *et al.*, 1998b; Grant *et al.*, 1999) with a mean of approximately 3.3. The range of uncertainty in the radiative forcings can be isolated from the uncertainties in the simulated sulphate loadings by considering the range in the normalised radiative forcing i.e., the radiative forcing per unit mass of sulphate aerosol (e.g., Nemesure *et al.*, 1995; Pilinis *et al.*, 1995). Table 6.4 shows that this is substantial, indicating that differences in the radiative forcing are not due solely to different mass loading.

The optical parameters for sulphate aerosol in each of the global studies vary. Although the single scattering albedo of pure sulphate and sulphate mixed with water is close to unity throughout most of the solar spectrum, some of the studies (e.g., Feichter *et al.*, 1997; van Dorland *et al.*, 1997; Hansen *et al.*,

Table 6.4: *The global and annual mean direct radiative forcing (DRF) for the period from pre-industrial (1750) to present day (2000) due to sulphate aerosols from different global studies. The anthropogenic column burden of sulphate and the source of the sulphate data are also shown together with the normalised radiative forcing. "Frac" indicates a cloud scheme with fractional grid box cloud amount, and "On/off" indicates that a grid box becomes overcast once a certain relative humidity threshold is reached. An asterisk indicates that the maximum hygroscopic growth of the aerosols was restricted to a relative humidity of 90%. The ratio of the Northern to the Southern Hemisphere (NH/SH) DRF and the ratio of the mean radiative forcing over land to the mean radiative forcing over oceans is also shown. NA indicates data is not available. "Langner and Rodhe (1991)s" indicates that the slow oxidation case was used in the calculations.*

Study	DRF (Wm^{-2})	Column burden (mgm^{-2})	Normalised DRF (Wg^{-1})	Cloud scheme	DRF NH/SH	DRF land/ ocean	Source of sulphate data
Ghan *et al.* (2001a)	−0.44	4.0	−110	On/off	5.2	1.9	Ghan *et al.* (2001a)
Jacobson (2001)	−0.32	2.55	−125	Frac	2.7	1.2	Jacobson (2001)
Boucher and Anderson (1995)	−0.29	2.32	−125	Frac	4.3	3.4	Langner and Rodhe (1991)
Graf *et al.* (1997)	−0.26	1.70	−153	Frac	2.0	NA	Graf *et al.* (1997)
Feichter *et al.* (1997)	−0.35	2.23	−157	Frac	4.2	1.4	Feichter *et al.* (1997)
Kiehl and Briegleb (1993)	−0.28	1.76	−159	Frac	3.3	NA	Langner and Rodhe (1991)s
Iversen *et al.* (2000)	−0.41	2.40	−167	Frac	4.1	NA	Iversen *et al.* (2000)
Myhre *et al.* (1998c)	−0.32	1.90	−169	Frac	6.9	NA	Restad *et al.* (1998)
van Dorland *et al.* (1997)	−0.36	2.11	−171	Frac	5.0	NA	van Dorland *et al.* (1997)
Koch *et al.* (1999)	−0.68	3.3	−200	Frac	NA	NA	Koch *et al.* (1999)
Kiehl and Rodhe (1995)	−0.66	3.23	−204	Frac	NA	NA	Pham *et al.* (1995)
	−0.29	1.76	−165	Frac	NA	NA	Langner and Rodhe (1991)s
Chuang *et al.* (1997)	−0.43	2.10	−205	On/off*	4.7	2.4	Chuang *et al.* (1997)
Haywood *et al.* (1997a)	−0.38	1.76	−215	Frac	4.0	NA	Langner and Rodhe (1991)s
Hansen *et al.* (1998)	−0.28	1.14	−246	Frac	NA	NA	Chin and Jacob (1996)
Kiehl *et al.* (2000)	−0.56	2.23	−251	Frac	2.7	1.3	Kiehl *et al.* (2000)
Haywood and Ramaswamy (1998)	−0.63	1.76	−358	On/off	3.6	2.6	Langner and Rodhe (1991)s
	−0.82	1.76	−460	On/off	5.8	2.7	Kasibhatla *et al.* (1997)
Penner *et al.* (1998b) and Grant *et al.* (1999)	−0.81	1.82	−445	On/off	4.5	2.3	Penner *et al.* (1998b)

1998) include some absorption. Charlson *et al.* (1999) show considerable variation in the specific extinction coefficient used in different studies, particularly when accounting for relative humidity effects. The treatment of the effects of relative humidity and clouds appear to be particularly important in determining the radiative forcing. The studies of Haywood and Ramaswamy (1998), Penner *et al.* (1998b) and Grant *et al.* (1999) produce normalised radiative forcings a factor of two to three higher than the other studies. Both Haywood and Ramaswamy (1998) and Penner *et al.* (1998b) acknowledge that their use of on/off cloud schemes where cloud fills an entire grid box once a threshold relative humidity is exceeded may lead to strong radiative

forcings due to strong non-linear relative humidity effects. Chuang *et al.* (1997) use an on/off cloud scheme and report a radiative forcing lower than these two studies, but the hygroscopic growth is rather suppressed above a relative humidity of 90%. The use of monthly mean relative humidity fields in some of the calculations leads to lower radiative forcings as temporal variations in relative humidity and associated non-linear effects are not accounted for (e.g., Kiehl and Briegleb, 1993; Myhre *et al.*, 1998c). Kiehl *et al.* (2000) improve the treatment of relative humidity compared to Kiehl and Briegleb (1993) and Kiehl and Rodhe (1995) by improving the relative humidity dependence of the aerosol optical properties and by
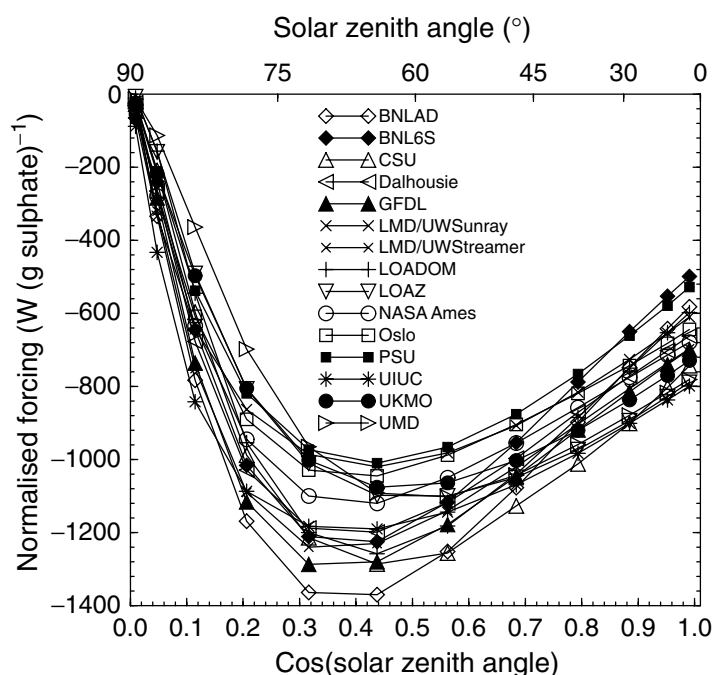
Figure 6.3: The normalised radiative forcing for sulphate aerosol from the intercomparison study of Boucher *et al.* (1998). A log-normal distribution with a geometric mean diameter of 0.170 μm and a geometric standard deviation of 1.105 together with an aerosol optical depth of 0.20 at 0.55 μm and a Lambertian surface reflectance of 0.15 was assumed. For details of the acronyms and the radiation codes used in the calculations see Boucher *et al.* (1998).

using interactive GCM relative humidities rather than monthly mean ECMWF analyses, resulting in a larger normalised radiative forcing. Ghan *et al.* (2001a) perform a sensitivity study and find that application of GCM relative humidities changes the direct radiative forcing by −0.2 Wm⁻² compared to the use of ECMWF analyses because the frequency of occurrence of relative humidities over 90% is higher when using GCM relative humidities. Haywood and Ramaswamy's (1998) GCM study indicates a stronger radiative forcing when sulphate resides near the surface because the relative humidity and subsequent hygroscopic growth of sulphate particles is higher. GCM sensitivity studies (Boucher and Anderson, 1995) and column calculations (Nemesure *et al.*, 1995) show that the radiative forcing is a strong function of relative humidity but relatively insensitive to chemical composition. Ghan *et al.* (2001a) suggest a number of reasons for the relatively low DRF from their study, including the relatively large fraction of anthropogenic sulphate in winter when the insolation is lowest, and the fact that sulphate aerosols are smaller in this study and therefore have smaller scattering efficiencies (see also Boucher and Anderson, 1995). The contribution to the global forcing from cloudy regions is predicted to be 4% (Haywood *et al.*, 1997a), 11% (Haywood and Ramaswamy, 1998), 22% (Boucher and Anderson, 1995) and 27% (Myhre *et al.*, 1998c) and hence remains uncertain. However, it should be noted that all of these studies suggest the majority of the global annual mean direct radiative forcing due to

sulphate occurs in cloud-free regions. The global mean long-wave radiative forcing has been estimated to be less than 0.01 Wm⁻² and is insignificant (Haywood *et al.*, 1997a).

Boucher and Anderson (1995) investigate the effects of different size distributions, finding a 20 to 30% variation in the radiative forcing for reasonable size distributions. Nemesure *et al.* (1995) and Boucher *et al.* (1998) find a much larger sensitivity to the assumed size distribution as sulphate is modelled by much narrower size distributions. Column radiative forcing calculations by fifteen radiative transfer codes of varying complexity (Boucher *et al.*, 1998) show that, for well constrained input data, differences in the computed radiative forcing when clouds are excluded are relatively modest at approximately 20% (see Figure 6.3). This indicates that uncertainties in the input parameters and in the implementation of the radiative transfer codes and the inclusion of clouds lead to the large spread in estimates as suggested by Penner *et al.* (1994).

Additional column calculations show a weakened radiative forcing when the cloud optical depth is much greater than the aerosol optical depth (Haywood and Shine, 1997; Liao and Seinfeld, 1998) and show that the forcing is insensitive to the relative vertical position of the cloud and aerosol. Haywood *et al.* (1997b, 1998b) and Ghan and Easter (1998) used a cloud resolving model to investigate effects of sub-grid scale variations in relative humidity and cloud. For their case study, the optical depth and radiative forcing in a GCM sized grid box were underestimated by 60%. Effects of sub-grid scale variations in relative humidity and cloud on a global scale have not been rigorously investigated.

Until differences in estimates of radiative forcing due to sulphate aerosol can be reconciled, a radiative forcing of −0.4 Wm⁻² with a range of −0.2 to −0.8 Wm⁻² is retained. This estimate is based on the range of radiative forcings provided by the model estimates shown in Table 6.4. It is not possible to perform standard statistical procedures because of the limited number of studies and the fact that the resulting DRFs are not normally distributed. However, these results are broadly consistent with the estimates of the uncertainties derived in Chapter 5 (see Sections 5.4.2, and Sections 6.7.8).

6.7.3 Fossil Fuel Black Carbon Aerosol

Since the SAR there have been a number of more refined three-dimensional global model estimates of the radiative forcing due to black carbon (BC) aerosol from fossil fuel burning which have superseded calculations using a simple expression for the radiative forcing where the contribution from cloudy regions was not included (e.g., Chylek and Wong, 1995; Haywood and Shine, 1995). These estimates now include the contribution to the total radiative forcing from areas where BC exists either above or within clouds, although the treatment of BC within clouds remains crude. Table 6.5 includes recent global annual mean estimates of the radiative forcing due to BC aerosol from fossil fuels. Haywood *et al*. (1997a) and Myhre *et al*. (1998c) assumed that fossil fuel BC was directly proportional to the mass of sulphate from Langner and Rodhe (1991) and Restad *et al.* (1998), respectively, by applying a 7.5% mass scaling (equivalent

to a global mean burden of approximately 0.13 mgm^{-2} to 0.14 mgm^{-2}). Global annual mean radiative forcings of +0.20 Wm^{-2} and +0.16 Wm^{-2} are calculated for external mixtures. Both studies suggest that BC internally mixed with sulphate will exert a stronger forcing although the method of mixing was fairly crude in both of these studies. These estimates of the radiative forcing were performed before global modelling studies for BC were generally available.

Penner *et al*. (1998b) and Grant *et al*. (1999) used a chemical transport model in conjunction with a GCM to estimate a global column burden of BC from fossil fuel emissions of 0.16 mgm^{-2} and a radiative forcing of +0.20 Wm^{-2} for an external mixture. Cooke *et al*. (1999) estimated the global burden of optically active BC aerosol from fossil fuel burning from a 1° by 1° inventory of emissions to be 0.14 mgm^{-2} (note the good agreement with the assumed column burdens of Haywood *et al*. (1997a) and Myhre *et al*. (1998c)) and a subsequent radiative forcing of +0.17 Wm^{-2}. Haywood and Ramaswamy (1998) estimated the BC radiative forcing due to fossil fuel and biomass burning to be approximately +0.4 Wm^{-2} (see also Section 6.7.5), approximately half of which (+0.2 Wm^{-2}) is due to fossil fuel sources. Jacobson (2000, 2001) modelled BC from both fossil fuels and biomass burning sources and investigated the effects of different mixing schemes, finding a direct radiative forcing of +0.54 Wm^{-2} and a normalised direct radiative forcing of 1,200 Wg^{-1} when BC was modelled as an absorbing spherical core. These studies suggest that the global mean radiative forcing due to fossil fuel BC is strongest in June/July/August owing to the larger insolation coupled with higher atmospheric concentrations in the Northern Hemisphere. From these studies the normalised radiative forcing for an external mixture of BC aerosol appears better defined than for sulphate aerosol ranging from +1,123 Wg^{-1} to +1,525 Wg^{-1}. However, all these studies used the same size distribution and exclude effects of relative humidity, thus the modelled specific extinction is independent of the relative humidity at approximately 10 m^{2}g^{-1} at 0.55 μm. Observational studies show a wide range of specific extinction coefficients, α_{sp}, (see Section 5.1.2 and Table 5.1) of approximately 5 to 20 m^{2}g^{-1} at 0.55 μm, thus the uncertainty in the associated radiative forcing is likely to be higher than the global model results suggest. Additionally, if BC were modelled as an internal mixture, Haywood *et al*. (1997a) and Myhre *et al*. (1998c) suggest the degree of absorption may be considerably enhanced, the radiative forcing being estimated as +0.36 Wm^{-2} and +0.44 Wm^{-2}, respectively. Both of these studies use relatively simple effective medium mixing rules for determining the composite refractive index of internally mixed BC with sulphate and water which may overestimate the degree of absorption (e.g., Jacobson, 2000). Detailed scattering studies including a randomly positioned black carbon sphere in a scattering droplet show that the absorption is relatively well represented by effective medium approximations (Chylek *et al*., 1996b). Column studies by Haywood and Shine (1997) and Liao and Seinfeld (1998) and the global studies by Haywood and Ramaswamy (1998) and Penner *et al*. (1998b) suggest that the radiative forcing due to BC will be enhanced if BC exists within or above the cloud, but reduced if the BC is below the cloud; thus the vertical profile of BC aerosol must be determined from observations and modelled accurately.

On the basis of the calculations summarised above, the estimate of the global mean radiative forcing for BC aerosols from fossil fuels is revised to +0.2 Wm^{-2} (from +0.1 Wm^{-2}) with a range +0.1 to +0.4 Wm^{-2}. The significant contribution to the global annual mean radiative forcing from cloudy regions is the main reason for the increase in the radiative forcing since the SAR. Uncertainties in determining the radiative forcing lie in modelling the mixing of BC with hygroscopic aerosols and the subsequent wet deposition processes which consequently influence the modelled atmospheric lifetime and burden of BC aerosol. Additionally, mixing of BC with other aerosol types and cloud droplets influences the optical parameters.

6.7.4 Fossil Fuel Organic Carbon Aerosol

Anthropogenic organic aerosols are a by-product of fossil fuel and biomass combustion and they consist of many complex chemical compounds and are released either as primary aerosol particles or as volatile organic gases (see Chapter 5). Studies that investigate the radiative forcing due to organic carbon (OC) from fossil fuels are included in Table 6.5. Penner *et al*. (1998b) and Grant *et al*. (1999) found a DRF of +0.16 Wm^{-2} when modelling the direct radiative forcing due to an internal mixture of fossil fuel BC and OC, and +0.2 Wm^{-2} when modelling the radiative forcing due to externally mixed fossil fuel BC. From these results, an annual global mean radiative forcing of −0.04 Wm^{-2} for fossil fuel OC from a global mean burden of approximately 0.7 mgm^{-2} may be derived. However, if OC were modelled as an external mixture with BC and/or if the effects of relative humidity are included, the radiative forcing due to OC from fossil fuels is likely to be more negative, thus this represents an approximate weakest limit. An alternative method for calculating the DRF due to fossil fuel OC from the results of Penner *et al*. (1998b) is to note that the absorption is approximately doubled when BC is modelled as an internal mixture rather than an external mixture (e.g., Haywood *et al*., 1997a). Thus, for an external mixture of fossil fuel OC a radiative forcing of −0.24 Wm^{-2} may be more appropriate. Cooke *et al*. (1999) performed GCM calculations for externally mixed fossil fuel OC, finding a radiative forcing of −0.02 Wm^{-2} from a global mean burden of 0.34 mgm^{-2}. Myhre *et al*. (2001) scale the atmospheric concentrations of fossil fuel OC to modelled sulphate aerosol concentrations and include the effects of relative humidity to estimate a radiative forcing of −0.09 Wm^{-2} from a global mean burden of 0.66 mgm^{-2}. Thus, modelling estimates suggest that the normalised radiative forcing for OC is in the range −60 to −340 Wg^{-1}, which is smaller in magnitude than that due to BC due to the larger specific extinction coefficient for BC and the fact that BC may exert a significant radiative forcing in cloudy regions. Cooke *et al*. (1999) assume that OC is partially absorbing with a modelled single scattering albedo of approximately 0.97 at a wavelength of 0.55 μm. Hansen *et al*. (1998) use a three-dimensional GCM and the OC distribution from Liousse *et al*. (1996) and estimate the radiative forcing due to combined fossil fuel and biomass sources to be −0.41 Wm^{-2}. The approximate fraction of the atmospheric burden of the fossil fuel component may be estimated from the emission inventory of Liousse *et al*. (1996)

Table 6.5: *The global and annual mean direct radiative forcing for the period from pre-industrial (1750) to present day (2000) due to black carbon (BC) and organic carbon (OC) aerosols from different global studies. The anthropogenic column burden of BC and OC is shown, where appropriate, together with the normalised direct radiative forcing (DRF).*

Aerosol	Author and type of study	Mixing or optical parameters	DRF (Wm^{-2})	Column burden (mgm^{-2})	Normalised DRF (Wg^{-1})	Remarks
Fossil fuel BC	Haywood *et al.* (1997a)	External	+0.20	0.13	1525	GCM study. 7.5% mass scaling of BC to SO$_4$ assumed. SO$_4$ from Langner and Rodhe (1991) (slow oxidation case).
		Internal with sulphate	+0.36		2770	Internal mixing approximated by volume weighting the refractive indices of BC and SO$_4$
	Myhre *et al.* (1998c)	External	+0.16	0.14	1123	Three-dimensional study using global climatologies for cloud, surface reflectance etc. 7.5% mass scaling of BC to SO$_4$ assumed. SO$_4$ from Restad *et al.* (1998).
		Internal with sulphate	+0.42		3000	Internal mixing approximated by volume weighting the refractive indices of BC and SO$_4$
	Penner *et al.* (1998b) and Grant *et al.* (1999)	Internal with fossil fuel OC	+0.20	0.16	1287	BC modelled using chemical transport model and GCM.
	Cooke *et al.* (1999)	External	+0.17	0.14	1210	BC modelled using chemical transport model and GCM.
	Haywood and Ramaswamy (1998)	External mixture	+0.2	0.13	1500	Three-dimensional GCM study using Cooke and Wilson (1996) BC data scaled to Liousse *et al.* (1996) total BC mass. 50% of the BC mass assumed to be from fossil fuels.
Fossil fuel OC	Penner *et al.* (1998b)	Internal/external with fossil fuel BC	−0.04 to −0.24	−0.7	−60 to −340	OC modelled using chemical transport model and GCM. Weakest estimate corresponds to internal mixing with BC, strongest estimate corresponds to external mixing with BC.
	Cooke *et al.* (1999)	External mixture	−0.02	0.34	−70	OC modelled using chemical transport model and GCM. May be more negative due to effects of RH and assumption of partial absorption of OC.
	Myhre *et al.* (2001)	External mixture	−0.09	0.66	−135	Three-dimensional study using global climatologies for cloud, surface reflectance etc. OC scaled linearly to SO$_4$. SO$_4$ from Restad *et al.* (1998).
Biomass burning (BC+OC)	Hobbs *et al.* (1997)	Optical parameters of biomass smoke	−0.3	3.7	−80	Uses simplified expression from Chylek and Wong (1995). Neglects radiative forcing from cloudy areas. Other parameters including estimated column burden from Penner *et al.* (1992).
	Iacobellis *et al.* (1999)	Optical parameters of biomass smoke	−0.74	3.5	−210	Three-dimensional chemical transport model and GCM. Simplified expressions also examined.
	Penner *et al.* (1998b) and Grant *et al.* (1999)	Internal/external mixture of OC and BC	−0.14 to −0.23	1.76	−80 to −120	Three-dimensional chemical transport model and GCM using biomass optical parameters modelled from two observational studies.
Fossil fuel and biomass burning BC	Haywood and Ramaswamy (1998)	External mixture	+0.4	0.27	1500	Three-dimensional GCM study using Cooke and Wilson (1996) BC data scaled to Liousse *et al.* (1996) total BC mass.
	Hansen *et al.* (1998)	Observed single scattering albedo	+0.27	NA	NA	Adjustment of modelled single scattering albedo from 1.0 to 0.92-0.95 to account for the absorption properties of BC.
	Jacobson (2001)	Internal with BC core.	+0.54	0.45	1200	GCM study using data from Cooke and Wilson (1996) scaled by a factor of 0.85.
Fossil fuel and biomass burning OC	Hansen *et al.* (1998)	External mixture	−0.41	NA	NA	Three-dimensional GCM study using Liousse *et al.* (1996) OC data. OC modelled as scattering.
	Jacobson (2001)	Internal with BC core.	−0.04 to −0.06	1.8	−17	OC treated as shell with BC core. Strongest forcing for non-absorbing OC.

who estimate that fossil fuels contribute 38% to the total OC emissions. Thus the radiative forcing due to fossil fuel OC may be inferred to be approximately -0.16 Wm^{-2}. This may constitute an approximate upper estimate as the majority of fossil fuel OC occurs over mid-latitude land areas where the surface reflectance is generally higher and insolation is lower than in the equatorial regions where biomass burning is the major source of OC. From these calculations, the radiative forcing due to fossil fuel OC is estimated to be -0.10 Wm^{-2}. The uncertainty associated with this estimate is necessarily high due to the limited number of detailed studies and is estimated to be at least a factor of three.

6.7.5 Biomass Burning Aerosol

Biomass burning aerosol consists of two major chemical components: black carbon (BC), which primarily absorbs solar radiation, and organic carbon (OC), which primarily scatters solar radiation. Sources of biomass burning aerosol include burning of forests and savanna for colonisation and agriculture, burning of agricultural waste, and substances burned for fuel such as wood, dung and peat. Not all biomass aerosol comes from anthropogenic activities, as naturally occurring vegetation fires regularly occur. The fraction of anthropogenic biomass aerosol remains difficult to deduce. As for sulphate and fossil fuel BC aerosol, three-dimensional GCM estimates (e.g., Penner *et al*., 1998b) have superseded earlier simple box-model calculations (e.g., Penner *et al*., 1992) (see Table 6.5). Penner *et al*. (1998b) and Grant *et al*. (1999) used a GCM to model the radiative forcing from biomass aerosol, finding a combined total radiative forcing of -0.14 to -0.23 Wm^{-2} depending upon the mixing assumptions and size distributions used. The radiative forcing is calculated to be negative over the majority of the globe, but some limited areas of positive forcing exist over areas with a high surface reflectance (see Section 6.14.2). The seasonal cycle is strongly influenced by the seasonal cycle of biomass burning emissions (Grant *et al*., 1999; Iacobellis *et al*., 1999), the global mean being estimated to be a maximum during June/July/August. Hobbs *et al*. (1997) performed aircraft measurements of smoke from biomass burning during the Smoke Cloud and Radiation-Brazil (SCAR-B) experiment and used the model of Penner *et al*. (1992) to estimate a global mean radiative forcing of -0.3 Wm^{-2} as an approximate upper limit due to modified optical parameters. Ross *et al*. (1998) performed a similar measurement and modelling study estimating a local annual mean radiative forcing of -2 to -3 Wm^{-2} in intensive biomass burning regions, indicating that the global mean radiative forcing is likely to be significantly smaller than in Penner *et al*. (1992). Iacobellis *et al*. (1999) model the global radiative forcing as -0.7 Wm^{-2} but use an emission factor for biomass aerosols that Liousse *et al*. (1996) suggest is a factor of three too high, thus a radiative forcing of -0.25 Wm^{-2} is more likely. These estimates neglect any long-wave radiative forcing although Christopher *et al*. (1996) found a discernible signal in AVHRR data from Brazilian forest fires that opposes the short-wave radiative forcing; the magnitude of the long-wave signal will depend upon the size, optical parameters, and altitude of the aerosol.

The radiative effects of the individual BC and OC components from biomass burning have also received attention. Haywood and Ramaswamy (1998) re-scaled the global column burden of BC from Cooke and Wilson (1996) to that of Liousse *et al*. (1996) which is thought to be more representative of optically active BC and estimated the radiative forcing due to fossil fuel and biomass burning to be approximately $+0.4$ Wm^{-2}, approximately half of which, or $+0.2$ Wm^{-2}, is due to biomass sources. Hansen *et al*. (1998) adjusted the single scattering albedo of background aerosols from unity to 0.92 to 0.95 to account for the absorbing properties of BC from combined fossil fuel and biomass emissions and found a radiative forcing of $+0.27$ Wm^{-2}.

The radiative forcing due to the purely scattering OC component from combined fossil fuel and biomass emissions is estimated by Hansen *et al*. (1998) to be -0.41 Wm^{-2} with a approximate upper limit for the radiative forcing due to fossil fuel OC from this study of approximately -0.16 Wm^{-2} (see Section 6.7.4). Thus an approximate weakest limit for the radiative forcing due to biomass burning OC is -0.25 Wm^{-2}. Jacobson (2001) used a multi-component aerosol model to investigate the radiative forcing due to OC from combined fossil fuel and biomass aerosols using emissions from Liousse *et al*. (1996) finding a resultant radiative forcing of between -0.04 and -0.06 Wm^{-2}, the strongest forcing being for purely scattering aerosol. The small radiative forcings of Jacobson (2001) may be due to the aerosol being modelled as tri-modal with less aerosol in the optically active region of the spectrum, or due to the fact that absorption by BC may be enhanced in the modelled multi-component mixture.

On the basis of these studies, the estimate of the radiative forcing due to biomass burning aerosols remains the same at -0.2 Wm^{-2}. The uncertainty associated with the radiative forcing is very difficult to estimate due to the limited number of studies available and is estimated as at least a factor of three, leading to a range of -0.07 to -0.6 Wm^{-2}.

6.7.6 Mineral Dust Aerosol

Recent studies have suggested that 20% (Sokolik and Toon, 1996) and up to 30 to 50% (Tegen and Fung, 1995) of the total mineral dust in the atmosphere originates from anthropogenic activities, the precise fraction of mineral dust of anthropogenic origin being extremely difficult to determine. Only the radiative forcing from this anthropogenic component is considered as there is no evidence that the naturally occurring component has changed since 1750, although ice core measurements suggest that atmospheric concentrations of dust have varied substantially over longer time-scales (e.g., Petit, 1990). Because mineral dust particles are of a relatively large size and because it becomes lofted to high altitudes in the troposphere, in addition to the short-wave radiative forcing, it may exert a significant long-wave radiative forcing. The global mean short-wave radiative forcing will be negative due to the predominantly scattering nature in the solar spectrum (although partial absorption may lead to a local positive radiative forcing over high surface albedos and clouds) and the global mean long-wave forcing will be positive.

Sokolik and Toon (1996) used a simple box model and neglected forcing in cloudy regions to estimate a short-wave radiative forcing of -0.25 Wm^{-2} over ocean and -0.6 Wm^{-2} over land, leading to a global forcing of approximately -0.46 Wm^{-2}. They point out that this is offset to some extent by a positive long-wave forcing. Tegen and Fung (1995) performed a more detailed three-dimensional GCM modelling study of dust aerosol and estimated that approximately 30 to 50% of the total dust burden is due to changes in land use associated with anthropogenic activity. The radiative forcing using this data was estimated by Tegen *et al.* (1996) to be -0.25 Wm^{-2} in the short-wave and $+0.34$ Wm^{-2} in the long-wave, resulting in a net radiative forcing of $+0.09$ Wm^{-2}. Updated calculations of the net radiative forcing based on Miller and Tegen (1998) estimate the radiative forcing to be -0.22 Wm^{-2} in the short-wave and $+0.16$ Wm^{-2} in the long-wave, resulting in a net radiative forcing of -0.06 Wm^{-2}. Hansen *et al.* (1998) perform similar calculations and calculate a net radiative forcing of -0.12 Wm^{-2} by assuming a different vertical distribution, different optical parameters and using a different global model. Jacobson (2001) used a multi-component global aerosol model to estimate the direct radiative forcing to be -0.062 Wm^{-2} in the short-wave and $+0.05$ Wm^{-2} in the long-wave, resulting in a net radiative forcing of -0.012 Wm^{-2}. The effects of non-sphericity of the mineral dust are not accounted for in these calculations. Mishchenko *et al.* (1997) suggest that differences in the optical parameters between model spheroids and actual dust particles do not exceed 10 to 15%, although changes of this magnitude may have a large effect on the radiative forcing (Miller and Tegen, 1998). An example of the geographical distribution of the radiative forcing is shown in Figure 6.7g (data from Tegen *et al.*, 1996) which shows regions of positive and negative forcing. Positive forcing tends to exist over regions of high surface reflectance and negative radiative forcings tend to exist over areas of low surface reflectance. This is due to the dependency of the forcing on surface reflectance and the additional effects of the long-wave radiative forcing.

One problem that needs to be solved is uncertainty in representative refractive indices (Claquin *et al.*, 1998), and how they vary geographically due to different mineral composition of different source regions (e.g., Lindberg *et al.,* 1976). Sokolik *et al.* (1993) summarise the imaginary part of the refractive index for different geographic regions finding a range (-0.003i to approximately -0.02i) at a wavelength of 0.55 μm, and differences in refractive index in the long-wave from different geographical sources are also reported by Sokolik *et al.* (1998). Kaufman *et al.* (2001) use observations from the Landsat satellite coupled with ground-based sun photometer measurements and suggest that Saharan dust has a smaller imaginary refractive index (-0.001i) at 0.55 μm and absorbs less solar radiation than that used in the above modelling studies leading to a much enhanced shortwave radiative forcing. However, the increase is much less in the modelling study of Hansen *et al.* (1998) who find the net radiative forcing changes from -0.12 Wm^{-2} to -0.53 Wm^{-2} when dust is treated as conservatively scattering. von Hoyningen-Huene *et al.* (1999) determine the imaginary part of the refractive index from surface based absorption and scattering measurements and find that a refrac-

tive index of -0.005i best fits the observations for Saharan dust, which is in agreement with the values reported by Sokolik *et al.* (1993). The refractive indices together with the assumed size distributions determine the optical parameters. The radiative forcing is particularly sensitive to the single scattering albedo (Miller and Tegen, 1999). Additional uncertainties lie in modelling the size distributions (Tegen and Lacis, 1996; Claquin *et al.*, 1998) which, together with the refractive indices, determine the optical parameters. Measurements made by the Advanced Very High Resolution Radiometer (AVHRR) by Ackerman and Chung (1992), showed a local short-wave radiative perturbation off the west coast of Africa of -40 to -90 Wm^{-2} and a corresponding long-wave perturbation of $+5$ to $+20$ Wm^{-2} at the top of the atmosphere. Relating instantaneous observational measurements that do not account for the effects of clouds, diurnal averaging of the radiation, the seasonal signal associated with emissions and the fraction of mineral dust that is anthropogenic to the global mean radiative forcing is very difficult. Because the resultant global mean net radiative forcing is a residual obtained by summing the short-wave and the long-wave radiative forcings which are of roughly comparable magnitudes, the uncertainty in the radiative forcing is large and even the sign is in doubt due to the competing nature of the short-wave and long-wave effects. The studies above suggest, on balance, that the shortwave radiative forcing is likely to be of a larger magnitude than the long-wave radiative forcing, which indicates that the net radiative forcing is likely to be negative, although a net positive radiative forcing cannot be ruled out. Therefore a tentative range of -0.6 to $+0.4$ Wm^{-2} is adopted; a best estimate cannot be assigned as yet.

6.7.7 Nitrate Aerosol

Although IPCC (1994) identified nitrate aerosol as a significant anthropogenic source of aerosol, only three estimates of the radiative forcing are available. Van Dorland *et al.* (1997) has produced a very speculative radiative forcing estimate of approximately -0.03 Wm^{-2} for ammonium nitrate, while Adams *et al.* (2001) derived a radiative forcing of -0.22 Wm^{-2} from an anthropogenic burden of 0.62 mg(NO$_3$)m^{-2}, and Jacobson (2001) derived a radiative forcing of approximately -0.02 Wm^{-2} for a column burden of 0.7 mg(NO$_3$)m^{-2}. It appears that the large discrepancy between the results of Jacobson (2001) and Adams *et al.* (2001) is that 90% of the nitrate is in the coarse mode in Jacobson (2001), which reduces the scattering efficiency. Recent measurement studies by Veefkind *et al.* (1996) and ten Brink *et al.* (1997) in the Netherlands have shown that nitrate aerosol in the form of ammonium nitrate is a locally important aerosol species in terms of aerosol mass in the optically active sub-micron size range and hence the associated radiative forcing. They also emphasise the problems in measuring the concentrations and size distributions of nitrate which is a semi-volatile substance. The contradictory nature of the global studies means that no "best estimate" or range for the radiative forcing due to anthropogenic nitrate aerosol is presented in this report, though future studies may prove that it exerts a significant radiative forcing.

6.7.8 Discussion of Uncertainties

While the radiative forcing due to greenhouse gases may be determined to a reasonably high degree of accuracy (Section 6.3), the uncertainties relating to aerosol radiative forcings remain large, and rely to a large extent on the estimates from global modelling studies that are difficult to verify at the present time. The range of estimates presented in this section represents mainly the structural uncertainties (i.e., differences in the model structures and assumptions) rather than the parametric uncertainties (i.e., the uncertainties in the key parameters) (see Pan *et al.*, 1997). This is because many of the model calculations for sulphate aerosol use identical size distributions and refractive indices which lead to identical optical parameters. Thus the model results are not necessarily independent, and certainly do not include the full range of parametric uncertainties. The response of the direct radiative forcing to parametric uncertainties is investigated in sensitivity studies for different aerosol species (e.g., Boucher and Anderson, 1995; Haywood and Ramaswamy, 1998). Three major areas of uncertainty exist; uncertainties in the atmospheric burden and the anthropogenic contribution to it, uncertainties in the optical parameters, and uncertainties in implementation of the optical parameters and burden to give a radiative forcing. The atmospheric burden of an anthropogenic aerosol species is determined by factors such as emission, aging, convective transport, scavenging and deposition processes, each of which have an associated uncertainty (see Chapter 5). The optical parameters have uncertainties associated with uncertainties in size distribution, chemical composition, state of mixing, method of mixing, and asphericity. The problem of the degree of external/internal mixing in the atmosphere deserves highlighting, as global modelling studies tend to assume external mixtures which make modelling the sources, atmospheric transport and radiative properties simpler (e.g., Tegen *et al.*, 1997). However, single particle analysis of particles containing mineral dust (e.g., Levin *et al.*, 1996) and sea salt (Murphy *et al.*, 1998) have often shown them to be internally mixed with sulphate and other aerosols of anthropogenic origin. Thus, heterogeneous conversion of SO_2 to sulphate aerosol on dust or sea salt particles may effectively lead to sulphate becoming internally mixed with larger super-micron particles (e.g., Dentener *et al.*, 1996) leading to a reduction in extinction efficiency, an effect that has not yet been accounted for in global modelling studies. Studies that model internal mixtures of absorbing and scattering aerosols necessarily apply simplifying assumptions such as volume weighting the refractive indices (e.g., Haywood *et al.*, 1997a; Myhre *et al.*, 1998c) which may overestimate the degree of absorption (e.g., Jacobson, 2000). Modelling studies that examine the effects of internal mixing of multi-component aerosols are only just becoming available (Jacobson, 2001). Uncertainties in calculating the radiative forcing from specified burdens and optical parameters arise from uncertainties in the parametrization of relative humidity effects, the horizontal and vertical distributions of the aerosol, the uncertainties and sub-grid scale effects in other model fields such as clouds, humidity, temperature and surface reflectance, the representation of the diurnal cycle, and the accuracy of the radiation code used in the calculations. The short atmospheric lifetime of aerosols and the resultant large spatial variability imply a strong requirement for global observational data. Until a reliable global observational method for verifying the radiative effects of anthropogenic aerosols is available, it is likely that the radiative forcing of any aerosol species will remain difficult to quantify. Although satellite retrievals of aerosol optical properties have advanced substantially since the SAR, the difficult problem of separating anthropogenic from natural aerosol still remains (Chapter 5). Nevertheless, new analyses reiterate that global satellite measurements contain tropospheric aerosol signatures that include those due to anthropogenic aerosols (Haywood *et al.*, 1999; Boucher and Tanré, 2000). While the general spatial distribution of the radiative forcing for sulphate aerosol appears to be similar among the studies listed in Table 6.4, some important features, such as the seasonal cycle in the radiative forcing, remain highly uncertain which may have important consequences in terms of the detection and attribution of climate change (Chapter 12).

Here we examine the consistency of the ranges derived in this section with the ranges obtained using the approach of Chapter 5, Section 5.4.2. For the industrial sulphate, fossil fuel BC, and fossil fuel OC aerosols, the "best estimates" of the direct radiative forcing are -0.4 Wm^{-2} with a factor of 2 uncertainty, $+0.2$ Wm^{-2} with a factor of 2 uncertainty and -0.1 Wm^{-2} with a factor of 3 uncertainty, respectively. An estimate of the total direct radiative forcing from industrial aerosols (using RMS errors) leads to a range -0.07 to -1.24 Wm^{-2} which is reasonably consistent with -0.1 to -1.0 Wm^{-2} (one standard deviation) from Chapter 5, Section 5.4.2. For biomass burning aerosols the "best estimate" of the direct radiative forcing is -0.2 Wm^{-2} with a range -0.07 to -0.6 Wm^{-2}, which is reasonably consistent with -0.1 to -0.5 Wm^{-2} (one standard deviation) obtained from Section 5.4.2.

Additionally, while this section has concentrated upon the radiative forcing at the top of the atmosphere, the effects of anthropogenic aerosols upon the radiative budget at the surface of the Earth has not been considered in detail. For purely scattering aerosols in cloud-free conditions, the radiative effect at the surface is within a few per cent of that at the top of the atmosphere (e.g., Haywood and Shine, 1997). However, for partially absorbing aerosols, the radiative effect at the surface may be many times that at the top of the atmosphere, as evidenced by modelling and measurement studies (e.g., Haywood and Shine, 1997; Haywood *et al.*, 1999; Chapter 5). This is because, for partially absorbing aerosols, energy is transferred directly to the atmospheric column. Ackerman *et al.* (2000) point out that this can warm the atmosphere and "burn off" clouds. They conclude that during the northeast monsoon (dry season over India) daytime trade cumulus cloud cover over the northern Indian Ocean can be reduced by nearly half, although these results depend strongly upon the meteorological conditions and modelling assumptions. This process may also be important over the global domain as indicated by Hansen *et al.* (1997a), as the climate sensitivity parameter (Section 6.2) may differ significantly for absorbing aerosols due to diabatic heating in the aerosol layer modifying the temperature structure of the atmosphere, which affects the formation of clouds. The vertical partitioning of the forcing by absorbing aerosols is also a potentially important factor in determining climatic changes at the surface (e.g., evaporation, soil moisture).

6.8 The Indirect Radiative Forcing of Tropospheric Aerosols

6.8.1 Introduction

Aerosols serve as cloud condensation and ice nuclei, thereby modifying the microphysics, the radiative properties, and the lifetime of clouds. The physics and chemistry of the indirect effect of aerosols is discussed in detail in Chapter 5. Only aspects directly relevant to quantifying the indirect radiative forcing by aerosols are presented here. The aerosol indirect effect is usually split into two effects: the first indirect effect, whereby an increase in aerosols causes an increase in droplet concentration and a decrease in droplet size for fixed liquid water content (Twomey, 1974), and the second indirect effect, whereby the reduction in cloud droplet size affects the precipitation efficiency, tending to increase the liquid water content, the cloud lifetime (Albrecht, 1989), and the cloud thickness (Pincus and Baker, 1994). Until recently, the first indirect effect has received much more attention than the second. IPCC (1994) and the SAR only considered the first indirect effect. Shine *et al.* (1996) retained a range of radiative forcing from 0 to -1.5 Wm^{-2} with no best estimate, although a value of -0.8 Wm^{-2} was used for the year 1990 in the IS92a scenario (Kattenberg *et al.*, 1996). Here we review and discuss the various estimates for the globally averaged aerosol indirect forcing available in the literature. Because of the inherent complexity of the aerosol indirect effect, GCM studies dealing with its quantification necessarily include an important level of simplification. While this represents a legitimate approach, it should be clear that the GCM estimates of the aerosol indirect effect are very uncertain. Section 6.8.2 investigates the indirect radiative forcing due to sulphate aerosols, on which most efforts have concentrated, while other aerosol types are treated in Section 6.8.3. Section 6.8.4 is devoted to alternative approaches, while Section 6.8.6 describes the aerosol indirect effects on ice clouds.

6.8.2 Indirect Radiative Forcing by Sulphate Aerosols

6.8.2.1 Estimates of the first indirect effect

The studies reported in Table 6.6 use different GCMs and methods for computing the droplet number concentration (i.e., empirical relationships between the sulphate mass and the cloud droplet number concentration, empirical relationships between the sulphate aerosol number concentration and the cloud droplet number concentration, or parametrization of cloud nucleation processes). The forcing estimates for the first indirect effect from sulphate aerosols range from -0.3 to -1.8 Wm^{-2}, which is close to the range of 0 to -1.5 Wm^{-2} given in the SAR when only a few estimates were available.

There is a tendency for more and more studies to use interactive (on-line) rather than prescribed (monthly or annual mean) sulphate concentrations. Feichter *et al.* (1997) pointed out that the first indirect effect calculated from monthly mean sulphate concentrations is 20% larger than calculated from interactive sulphate concentrations. Jones *et al.* (1999) found that the total indirect effect was overesti-

mated by about 60% when they used seasonal or annual mean sulphate concentrations.

The various GCM studies show some disagreement on the spatial distribution of the forcing, an example of which is shown in Figure 6.7h. The Northern to Southern Hemisphere ratio varies from 1.4 to 4 depending on the models. It is generally smaller than the Northern to Southern Hemisphere ratio of anthropogenic sulphate aerosol concentrations because of the higher susceptibility of the clouds in the Southern Hemisphere (Platnick and Twomey, 1994; Taylor and McHaffie, 1994). The ocean to land ratio depends very much on the method used to relate the concentration of sulphate mass to the cloud droplet number concentration and on the natural background aerosol concentrations. It was generally found to be smaller than unity (Boucher and Lohmann, 1995; Jones and Slingo, 1997; Kiehl *et al.*, 2000). Larger ratios, such as 1.6 (Chuang *et al.*, 1997) and 5 (Jones and Slingo, 1997), are reported in some of the sensitivity experiments. Using a detailed inventory of ship sulphur emissions and a simple calculation of the aerosol indirect effect, Capaldo *et al.* (1999) suggested that a significant fraction of the effect over the oceans (-0.11 Wm^{-2}, averaged globally) could be due to ship-emitted particulate matter (sulphate plus organic material). So far this source of aerosols has not been included in the GCM studies.

Kogan *et al.* (1996, 1997) used the Warren *et al.* (1988) cloud climatology over the oceans rather than a GCM to predict the indirect effect by sulphate aerosols on cloud albedo. The cloud albedo susceptibility was evaluated from a large eddy simulation model applied to stratocumulus clouds. They found an indirect short-wave forcing of -1.1 Wm^{-2} over the oceans with a small hemispheric difference of 0.4 Wm^{-2} (i.e., a Northern to Southern Hemisphere ratio of about 1.4). In their study, the forcing had a strong seasonal cycle, with the Southern Hemisphere forcing prevailing in some seasons.

6.8.2.2 Estimates of the second indirect effect and of the combined effect

Whereas the first indirect effect can be computed diagnostically, assessment of the second indirect effect implies that two independent (i.e., with the same fixed sea surface temperatures, but with different meteorologies) GCM simulations be made, a first one with pre-industrial and a second one with present day aerosols. The difference in top of the atmosphere fluxes or cloud radiative forcings between two such simulations is used as a proxy for the forcings due to the second indirect and the combined effects. The simulations need to be sufficiently long (usually 5 years) so that the effects of natural variability are expected to average out. However, as a consequence, the estimates of the aerosol indirect effect may include some undesirable feedbacks involving climate parameters which would violate the definition adopted for radiative forcing of climate change by IPCC (see also Section 6.1.1). Rotstayn and Penner (2001) showed that, at least in their model, the difference in top of the atmosphere fluxes between two simulations did not differ by more than 10% from the radiative forcing for the first indirect effect computed diagnostically. Caution should nevertheless be exercised before this result can be generalised to other models and to the second indirect effect.

Table 6.6: *The global mean annual average aerosol indirect radiative forcing from different global studies. Letters P (prescribed) and C (computed) refer to off-line and on-line sulphate aerosol calculations, respectively. CCN and CDN stand for cloud condensation nuclei and cloud droplet number, respectively. In studies indicated by an asterisk, the estimate in flux change due to the indirect effect of aerosols was computed as the difference in top of atmosphere fluxes between two distinct simulations and therefore does not represent a forcing in the strict sense (see text). When several simulations are performed in the same study, "base" indicates the baseline calculation, while the range of estimates is given in parenthesis.*

Reference	Aerosol Type	Forcing estimate (Wm^{-2})				Remarks	
		First effect	**Second effect**	**Both effects**			
Boucher and Rodhe (1994)*	Sulphate			−0.65 to −1.35	P	Uses 3 relationships between sulphate mass and CCN/CDN concentrations.	
Chuang *et al.* (1994)	Sulphate	−0.47			C	Includes a parametrization of cloud nucleation processes.	
Jones *et al.* (1994)	Sulphate	−1.3			P	Uses a relationship between aerosol and droplet number concentrations.	
Boucher and Lohmann (1995)	Sulphate	−0.5 to −1.4			P	LMD GCM	Uses 4 different relationships between sulphate mass and
Boucher and Lohmann (1995)	Sulphate	−0.45 to −1.5			P	ECHAM	CCN/CDN concentrations (A, B, C, and D).
Jones and Slingo (1996)	Sulphate	−0.3 to −1.5			P	Uses 2 different sulphate distributions. Follows Jones *et al.* (1994), Hegg (1994), Boucher and Lohmann (1995) 'D'.	
Kogan *et al.* (1996) Kogan *et al.* (1997)	Sulphate	−1.1				Uses a cloud climatology rather than GCM-simulated clouds.	
Chuang *et al.* (1997)	Sulphate	−0.4 to −1.6			C	Includes a parametrization of cloud nucleation processes. Uses a mixture of pre-existing aerosols.	
Feichter *et al.* (1997)	Sulphate	−0.76			C	Uses Boucher and Lohmann (1995) 'A' relationship.	
Jones and Slingo (1997)	Sulphate	−0.55 to −1.50			P	Uses 2 different versions of the Hadley Centre model.	
Lohmann and Feichter (1997)*	Sulphate	−1		−1.4 to −4.8	C	Uses Boucher and Lohmann (1995) 'A' relationship.	
Rotstayn (1999)*	Sulphate	base −1.2 (−1.1 to −1.7)	base −1.0 (−0.4 to −1.0)	base −2.1 (−1.6 to −3.2)	P	Includes a (small) long-wave radiative forcing.	
Jones *et al.* (1999)* [a]	Sulphate	−0.91	base −0.66	−1.18	C	Includes a (small) long-wave radiative forcing. The two effects add non-linearly.	
Kiehl *et al.* (2000)	Sulphate	−0.40 to −1.78			C		
Ghan *et al.* (2001a)*	Sulphate	~50% for base	~50% for base	base −1.7 (−1.6 to −3.2)	C	Includes a parametrization of cloud nucleation. Predicted aerosol size distribution.	
Lohmann *et al.* (2000)*	Sulphate			base −0.4 (0 to −0.4)	C	Includes a parametrization of cloud nucleation processes.	
	Carb.			base −0.9 (−0.9 to −1.3)	C		
	Sulphate and Carb.	−40% for base	−60% for base	base −1.1 (−1.1 to −1.9)	C		
Chuang *et al.* (2000b)	Sulphate	−0.30			C	Includes a parametrization of cloud nucleation processes. Includes the effect of BC absorption in clouds.	
	Carb.	base −1.51 (−1.27 to −1.67)			C		
	Sulphate and Carb.	−1.85			C		

[a] This model predicts too low sulphate concentrations on average.

Jones *et al.* (1999) and Rotstayn (1999) provide estimates for the second indirect effect alone with ranges of −0.53 to −2.29 Wm^{-2} and −0.4 to −1.0 Wm^{-2}, respectively. For the combined effect (first and second effects estimated together), Jones *et al.* (1999) and Rotstayn (1999) give best estimates of −1.18 and −2.1 Wm^{-2}. Larger radiative impacts are found in sensitivity tests by Rotstayn (1999) and Lohmann and Feichter (1997), with values of −3.2 and −4.8 Wm^{-2}, respectively. Rotstayn (1999) tried an alternative parametrization for cloud droplet concentration (Roelofs *et al.*, 1998) and Lohmann and Feichter (1997) tried an alternative cloud scheme. In contrast to these studies, Lohmann *et al.* (2000) adopted a "mechanistic" approach, where they introduced a prognostic equation for the cloud droplet number concentration. They predict a much smaller combined effect with radiative impact of 0.0 and −0.4 Wm^{-2}, assuming externally and internally mixed sulphate aerosols, respectively. The authors attribute this rather small radiative impact to the small increase in anthropogenic sulphate aerosol number concentrations. Ghan *et al.* (2001a) estimate a combined effect of −1.7 Wm^{-2} using a mechanistic approach similar to that of Lohmann *et al.*, but with aerosol size distribution predicted rather than prescribed. The larger forcing is due to the absence of lower bounds on droplet and aerosol number concentrations in the simulations by Ghan *et al.* (2001a). Studies by Rotstayn (1999) and Jones *et al.* (1999) both indicate that the positive long-wave forcing associated with the indirect aerosol effect is small (between 0.0 and 0.1 Wm^{-2} for each of the effects).

The partitioning of the total indirect radiative impact between the first and second effect is uncertain. Jones *et al.* (1999) found that the ratio between their best estimates of the first and second indirect effects, taken separately, was 1.38, while Lohmann *et al.* (2000) predicted a ratio of 0.71 (for sulphate and carbonaceous aerosols taken together). Rotstayn (1999) and Lohmann *et al.* (2000) estimated that the radiative impact for the combined effects was of similar magnitude than the sum of the two effects considered separately. In contrast, Jones *et al.* (1999) found that the combined radiative impact (−1.18 Wm^{-2}) was less than the sum of the two effects (estimated as −0.91 and −0.66 Wm^{-2}, respectively, yielding a sum of −1.57 Wm^{-2}).

6.8.2.3 Further discussion of uncertainties
Some authors have argued that sea salt particles may compete with sulphate aerosols as cloud condensation nuclei, thereby reducing the importance of anthropogenic sulphate in droplet nucleation (Ghan *et al.*, 1998; O'Dowd *et al.*, 1999). While this process is empirically accounted for in some of the above mentioned estimates (e.g., Jones *et al.*, 1999), it certainly adds further uncertainty to the estimates. Considerable sensitivity is found to the parametrization of the autoconversion process (Boucher *et al.*, 1995; Lohmann and Feichter, 1997; Delobbe and Gallée, 1998; Jones *et al.*, 1999) which complicates matters because there is a need to "tune" the autoconversion onset in GCMs (Boucher *et al.*, 1995; Fowler *et al.*, 1996; Rotstayn, 1999, 2000) to which the indirect aerosol forcing is sensitive (Jones *et al.*, 1999; Rotstayn, 1999; Ghan *et al.*, 2001a). The indirect aerosol forcing is also sensitive to the treatment of the pre-industrial aerosol concentration and properties (Jones *et al.*, 1999; Lohmann *et al.*, 2000) which

remain poorly characterised, the representation of the microphysics of mid-level clouds (Lohmann *et al.*, 2000), the representation of aerosol size distribution (Ghan *et al.*, 2001a), the parametrization of sub-grid scale clouds, the horizontal resolution of the GCM (Ghan *et al.*, 2001a), and the ability of GCMs to simulate the stratocumulus cloud fields. Finally, it should be noted that all the studies discussed above cannot be considered as truly "independent" because many of them (with the exceptions of Lohmann *et al.* (2000) and Ghan *et al.* (2001a)) use similar methodologies and similar relationships between sulphate mass and cloud droplet number concentration. Therefore it is suspected that the range of model results does not encompass the total range of uncertainties. In an overall sense, it can be concluded that the considerable sensitivities to the treatment of microphysical details associated with aerosol-cloud interactions, and their linkages with macroscopic cloud and circulation parameters, remain to be thoroughly explored.

6.8.3 Indirect Radiative Forcing by Other Species

6.8.3.1 Carbonaceous aerosols
In this section, carbonaceous aerosols refer to the mixture (internal or external) of OC and BC aerosols. Carbonaceous aerosols (and in particular biomass burning aerosols) are efficient cloud condensation nuclei (see Chapter 5 and e.g., Novakov and Penner, 1993; Novakov and Corrigan, 1996). There have been few GCM studies estimating the indirect forcing from carbonaceous aerosols. Penner *et al.* (1996) reported a range of forcing from −2.5 to −4.5 Wm^{-2} (not included in Table 6.6), which is probably an overestimate because of neglect of other aerosol types such as dust and sea salt and underestimated natural emissions of organic aerosols. In a new set of simulations using an updated model accounting for dust and sea salt aerosols, Chuang *et al.* (2000b) obtained a forcing of −1.51 Wm^{-2} for the first indirect effect from carbonaceous aerosols (−0.52 and −1.16 Wm^{-2} for fossil fuel and biomass burning aerosols, respectively). This estimate includes the effect of black carbon absorption in cloud droplets. Lohmann *et al.* (2000) predicted a radiative impact for the combined effect (i.e., first and second effects) of −1.3 and −0.9 Wm^{-2} for externally and internally mixed carbonaceous aerosols, respectively. These estimates do not include the effects of secondary organic aerosols, nor the effects of absorption of solar radiation by black carbon within the cloud.

Kaufman and Nakajima (1993) used AVHRR data to analyse bright warm clouds over Brazil during the biomass burning season. They found a decrease in the cloud reflectance when the smoke optical thickness increased. Kaufman and Fraser (1997) used a similar approach to observe thinner and less reflective clouds. They showed that smoke from biomass burning aerosols reduced the cloud droplet size and increased the cloud reflectance for smoke optical depth up to 0.8. They estimated the indirect radiative forcing by smoke to be −2 Wm^{-2} over this region for the three months when biomass burning takes place, which would suggest a much smaller global average. However, using a combination of satellite observations and a global chemistry model, Remer *et al.* (1999) estimated that 50% of the cumulative biomass burning aerosol indirect forcing occurs for smoke optical depth smaller than 0.1, that is well away from the source regions.

6.8.3.2 Combination of sulphate and carbonaceous aerosols

Lohmann *et al.* (2000) found that the radiative impact of sulphate and carbonaceous aerosols considered simultaneously (−1.5 and −1.1 Wm^{-2} for the externally and internally mixed assumptions, respectively) is comparable to the sum of the radiative impacts calculated separately (see Table 6.6). Chuang *et al.* (2000b) reached a similar conclusion in their experiments where they considered only the first indirect effect, with a total radiative forcing of −1.85 Wm^{-2}. It is noteworthy, however, that in these two studies, the predicted radiative forcings for sulphate aerosols are on the low side. This indicates that it is not wise to add the radiative forcings due to sulphate and carbonaceous aerosols obtained separately from two different models. In fact, most of the GCM studies of the indirect aerosol effect used sulphate as a surrogate for the total anthropogenic fraction of the aerosol (e.g., Boucher and Lohmann, 1995; Feichter *et al.*, 1997; Lohmann and Feichter, 1997). In this case the computed forcings incorporate the effects of other aerosol types which have a similar spatial distribution to sulphate aerosols, such as nitrate aerosols or carbonaceous aerosols from fossil fuel combustion. It will not include, however, the effects of biomass burning aerosols which have a different spatial distribution from sulphate aerosols.

Another issue is the potential for light-absorbing aerosols to increase in-cloud absorption of solar radiation – and correspondingly decrease the cloud albedo – when incorporated inside cloud droplets. Twohy *et al.* (1989) concluded from measurements off the coast of California and from simple radiative calculations that the observed levels of soot would not lead to a significant impact on the cloud albedo. Chylek *et al.* (1996a) estimated an upper bound for increased absorption of solar radiation of 1 to 3 Wm^{-2} (global and annual average) for a black carbon concentration of 0.5 μgm^{-3}. Considering the modelled atmospheric concentrations of soot (Chapter 5 and Sections 6.7.3 and 6.7.5) and the fact that only a fraction of the soot is incorporated in the cloud droplets, the effect is probably smaller by one to two orders of magnitude. Heintzenberg and Wendisch (1996) showed that the decrease in radiative forcing due to a decrease in soot concentrations with increasing distances from the pollution sources could be compensated by a concurrent increase in the fraction of soot which is incorporated in the cloud droplets. Only one GCM study to date has considered the in-cloud absorption of soot. Chuang *et al.* (2000b) estimated a radiative forcing for in-cloud BC of +0.07 Wm^{-2} for the soot concentrations predicted by their model and using an effective medium approximation. More studies are needed to confirm these results.

6.8.3.3 Mineral dust aerosols

Levin *et al.* (1996) observed desert dust particles coated with sulphate. Such particles may originate from in-cloud scavenging of interstitial dust particles followed by evaporation of the cloud droplets, condensation of SO$_2$ onto dust followed by oxidation, or even coagulation of dust and sulphate particles. The presence of soluble material (which may be of anthropogenic origin) on the desert dust particles converts them into large and effective CCN which may affect the cloud microphysics. Whether this effect results in a significant climate forcing has not been investigated and cannot presently be quantified.

6.8.3.4 Effect of gas-phase nitric acid

Kulmala *et al.* (1993, 1995, 1998) argued that enhanced concentrations of condensable vapours (such as HNO$_3$ and HCl) in the atmosphere could affect cloud properties by facilitating the activation of cloud condensation nuclei. The impact of such an effect on the planetary cloud albedo has not been assessed.

6.8.4 Indirect Methods for Estimating the Indirect Aerosol Effect

6.8.4.1 The "missing" climate forcing

Hansen and colleagues have used two alternative approaches to characterise and quantify any "missing" climate forcing besides that due to greenhouse gases, solar constant, O$_3$, and aerosol direct effect. Hansen *et al.* (1995) used a simplified GCM to investigate the impacts of various climate forcings on the diurnal cycle of surface air temperature and compared them with observations. They found that, although the aerosol direct effect or an increase in continental cloud albedo could contribute to damp the surface temperature diurnal cycle, only an increase in continental cloud cover would be consistent with observations (Karl *et al.*, 1993). The required cloud increase depends on cloud height and would be of the order of 1% global coverage for low clouds (i.e., 2 to 5% over land). We cannot rule out that such a change is an unidentified cloud feedback rather than a forcing. Hansen *et al.* (1997b) also argued that agreement between observed and computed temperature trends requires the presence of another forcing of at least −1 Wm^{-2} which is inferred as being due to the *indirect* effect. In their calculations, the *direct* tropospheric aerosol effect does not play a large net role, because the moderately absorbing aerosol assumption leads to an offset between its sunlight reflecting and absorbing properties insofar as the top of the atmosphere irradiance change is concerned. However, this method assumes that the observed change in temperature since pre-industrial times is primarily a response to anthropogenic forcings, that all the other anthropogenic forcings are well quantified, and that the climate sensitivity parameter (Section 6.1) predicted by the GCM is correct (Rodhe *et al.*, 2000). Therefore it may simply be a coincidence that the estimate of Hansen *et al.* (1997b) is consistent with the GCM estimates discussed above.

6.8.4.2   Remote sensing of the indirect effect of aerosols

Han *et al.* (1994) analysed AVHRR satellite radiances to retrieve the cloud droplet size of low-level clouds. They reported significant inter-hemispheric differences for both maritime and continental clouds. Boucher (1995) showed that, if this difference is to be attributed to anthropogenic aerosols, it implies a differential forcing of about −1 Wm^{-2} between the two hemispheres. Assuming a Northern Hemisphere to Southern Hemisphere ratio of 2:1 for the aerosol indirect effect, this would imply a globally-averaged forcing of −1.5 Wm^{-2}. It is not clear, however, to what extent changes in cloud droplet size are related to change in aerosol concentrations. For instance, Han *et al.* (1998) showed that cloud albedo decreases with decreasing droplet size for the optically thinner clouds over the oceans. While this does not invalidate the aerosol indirect effect at all, it underlines the limita-

tions in using satellite observed changes in droplet size to compute the aerosol indirect forcing. Therefore it seems difficult at present to use satellite observations to estimate the first aerosol indirect forcing unless some changes in cloud albedo could be tied to changes in aerosol concentrations under the assumption of constant liquid water content. Satellite observations do play, however, a key role for evaluating models of the indirect aerosol radiative effect (Ghan *et al*., 2001b).

6.8.5 Forcing Estimates for This Report

Shine and Forster (1999) proposed a value of the aerosol indirect forcing due to all aerosols of -1 Wm^{-2} with at least a factor of two uncertainty. Several observational studies (see Chapter 5) support the existence of the first aerosol indirect effect on low-level clouds and a negative sign for the associated radiative forcing, but these studies do not give indications on what a (negative) upper bound of the forcing would be. GCM studies predict radiative forcing for the first indirect effect of industrial aerosols in the range of -0.3 to -1.8 Wm^{-2}. However, because of the uncertainties in the estimates discussed above, the limited validation of GCM parametrizations and results, and because in-cloud absorption by black carbon aerosols was not considered in all but one of the GCM studies, we retain 0 Wm^{-2} as an upper bound for the first aerosol indirect effect. A lower bound of -2 Wm^{-2} is selected on the basis of available GCM studies for the first indirect effect. Not too much emphasis should be given to the exact bounds of this interval because they do not carry any statistical meaning (Section 6.13.1) and because of the very low level of scientific understanding associated to this forcing (see Section 6.13.1 where this concept is defined).

Available GCM studies suggest that the radiative flux perturbations associated with the second effect could be of similar magnitude to that of the first effect. There are no studies yet to confirm unambiguously that the GCM estimates of the radiative impact associated with the second indirect effect can be interpreted in the strict sense of a radiative forcing (see Sections 6.1 and 6.8.2.2), and very few observations exist as yet to support the existence of a significant effect. Therefore we refrain from giving any estimate or range of estimates for the second aerosol indirect effect. However, this does not minimise the potential importance of this effect.

6.8.6 Aerosol Indirect Effect on Ice Clouds

6.8.6.1 Contrails and contrail-induced cloudiness
Using meteorological and air traffic data scaled to regional observations of contrail cover, Sausen *et al.* (1998) estimated the present day global mean cover by line-shaped contrails to be about 0.1%. This results in a global and annual mean radiative forcing by line-shaped contrails of 0.02 Wm^{-2} (Minnis *et al.*, 1999), subject to uncertainties in the contrail cover, optical depth, ice particle size and shape (Meerkötter *et al.*, 1999). We follow Fahey *et al.* (1999) and retain a range of 0.005 to 0.06 Wm^{-2} for the present day forcing, around the best estimate of 0.02 Wm^{-2}.

Contrails can evolve into extended cirrus clouds. Boucher (1999) and Fahey *et al.* (1999) have shown evidences that cirrus

occurrence and coverage may have increased in regions of high air traffic compared with the rest of the globe. Smith *et al.* (1998) reported the existence of nearly invisible layers of small ice crystals, which cause absorption of infrared radiation, and could be due to remnant contrail particles. From consideration of the spatial distribution of cirrus trends during the last 25 years, Fahey *et al.* (1999) gave a range of possible best estimates of 0 to 0.04 Wm^{-2} for the radiative forcing due to aviation-induced cirrus. The available information on cirrus clouds was deemed insufficient to determine a single best estimate or an uncertainty range.

6.8.6.2 Impact of anthropogenic aerosols on cirrus cloud microphysics
Measurements by Ström and Ohlsson (1998) in a region of high air traffic revealed higher crystal number concentrations in areas of the cloud affected by soot emissions from aircraft. If the observed enhancement in crystal number density (which is about a factor of 2) is associated with a reduction in the mean crystal size, as confirmed by the measurements of Kristensson *et al.* (2000), a change in cloud radiative forcing may result. Wyser and Ström (1998) estimated the forcing, although very uncertain, to be in the order of 0.3 Wm^{-2} in regions of dense air traffic under the assumption of a 20% decrease of the mean crystal size. No globally averaged radiative forcing is available.

The sedimentation of ice particles from contrails may remove water vapour from the upper troposphere. This effect is expected to be more important in strongly supersaturated air when ice particles can fall without evaporating (Fahey *et al.*, 1999). The impacts of such an effect on cirrus formation, vertical profile of humidity and the subsequent radiative forcing have not been assessed.

Aerosols also serve as ice nuclei although it is well recognised that there are fewer ice nuclei than cloud condensation nuclei. It is conceivable that anthropogenic aerosols emitted at the surface and transported to the upper troposphere affect the formation and properties of ice clouds. Jensen and Toon (1997) suggested that insoluble particles from the surface or soot particles emitted by aircraft, if they serve as effective ice nuclei, can result in an increase in the cirrus cloud coverage. Laaksonen *et al.* (1997) argued that nitric acid pollution is able to cause an increase in supercooled cirrus cloud droplet concentrations, and thereby influence climate (see Chapter 5, Section 5.3.6). Such effects, if significant at all, are not quantified at present.

6.9 Stratospheric Aerosols

IPCC (1992, 1994) and the SAR have dealt with the climatic effects of episodic, explosive volcanic events which result in significant enhancements of aerosol concentrations in the stratosphere. The most dramatic of these in recent times has been the 1991 eruption of Mt. Pinatubo. The radiative, chemical, dynamical and climatic consequences accompanying the transient duration of sulphuric acid aerosols in the stratosphere have been discussed in previous IPCC assessments. The eruption of Mt. Pinatubo reached a peak forcing of about -3 Wm^{-2} (uncertainty of 20%) in 1991 (Hansen *et al.*, 1998; Stenchikov *et al*., 1998), and was plausibly the largest volcanic aerosol forcing

of this century, perturbing the stratospheric and surface climate significantly (SAR). However, aerosol levels in the stratosphere have now fallen to well below the peak values seen in 1991 to 1993, and are comparable to the very low value seen in about 1979, which was a quiescent time as far as volcanic activity was concerned (WMO, 1999). It is likely that even the heterogeneous chemical effects initiated by aerosols upon the O_3 chemistry and its destruction (Solomon *et al.*, 1996) have diminished. One consequence of the aerosol-induced ozone depletion may have been a prolonged cooling of the lower stratosphere to abnormally low values through the mid-1990s, as estimated from satellite and radiosonde observations (WMO, 1999, Chapter 5). Although episodic in nature and transient in duration, volcanic events can exert a significant influence on the time history of the radiative forcing evolution and thereby on the long-term (interannual to decadal scale) temperature record (see Chapter 9).

As noted in previous IPCC Assessments, there are difficulties in compiling a good quantitative record of the episodic volcanic events (see also Rowntree, 1998), in particular the intensity of their forcings prior to the 1960s. Efforts have been made to compile the optical depths of the past volcanoes (SAR; Robock and Free, 1995, 1996; Andronova *et al.*, 1999); however, the estimated global forcings probably have an uncertainty of a factor of two or more. Several major volcanic eruptions occurred between 1880 and 1920, and between 1960 and 1991.

6.10 Land-use Change (Surface Albedo Effect)

Changes in land surface albedo can result from land-use changes (Henderson-Sellers, 1995) and thus be tied to an anthropogenic cause. Hansen *et al.* (1997b) estimate that a forcing of −0.4 Wm^{-2} has resulted, about half of which is estimated to have occurred in the Industrial Era. The largest effect is estimated to be at the high latitudes where snow-covered forests that have a lower albedo have been replaced by snow-covered deforested areas. Hansen *et al.* (1998) point out that the albedo of a cultivated field is affected more by a given snowfall than the albedo of an evergreen forest. They performed a simulation with pre-industrial vegetation replaced by current land-use patterns and found the global mean forcing to be −0.21 Wm^{-2}, with the largest contributions coming from deforested areas in Eurasia and North America. In a similar study, Betts (2001) estimates an instantaneous radiative forcing of −0.20 Wm^{-2} by surface albedo change due to present day land use relative to natural vegetation. In agreement with Hansen *et al.* (1997b), the greatest effect is seen in the high latitude agricultural regions. If, as above, half of the land clearance is assumed to have taken place since the industrial revolution, this suggests a forcing of −0.10 Wm^{-2} by land use over this period. In a parallel simulation with the climate free to respond to the change in albedo and other vegetation characteristics, lower temperatures are simulated in the northern mid-latitudes. These are mainly attributed to the increased surface albedo, although increases in cloud cover cause further localised reductions in the net surface short-wave radiation in some regions. However, some areas exhibit higher temperatures in their dry season, consistent with a decrease in evapotranspiration due to reduced access of soil moisture by the shallower roots of the crops compared with forest.

Following Hansen *et al.* (1997b), Shine and Forster (1999) recommended in their review a value of −0.2 Wm^{-2} with at least a 0.2 Wm^{-2} uncertainty. We adopt those values here for the best estimate and range, respectively; however, in view of the small number of investigations and uncertainty in historical land cover changes, there is very low confidence in these values at present.

Changes in land use can also exert other kinds of climatic impacts, e.g., changes in roughness length, turbulent fluxes, and soil moisture and heat budgets (see also Chapters 7 and 8). Further, there are a host of factors that are potentially affected by land-use change and that could have an impact on the atmospheric concentrations of radiatively active trace gases and aerosols. For instance, the dry deposition rates of species could be affected owing to the surface roughness change. Precipitation changes induced by deforestation etc. could affect the wet deposition of species and thereby bring about biogeochemical changes, leading to changes in lifetimes. The impacts due to such changes have not been comprehensively investigated.

6.11 Solar Forcing of Climate

In this section variations in total solar irradiance and how these translate into radiative forcing are described and potential mechanisms for amplification of solar effects are discussed. The detection of solar effects in observational records is covered in Chapters 2 and 12.

6.11.1 Total Solar Irradiance

6.11.1.1 The observational record

The fundamental source of all energy in the climate system is the Sun so that variation in solar output provides a means for radiative forcing of climate change. It is only since the late 1970s, however, and the advent of space-borne measurements of total solar irradiance (TSI), that it has been clear that the solar "constant" does, in fact, vary. These satellite instruments suggest a variation in annual mean TSI of the order 0.08% (or about 1.1 Wm^{-2}) between minimum and maximum of the 11-year solar cycle. While the instruments are capable of such precision their absolute calibration is much poorer such that, for example, TSI values for solar minimum 1986 to 1987 from the ERB radiometer on Nimbus 7 and the ERBE experiment on NOAA-9 disagree by about 7 Wm^{-2} (Lean and Rind, 1998). More recent data from ACRIM on UARS, EURECA and VIRGO on SOHO cluster around the ERBE value (see Figure 6.4) so absolute uncertainty may be estimated at around 4 Wm^{-2}. Although individual instrument records last for a number of years, each sensor suffers degradation on orbit so that construction of a composite series of TSI from overlapping records becomes a complex task. Figure 6.4 shows TSI measurements made from satellites, rockets, and balloons since 1979.

Willson (1997) used ERB data to provide cross-calibration between the non-overlapping records of ACRIM-I and ACRIM-II and deduced that TSI was 0.5 Wm^{-2} higher during the solar minimum of 1996 than during solar minimum in 1986. If this reflects an underlying trend in solar irradiance it would
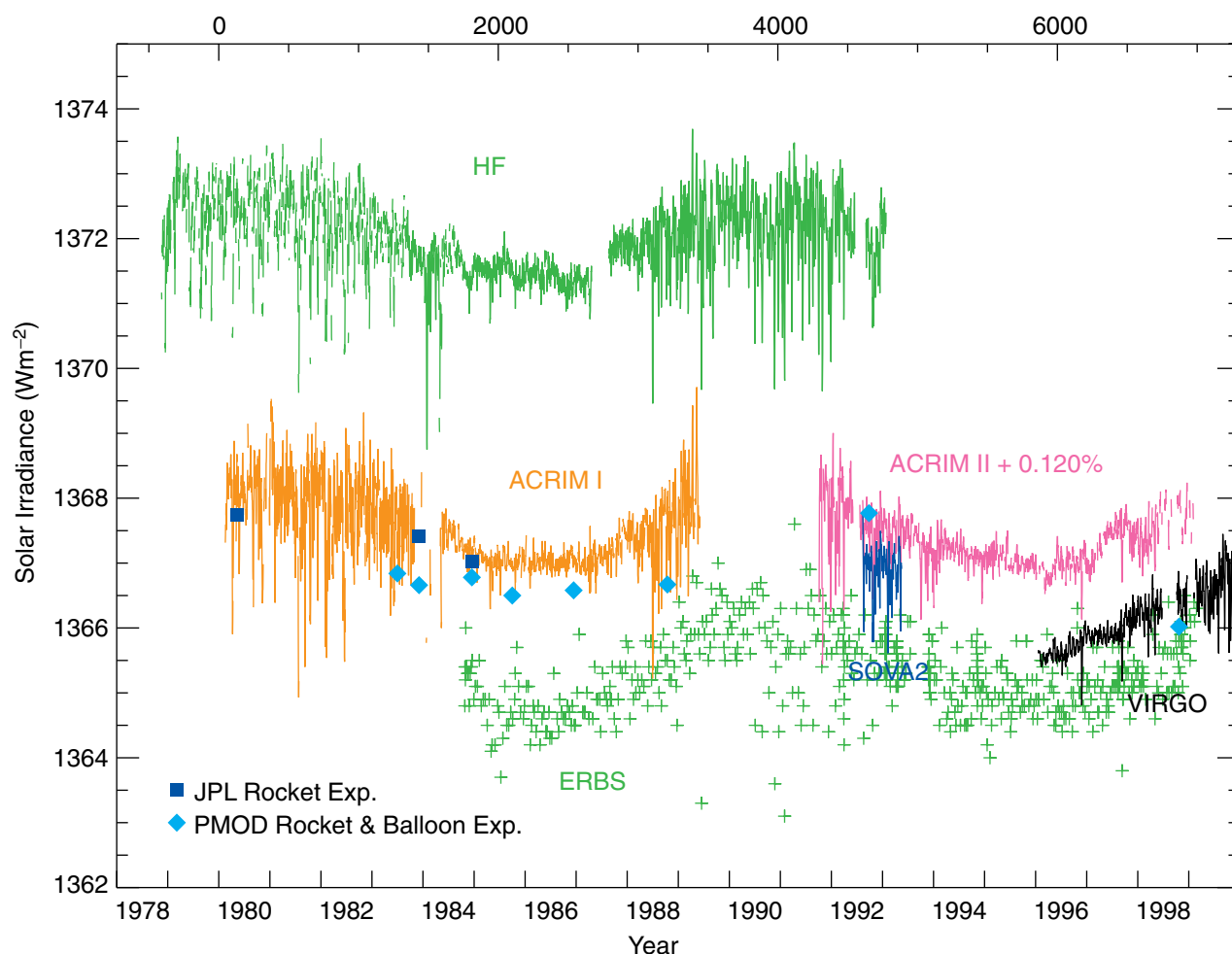
Figure 6.4: Measurements of total solar irradiance made between 1979 and 1999 by satellite, rocket and balloon instruments (http://www.pmodwrc.ch/solar_const/solar_const.html).

represent a radiative forcing[2] of 0.09 Wm⁻² over that decade compared with about 0.4 Wm⁻² due to well-mixed greenhouse gases. The factors used to correct ACRIM-I and ACRIM-II by Willson (1997) agree with those derived independently by Crommelynk *et al.* (1995) who derived a Space Absolute Radiometric Reference of TSI reportedly accurate to ± 0.15%. Fröhlich and Lean (1998), however, derived a composite TSI series which shows almost identical values in 1986 and 1996, in good agreement with a model of the TSI variability based on independent observations of sunspots and bright areas (faculae). The difference between these two assessments depends critically on the corrections necessary to compensate for problems of unexplained drift and uncalibrated degradation in both the Nimbus 7/ERB and ERBS time series. Thus, longer-

term and more accurate measurements are required before trends in TSI can be monitored to sufficient accuracy for application to studies of the radiative forcing of climate.

6.11.1.2 Reconstructions of past variations of total solar irradiance

As direct measurements of TSI are only available over the past two decades it is necessary to use other proxy measures of solar output to deduce variations at earlier dates. In the simplest type of reconstruction a proxy measure, such as sunspot number (Stevens and North, 1996) or solar diameter (Nesme-Ribes *et al.*, 1993), is calibrated against recent TSI measurements and extrapolated backwards using a linear relationship. The various proxies vary markedly as indicators of solar activity. For example, over the past century, sunspot number and 10.7 cm flux showed highest values at the solar maximum of 1958, whereas the aa index, which gives a measure of the magnitude of the solar magnetic field at the Earth, peaked during 1990. This is because whereas sunspot numbers return to essentially zero at each solar minimum the aa index shows 11-year cycles imposed on a longer-term modulation (Lean and Rind, 1998). Other terrestrially based indicators of solar activity recorded by cosmogenic isotopes in tree-rings and ice-

---

[2] Geometric factors affect the conversion from change in TSI to radiative forcing. It is necessary to divide by a factor of 4, representing the ratio of the area of the Earth's disc projected towards the Sun to the total surface area of the Earth, and to multiply by a factor of 0.69, to take account of the Earth's albedo of 31%. Thus a variation of 0.5 Wm⁻² in TSI represents a variation in global average instantaneous (i.e. neglecting stratospheric adjustment) radiative forcing of about 0.09 Wm⁻².

cores also show longer term modulation. However, direct solar proxies other than the sunspot number cover too short a period to reliably detect such a trend. Thus, it is not clear which proxy, if any, can be satisfactorily used to indicate past values of TSI.

A more fundamental approach recognises that solar radiative output is determined by a balance between increases due to the development of faculae and decreases due to the presence of sunspots. Longer-term changes are also speculated to be occurring in the quiet Sun against which these variable active regions are set. The sunspot darkening depends on the area of the solar disc covered by the sunspots while the facular brightening has been related to a variety of indices. These include sunspot number (Lean *et al.*, 1995), emission of singly ionised calcium (Ca II at 393.4 nm) (Lean *et al.*, 1992), solar cycle length, solar cycle decay rate, solar rotation rate and various empirical combinations of all of these (Hoyt and Schatten, 1993; Solanki and Fligge, 1998).

In addition to estimates of the impact of active regions on TSI potential contributions due to the variation in brightness of the quiet Sun have been estimated (Lean *et al.,* 1992; White *et al.*, 1992). These were largely based on observations of the behaviour of Sun-like stars (Baliunas and Jastrow, 1990) and the assumption that during the Maunder Minimum (an extended period during the late 17th century during which no sunspots were observed) the Sun was in a non-cycling state. The various reconstructions vary widely in the values deduced for TSI during the Maunder Minimum relative to the present. Mendoza (1997) has pointed out that uncertainties in the assumptions made about the state of the Sun during that period could imply a range of between 1 and 15 Wm^{-2} reduction in TSI less than present mean values although most estimates lie in the 3 to 5.5 Wm^{-2} range. Figure 6.5 shows group sunspot numbers from 1610 to 1996 (Hoyt and Schatten, 1998) together with five TSI reconstructions. The sunspot numbers (grey curve, scaled to correspond to Nimbus-7 TSI observations for 1979 to 1993) show little long-term trend. Lean *et al.* (1995, solid red curve) determine long-term variability from sunspot cycle amplitude; Hoyt and Schatten (1993, black solid curve) use mainly the length of the sunspot cycle; the two Solanki and Fligge (1998) blue curves (dotted) are similar in derivation to the Lean *et al*. and Hoyt and Schatten methods. Lockwood and Stamper (1999, heavy dash-dot green curve) use an entirely different approach, based not on sunspot numbers but on the aa geomagnetic index, and predict somewhat larger variation over individual cycles but less on the longer term. Clearly, even disregarding the shifts due to absolute scaling, there are large differences between the TSI reconstructions. Thus knowledge of solar radiative forcing is uncertain, even over the 20th century and certainly over longer periods.

An alternative approach which has been used to reconstruct TSI (Reid, 1997; Soon *et al.*, 1996) is to assume that time variations in global surface temperature are due to a combination of the effects of solar variability and enhanced greenhouse gas concentrations and to find that combination of these two forcings which best combine to simulate surface temperature measurements. However, these authors did not take natural climatic variability into account and a TSI series derived by such methods could not be used as an independent measure of radiative forcing of climate.
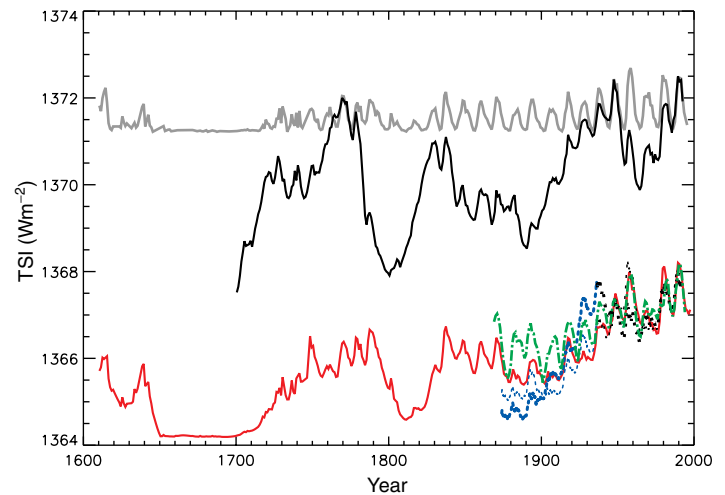
Figure 6.5: Reconstructions of total solar irradiance (TSI) by Lean *et al.* (1995, solid red curve), Hoyt and Schatten (1993, data updated by the authors to 1999, solid black curve), Solanki and Fligge (1998, dotted blue curves), and Lockwood and Stamper (1999, heavy dash-dot green curve); the grey curve shows group sunspot numbers (Hoyt and Schatten, 1998) scaled to Nimbus-7 observations for 1979 to 1993.

The estimate for solar radiative forcing since 1750 of 0.3 Wm^{-2}, shown in Figure 6.6, is based on the values in Figure 6.5 (taking the 11-year cycle minimum values in 1744 and 1996). Clearly the starting date of 1750 (chosen for the date of the pre-industrial atmosphere in Figure 6.6) is crucial here: a choice of 1700 would give values about twice as large; a choice of 1776 would give smaller values (particularly using the Hoyt and Schatten series). The range of 0.1 to 0.5 Wm^{-2} given in Figure 6.6 is based on the variability of the series, the differences between the reconstructions and uncertainties concerning stratospheric adjustment (see Section 6.11.2.1). However, because of the large uncertainty in the absolute value of TSI and the reconstruction methods our assessment of the "level of scientific understanding" is "very low".

6.11.2 Mechanisms for Amplification of Solar Forcing

6.11.2.1 Solar ultraviolet variation

The Sun emits radiation over the entire electromagnetic spectrum but with most energy in the near ultraviolet, visible, and near infrared regions: 80% of TSI lies between 400 and 1,600 nm. The variations in TSI, discussed above, of a few tenths of one per cent thus represent the integrated change across ultraviolet, visible, and near infrared wavelengths. Most of this radiation passes through the atmosphere unhindered to the tropopause but shorter wavelengths are absorbed in the middle atmosphere where they result in O_3 formation and local heating. In the ultraviolet the amplitude of variability is much higher. Since 1978 (see Cebula *et al.* (1998) for a review) satellite data have shown variations over the 27-day solar rotation period of e.g., 6% at 200 nm and 2.5% at 250 nm. Problems with sensor drift and calibration preclude direct detection of variability on the 11-year time-scale at wavelengths longer than about 250 nm. Instead ultraviolet irradiance cycles are

deduced from observations by scaling the 27-day variations to selected solar activity indices and assuming that the same scaling applies over longer time-scales (Lean *et al.*, 1997). With the launch of the SOLSTICE (Rottman *et al.*, 1993) and SUSIM (Brueckner *et al.*, 1993) instruments on UARS in 1991, measurements have now been made from near solar maximum to solar minimum with long-term precisions that approach 1% at some wavelengths (Rottman *et al.*, 1993; Floyd *et al.*, 1998). Careful cross-calibration of NOAA-11 SBUV/2 with Shuttle SBUV observations (Cebula *et al.*, 1998) have also produced spectral variations 1989 to 1994, but also with uncertainties of a few per cent, which exceeds the actual irradiance variability at the longer ultraviolet wavelengths. Comparison of the SOLSTICE, SUSIM, and SBUV/2 data show reasonable agreement during their 2 to 3 year overlap period (DeLand and Cebula, 1998) and suggest a decline of about 7% at 200 to 208 nm and of about 3.5% at 250 nm from solar maximum in 1989 to near solar minimum in 1994. These estimates agree well with the modelled scalings deduced from the 27-day variations (Lean *et al.*, 1997).

Variations in stratospheric composition and thermal structure resulting from ultraviolet irradiance changes may have an impact on tropospheric climate. The first mechanism whereby this might happen is through changes in radiative forcing (Haigh, 1994). Thus, in addition to a direct increase in downward short-wave irradiance at the tropopause, higher solar activity can cause an increase in downward infrared flux by heating the stratosphere and also radiative forcing due to O_3 changes. However, the sign of the O_3 effect is not well established. Haigh (1994) found that O_3 increases reduced the solar radiative forcing by about 0.1 Wm^{-2} at solar maximum, Wuebbles *et al.* (1998) computed a value of -0.13 Wm^{-2} due to O_3 increases since the Maunder Minimum and Myhre *et al.* (1998a) about -0.02 Wm^{-2} from minimum to maximum of the solar cycle. Hansen *et al.* (1997a) showed an additional forcing of about +0.05 Wm^{-2} from minimum to maximum of a solar cycle due to O_3 increases and lower stratospheric warming. Haigh (1999) and Larkin *et al.* (2000) suggest that the O_3 effect has little effect on radiative forcing at the tropopause but significant effect on where the additional radiation is absorbed (more within the troposphere rather than at the surface). These disparities may represent the different approaches used. Haigh (1994), Wuebbles *et al.* (1998), and Myhre *et al.* (1998a) calculated the O_3 response using two-dimensional chemical-transport models in which temperature changes are estimated using the fixed dynamic heating approximation. The Hansen *et al.* (1997a) value was deduced from studies with a simplified GCM of sensitivity to slab O_3 changes (of unspecified cause) and the assumption that the solar-induced O_3 change is all within the 10 to 150 hPa region. Haigh (1999) and Larkin *et al.* (2000) specified solar irradiance and O_3 changes and calculated the stratospheric temperature response in GCMs. The negative radiative forcing values probably correspond to O_3 change profiles which peak at higher altitudes, and thus have less impact on lower stratospheric temperature and long-wave radiative forcing, although the different methods for calculating temperature change may also be important.

The response of O_3 to solar variability is not well established. Two-dimensional models (e.g., Haigh, 1994; Fleming *et al.*,

1995; Wuebbles *et al.*, 1998) predict the largest fractional changes in the middle-upper stratosphere with monotonically decreasing effects towards the tropopause. Multiple regression analysis of satellite data as carried out with SBUV data by McCormack and Hood (1996) and SAGE data by Wang *et al.* (1996) suggest the largest changes in the upper and lower stratosphere and zero, or even slightly negative, changes in the middle stratosphere. However, as the data are only available over about one and a half solar cycles, have large uncertainties, especially in the lower stratosphere, and may not properly have accounted for the effects of volcanic aerosol (Solomon *et al.*, 1996), the true nature of solar-induced changes in stratospheric O_3 remains uncertain.

Chandra *et al.* (1999) have estimated tropical tropospheric O_3 column amounts by taking the difference between TOMS total columns in clear-sky areas and those with deep convective cloud. They deduced O_3 changes of the order 10% of the tropospheric column over the eleven year cycle occurring out of phase with the solar forcing. This they ascribed to a self-feedback effect on O_3 production with enhanced levels of O_3 aloft resulting in less ultraviolet reaching the troposphere. However, it is also possible that the O_3 changes reflect a response to solar effects in tropospheric dynamics. If the changes are real then solar radiative forcing, as represented in Figure 6.6, should be reduced by approximately 30% due to solar-induced decreases in tropospheric O_3

Changes in stratospheric thermal structure may also affect the troposphere through dynamical interactions rather than through radiative forcing. Kodera (1995) suggested that changes in stratospheric zonal wind structure, brought about by enhanced solar heating, could interact with vertically propagating planetary waves in the winter hemisphere to produce a particular mode of response. This mode, also seen in response to heating in the lower stratosphere caused by injection of volcanic aerosol, shows dipole anomalies in zonal wind structure which propagate down, over the winter period, into the troposphere. Rind and Balachandran (1995) investigated the impact of large increases in solar ultraviolet on the troposphere with a GCM and confirmed that altered refraction characteristics affect wave propagation in winter high latitudes. Solar cycle changes to wave propagation in the middle atmosphere were also investigated by Arnold and Robinson (1998) who used a three-dimensional model of the atmosphere between 10 and 140 km to study the effects of thermospheric heating. They found that non-linear interactions in the winter hemisphere resulted in changes to the stratospheric circulation. It is not clear that the signals discussed above are statistically robust in any of these studies.

Haigh (1996, 1999), Shindell *et al.* (1999), and Larkin *et al.* (2000) have introduced realistic changes in ultraviolet and O_3 into GCMs and found that the inclusion of the O_3 has a significant effect on simulated climate. Haigh (1999) using a GCM with a lid at 10 hPa and few stratospheric levels, showed a pattern of change in zonal mean temperature which was consistent over a range of assumptions concerning the magnitude of the ultraviolet and O_3 changes. This pattern consisted of warming in the stratosphere (except in winter high latitudes) and a vertical banding structure in the troposphere due to shifts in the positions of the sub-tropical

jets. The predicted changes in 30 hPa geopotential heights were of similar form to those observed by Labitzke and van Loon (1997) but of smaller magnitude (by about a factor 3). Larkin *et al.* (2000) found very similar patterns of change to those of Haigh (1999) using the same solar irradiance/O_3 changes but an entirely different GCM with a lid at 0.1 hPa. Shindell *et al.* (1999) used a model with a detailed representation of the middle atmosphere and a parametrized photochemical scheme which allows O_3 to respond to changes in ultraviolet flux but not to changes in wind fields. They showed larger amplitude changes in 30 hPa heights in the winter hemisphere, more like those of Labitzke and van Loon (1997) but with little summer hemisphere response. These experiments suggest that further work is needed to establish the response of O_3 to solar variability and to how this affects climate.

6.11.2.2 Cosmic rays and clouds

Svensmark and Friis-Christensen (1997) demonstrated a high degree of correlation between total cloud cover, from the ISCCP C2 data set, and cosmic ray flux between 1984 and 1991. Changes in the heliosphere arising from fluctuations in the Sun's magnetic field mean that galactic cosmic rays (GCRs) are less able to reach the Earth when the Sun is more active so the cosmic ray flux is inversely related to solar activity. Svensmark and Friis-Christensen analysed monthly mean data of total cloud using only data over the oceans between 60°S and 60°N from geostationary satellites. They found an increase in cloudiness of 3 to 4% from solar maximum to minimum and speculated that (a) increased GCR flux causes an increase in total cloud and that (b) the increase in total cloud causes a cooling of climate. Svensmark and Friis-Christensen (1997) also extended this analysis to cover the years 1980 to 1996 using cloud data from the DMSP and Nimbus-7 satellites and showed that the high correlation with GCR flux is maintained. However, it was not possible to intercalibrate the different data sets so the validity of the extended data set as a measure of variations in absolute total cloudiness is open to question.

Svensmark (1998) showed that, at least for the limited period of this study, total cloud varies more closely with GCRs than with the 10.7 cm solar activity index over the past solar cycle. On longer time-scales he also demonstrated that Northern Hemisphere surface temperatures between 1937 and 1994 follow variations in cosmic ray flux and solar cycle length more closely than total irradiance or sunspot number. There has been a long-term decrease in cosmic ray flux since the late 17th century, as evidenced by the [10]Be and ^{14}C cosmogenic isotope records (Stuiver and Reimer, 1993; Beer *et al.*, 1994), and this mirrors the long-term increase in TSI. However, the TSI reconstruction of Hoyt and Schatten (1993), which is based on solar cycle lengths, does not appear to track the cosmogenic isotope records any more closely than that of Lean *et al.* (1995), which is based on sunspot cycle amplitude (Lean and Rind, 1998). Such use of different solar indices may help to identify which physical mechanisms, if any, are responsible for the apparent meteorological responses to solar activity.

Kuang *et al.* (1998) have repeated Svensmark and Friis-Christensen's analysis of ISCCP data and showed high correlations with an El Niño-Southern Oscillation (ENSO) index

difficult to distinguish from the GCR flux. Farrar (2000) showed that the pattern of change in cloudiness over that period, particularly in the Pacific Ocean, corresponds to what would be expected for the atmospheric circulation changes characteristic of El Niño. Kernthaler *et al.* (1999) have also studied the ISCCP dataset, using both geostationary and polar orbiter data and suggested that the correlation with cosmic ray flux is reduced if high latitude data are included. This would not be expected if cosmic rays were directly inducing increases in cloudiness, as cosmic ray flux is greatest at high latitudes. Kernthaler *et al.* (1999), Jørgensen and Hansen (2000), and Gierens and Ponater (1999), also noted that a mechanism whereby cosmic rays resulted in greater cloud cover would be most likely to affect high cloud as ionisation is greatest at these altitudes. Even if high cloud did respond to cosmic rays, it is not clear that this would cause global cooling as for thin high cloud the long-wave warming effects dominate the short-wave cooling effect. Kristjánsson and Kristiansen (2000) have additionally analysed the ISCCP D2 dataset, 1989 to 1993, and found little statistical evidence of a relationship between GCRs and cloud cover with the possible exception of low marine clouds in mid-latitudes. They also noted that there was no correlation between outgoing long-wave radiation, as represented in ERBE data, and GCRs. Thus the evidence for a cosmic ray impact on cloudiness remains unproven.

A further consideration must be potential physical mechanisms whereby cosmic rays might enhance cloudiness. Cosmic rays are the principal source of ionisation in the free troposphere. Furthermore, ionisation rates and atmospheric conductivity are observed to vary with solar activity. Svensmark and Friis-Christensen (1997) propose that the correlation between cosmic rays and cloud cover that they observed is due to an increase in efficiency of charged particles, over uncharged ones, in acting as cloud condensation nuclei. There is evidence for this occurring in thunderstorms (Pruppacher and Klett, 1997) but it is not clear to what extent this affects cloud development. There is also evidence that ions are sometimes critical in gas-to-particle conversion but again there is no evidence that this has any impact on cloud formation.

In a series of papers, Brian Tinsley has developed a more detailed mechanism for a link between cosmic rays and cloudiness (e.g., Tinsley, 1996). This is based on the premise that aerosols ionised by cosmic rays are more effective as ice nuclei and cause freezing of supercooled water in clouds. In clouds that are likely to cause precipitation the latent heat thus released then causes enhanced convection which promotes cyclonic development and hence increased storminess. There is some laboratory evidence to suggest that charging increases ice nucleation efficiency (Pruppacher, 1973) although there is no observational evidence of this process taking place in the atmosphere. Furthermore, only a small proportion of aerosol particles are capable of acting as ice nuclei, depending on chemical composition or shape. There are also laboratory studies (Abbas and Latham, 1969) which indicate the existence of "electrofreezing", but again no evidence in the real atmosphere. Thus Tinsley's mechanism is plausible but requires further observational and modelling studies to establish whether or not it could be of sufficient magnitude to result in the claimed effects (Harrison and Shine, 1999).

We conclude that mechanisms for the amplification of solar forcing are not well established. Variations in ultraviolet and solar-induced changes in O_3 may have a small effect on radiative forcing but additionally may affect climate through changing the distribution of solar heating and thus indirectly through a dynamical response. At present there is insufficient evidence to confirm that cloud cover responds to solar variability.

6.12 Global Warming Potentials

6.12.1 Introduction

Just as radiative forcing provides a simplified means of comparing the various factors that are believed to influence the climate system to one another, Global Warming Potentials (GWPs) are one type of simplified index based upon radiative properties that can be used to estimate the potential future impacts of emissions of different gases upon the climate system in a relative sense. The formulation of GWPs, reasons for the choice of various time horizons, and the effects of clouds, scenarios, and many other factors upon GWP values were discussed in detail in IPCC (1994). That discussion will not be repeated here. Section 6.2 discusses the relationship between radiative forcing and climate response and describes recent studies that have supported the view that many different kinds of forcing agents (e.g., various greenhouse gases, sulphate aerosols, solar activity, etc.) yield similar globally averaged climate responses per Wm^{-2} of forcing (albeit with different spatial patterns in some important cases). These parallels in global mean climate responses have motivated the use of simplified measures to estimate in an approximate fashion the relative effects of emissions of different gases on climate. The emphasis on relative rather than absolute effects (such as computed temperature change) avoids dependence upon any particular model of climate response.

The impact of greenhouse gas emissions upon the atmosphere is related not only to radiative properties, but also to the time-scale characterising the removal of the substance from the atmosphere. Radiative properties control the absorption of radiation per kilogram of gas present at any instant, but the lifetime (or adjustment time, see Chapter 4) controls how long an emitted kilogram is retained in the atmosphere and hence is able to influence the thermal budget. The climate system responds to changes in the thermal budget on time-scales ranging from the order of months to millennia depending upon processes within the atmosphere, ocean, cryosphere, etc. GWPs are a measure of the relative radiative effect of a given substance compared to another, integrated over a chosen time horizon. The choice of the time horizon depends in part upon whether the user wishes to emphasise shorter-term processes (e.g., responses of cloud cover to surface temperature changes) or longer-term phenomena (such as sea level rise) that are linked to sustained alterations of the thermal budget (e.g., the slow transfer of heat between, for example, the atmosphere and ocean). In addition, if the speed of potential climate change is of greatest interest (rather than the

eventual magnitude), then a focus on shorter time horizons can be useful (IPCC, 1994; Skodvin and Fuglestvedt, 1997; Fuglestvedt *et al.*, 2000; Smith and Wigley, 2000a,b).

As in previous reports, here we present GWPs for 20, 100, and 500 year time horizons. The most recent GWP evaluations are those of WMO (1999) and the SAR, and the results presented here are drawn in large part from those assessments, with updates for those cases where significantly different new laboratory or radiative transfer results have been published. The sources used for input variables for the GWP calculations are indicated in this section and in the headers and footnotes to the tables, where sources of new estimates since the SAR are identified.

The GWP has been defined as the ratio of the time-integrated radiative forcing from the instantaneous release of 1 kg of a trace substance relative to that of 1 kg of a reference gas (IPCC, 1990):

$$GWP(x) = \frac{\int_0^{TH} a_x \cdot [x(t)] \, dt}{\int_0^{TH} a_r \cdot [r(t)] \, dt} \qquad (6.2)$$

where *TH* is the time horizon over which the calculation is considered, a_x is the radiative efficiency due to a unit increase in atmospheric abundance of the substance in question (i.e., $Wm^{-2} kg^{-1}$), [x(t)] is the time-dependent decay in abundance of the instantaneous release of the substance, and the corresponding quantities for the reference gas are in the denominator. The GWP of any substance therefore expresses the integrated forcing of a pulse (of given small mass) of that substance relative to the integrated forcing of a pulse (of the same mass) of the reference gas over some time horizon. The numerator of Equation 6.2 is the absolute (rather than relative) GWP of a given substance, referred to as the AGWP. The GWPs of various greenhouse gases can then be easily compared to determine which will cause the greatest integrated radiative forcing over the time horizon of interest. The direct relative radiative forcings per ppbv are derived from infrared radiative transfer models based on laboratory measurements of the molecular properties of each substance and considering the molecular weights. Updated information since the SAR is presented for many gases in Section 6.3. Many important changes in these quantities were recently reviewed in WMO (1999) and will be briefly summarised here. In addition, some gases can indirectly affect radiative forcing, mainly through chemical processes. For example, tropospheric O_3 provides a significant radiative forcing of the climate system, but its production occurs indirectly, as a result of atmospheric chemistry following emissions of precursors such as NO_x, CO, and NMHCs (see Section 6.6 and Chapter 4). Indirect effects will be described below for a number of key gases.

It is important to distinguish between the integrated relative effect of an emitted kilogram of gas which is represented by a GWP and the actual radiative forcings for specific gas amounts presented, for example, in Section 6.3 and in Figure 6.6. GWPs are intended for use in studying relative rather than absolute impacts of emissions, and pertain to specific time horizons.

The radiative efficiencies a_r and a_x are not necessarily constant over time. While the absorption of infrared radiation by many greenhouse gases varies linearly with their abundance, a

few important ones display non-linear behaviour for current and likely future abundances (e.g., CO_2, CH_4, and N_2O). For those gases, the relative radiative forcing will depend upon abundance and hence upon the future scenario adopted. These issues were discussed in detail and some sensitivities to chosen scenarios were presented in IPCC (l994).

A key aspect of GWP calculations is the choice of the reference gas, taken here to be CO_2. In IPCC (l994), it was shown, for example, that a particular scenario for future growth of CO_2 (S650, see Chapter 3) would change the denominator of Equation 6.2 by as much as 15% compared to a calculation employing constant pre-industrial CO_2 mixing ratios.

The atmospheric response time of CO_2 is subject to substantial scientific uncertainties, due to limitations in our knowledge of key processes including its uptake by the biosphere and ocean. When CO_2 is used as the reference, the numerical values of the GWPs of all greenhouse gases can change substantially as research improves the understanding of the removal processes of CO_2. The removal function for CO_2 used for the GWPs presented here is based upon carbon cycle models such as those discussed in Chapter 3. The CO_2 radiative efficiency (a_r) used in this report has been updated since the SAR, as discussed in Section 6.3 (see below).

The lifetimes of non-CO_2 greenhouse gases are dependent largely on atmospheric photochemistry, which controls photolysis and related removal processes as discussed in Chapter 4. When the lifetime of the gas in question is comparable to the response time of CO_2 (nominally about 150 years, although it is clear that the removal of CO_2 cannot be adequately described by a single, simple exponential lifetime; see IPCC (l994) and the discussion below), the GWP is relatively insensitive to choice of time horizon, i.e., for N_2O. When the lifetime of the gas in question differs substantially from the response time of the reference gas, the GWP becomes sensitive to the choice of time horizon, which in turn implies a decision regarding climate processes and impacts of interest, as noted above. For longer time horizons, those species that decay more rapidly than the reference gas display decreasing GWPs, with the slope of the decay being dependent mainly on the lifetime of the gas in question. Gases with lifetimes much longer than that of the reference gas (e.g., C_2F_6) display increasing GWPs over long time horizons (i.e., greater than a hundred years). We emphasise that the GWP is an integral from zero to the chosen time horizon; hence the values presented in the table for 25, 100, and 500 years are not additive.

A number of studies have suggested modified or different indices for evaluating relative future climate effects. Here we provide only an indication of the kinds of issues that are being considered in these alternative indices. Wuebbles and Calm (l997) emphasised the fact that some halocarbon substitutes used, for example, in refrigeration are less efficient than the CFCs they are replacing, so that more energy is consumed through their use and hence more CO_2 emitted per hour of operation. Evaluation of these technological factors would only be possible through detailed emission inventories coupled with scenarios, and are not included here. Some studies have argued for use of "discount rates" to reflect increasing uncertainty and

changing policies with time (e.g., to account for the possibility that new technologies will emerge to solve problems; see for example Lashof and Ahuja, l990; Reilly *et al.*, l999). Economic factors could be considered along with the technological ones mentioned above, adding another aspect to any scenario. These are not included here. Smith and Wigley (2000a,b), Fuglestvedt *et al.* (2000), and Reilly *et al.* (l999) have examined the relationship between GWPs and climate response using simple energy balance models. These studies emphasised the point made above regarding the links between choice of time horizon, lifetime of a particular substance, and the climate response of interest, noting for example that while the 100-year GWP for N_2O represented the model-calculated temperature responses (both instantaneous and integrated over time), and the calculated sea level rise to good accuracy, that for CH_4 (a short-lived gas with a lifetime of about 10 years) represented sea level rise far better than it did the instantaneous temperature change for that time horizon. For very short-lived gases, GWPs are often calculated using a 'slab' (continuous) rather than pulse emission. This approach involves the assumption of specific scenarios for the magnitudes of the slabs. For some very short-lived gases such as NMHCs, models must employ 'slab' emissions in GWP analyses since their impact depends critically on non-linear coupled chemical processes. Some examples are given in Sections 6.12.3.2 and 6.12.3.4.

6.12.2 Direct GWPs

The CO_2 response function used in this report is the same as that in WMO (l999) and the SAR and is based on the "Bern" carbon cycle model (see Siegenthaler and Joos, 1992; Joos *et al.*, l996) run for a constant future mixing ratio of CO_2 over a period of 500 years. The Bern carbon cycle model was compared to others in IPCC (l994), where it was shown that different models gave a range of as much as 20% in the CO_2 response, with the greatest differences occurring over time-scales greater than 20 years.

The radiative efficiency per kilogram of CO_2 has been updated compared to previous IPCC assessments (IPCC, 1994; SAR). Here we employ the approach discussed in WMO (l999) using the simplified formula presented in Table 6.2. We assume a background CO_2 mixing ratio of 364 ppmv, close to the present day value (WMO (1995) used 354 ppmv). For this assumption, this expression agrees well with the adjusted total-sky radiative forcing calculations of Myhre and Stordal (1997); see also Myhre *et al.* (1998b). The revised forcing is about 12% lower than that in the SAR. For a small perturbation in CO_2 from 364 ppmv, the radiative efficiency is $0.01548 \ Wm^{-2} \ ppmv^{-1}$. This value is used in the GWP calculations presented here. We emphasise that it applies only to GWP calculations and cannot be used to obtain the total radiative forcing for this key gas since pre-industrial times, due to time-dependent changes in mixing ratio as noted above. Because of this change in the CO_2 forcing per mass, the CO_2 AGWPs are 0.207, 0.696, and 2.241 Wm^{-2}/yr /ppmv^{-1} for 20, 100, and 500 year time horizons, respectively. These are smaller than the values used in the SAR by 13%. AGWPs for any gas can be obtained from the GWP values given in the tables presented here by multiplying by these numbers.

The decreases in the CO_2 AGWPs will lead to proportionately larger GWPs for other gases compared to previous IPCC assessments, in the absence of other changes. In Tables 6.7 and 6.8, GWPs (on a mass basis) for 93 gases are tabulated for time horizons of 20, 100, and 500 years. The list includes CH_4, N_2O, CFCs, HCFCs, HFCs, hydrochlorocarbons, bromocarbons, iodocarbons, fully fluorinated species, fluoroalcohols, and fluoroethers. The radiative efficiencies per kilogram were derived from the values given per ppbv in Section 6.3. Several of these have been updated since the SAR, most notably that of CFC-11. Since the radiative forcings of the halocarbon replacement gases are scaled relative to CFC-11 in GWP calculations, the GWPs of those gases are also affected by this change. As discussed further in Section 6.3, the change in radiative forcing for CFC-11 reflects new studies (Pinnock *et al.,* 1995; Christidis *et al.,* l997; Hansen *et al.*, l997a; Myhre and Stordal, 1997; Good *et al.*, 1998) suggesting that the radiative forcing of this gas is about 0.25 Wm^{-2} $ppbv^{-1}$, an increase of about 14% compared to the value adopted in earlier IPCC reports, which was based on the study of Hansen *et al.* (l988).

The lifetimes and adjustment times used in Tables 6.7 and 6.8 come from Chapter 4 except where noted. For some gases (including several of the fluoroethers), lifetimes have not been derived from laboratory measurements, but have been estimated by various other means. For this reason, the lifetimes for these gases, and hence the GWPs, are considered to be much less reliable, and so these gases are listed separately in Table 6.8. NF_3 is listed in Table 6.8 because, although its photolytic destruction has been characterised, other loss processes may be significant but have not yet been characterised (Molina *et al.*, 1995). Note also that some gases, for example, trifluoromethyl iodide (CF_3I) and dimethyl ether (CH_3OCH_3) have very short lifetimes (less than a few months); GWPs for such very short-lived gases may need to be treated with caution, because the gases are unlikely to be evenly distributed globally, and hence estimates of, for example, their radiative forcing using global mean conditions may be subject to error.

Uncertainties in the lifetimes of CFC-11 and CH_3CCl_3 are thought to be about 10%, while uncertainties in the lifetimes of gases obtained relative to CFC-11 or CH_3CCl_3 are somewhat larger (20 to 30%) (SAR; WMO, l999). Uncertainties in the radiative forcing per unit mass of the majority of the gases considered in Table 6.7 are approximately ± 10%. The SAR suggested typical uncertainties of ± 35% (relative to the reference gas) for the GWPs, and we retain this uncertainty estimate for gases listed in Table 6.7. In addition to uncertainties in the CO_2 radiative efficiency per kilogram and in the response function, AGWPs of CO_2 are affected by assumptions concerning future CO_2 abundances as noted above. Furthermore, as the CO_2 mixing ratios and climate change, the pulse response function changes as well. In spite of these dependencies on the choice of future emission scenarios, it remains likely that the error introduced by these assumptions is smaller than the uncertainties introduced by our imperfect understanding of the carbon cycle (see Chapter 3). Finally, although any induced error in the CO_2 AGWPs will certainly affect the non-CO_2 GWPs, it will not affect intercomparisons among non-CO_2 GWPs.

6.12.3 Indirect GWPs

We next consider discuss indirect effects in more detail, and present GWPs for other gases, including estimates of their impacts. While direct GWPs are usually believed to be known reasonably accurately (±35%), indirect GWPs can be highly uncertain. A number of different processes contribute to indirect effects for various molecules; many of these are also discussed in Section 6.6.

6.12.3.1 Methane

Four types of indirect effects due to the presence of atmospheric CH_4 have been identified (see Chapter 4 and Section 6.6). The largest effect is potentially the production of O_3 (25% of the direct effect, or 19% of the total, as in the SAR). This effect is difficult to quantify, however, because the magnitude of O_3 production is highly dependent on the abundance and distribution of NO_x (IPCC, 1994; SAR). Other indirect effects include the production of stratospheric water vapour (assumed here to represent 5% of the direct effect, or 4% of the total, as in the SAR), the production of CO_2 (from certain CH_4 sources), and the temporal changes in the CH_4 adjustment time resulting from its coupling with OH (Lelieveld and Crutzen, 1992; Brühl, 1993; Prather, 1994, 1996; SAR; Fuglestvedt *et al.*, 1996). Here we adopt the values for each of these terms as given in the SAR, with a correction for the updated CO_2 AGWPs and adopting the perturbation lifetime given in Chapter 4. It should be noted that the climate forcing caused by CO_2 produced from the oxidation of CH_4 is not included in these GWP estimates. As discussed in the SAR, it is often the case that this CO_2 is included in national carbon production inventories. Therefore, depending on how the inventories are combined, including the CO_2 production from CH_4 could result in double counting this CO_2.

6.12.3.2 Carbon monoxide

CO has a small direct GWP but leads to indirect radiative effects that are similar to those of CH_4. As in the case of CH_4, the production of CO_2 from oxidised CO can lead to double counting of this CO_2 and is therefore not considered here. The emission of CO perturbs OH, which in turn can then lead to an increase in the CH_4 lifetime (Fuglestvedt *et al*., l996; Prather, 1996; Daniel and Solomon, 1998). This term involves the same processes whereby CH_4 itself influences its own lifetime and hence GWP values (Prather, l996) and is subject to similar uncertainty. This term can be evaluated with reasonable accuracy using a box model, as shown by Prather (l996) and Daniel and Solomon (1998). Emissions of CO can also lead to the production of O_3 (see Chapter 4), with the magnitude of O_3 formation dependent on the amount of NO_x present. As with CH_4, this effect is quite difficult to quantify due to the highly variable and uncertain NO_x distribution (e.g., Emmons *et al.*, 1997). Because of the difficulty in accurately calculating the amount of O_3 produced by CO emissions, an accurate estimate of the entire indirect forcing of CO requires a three-dimensional chemical model. Table 6.9 presents estimates of the CO GWP due to O_3 production and to feedbacks on the CH_4 cycle from two recent multi-dimensional model studies (in which a "slab" emission of CO was imposed),

Table 6.7: *Direct Global Warming Potentials (mass basis) relative to carbon dioxide (for gases for which the lifetimes have been adequately characterised).*

Gas		Radiative efficiency $(Wm^{-2}ppb^{-1})$ (from (b) unless indicated)	Lifetime (years) (from Chapter 4 unless indicated)	Global Warming Potential Time horizon		
				20 years	100 years	500 years
Carbon dioxide	CO_2	See Section 6.12.2	See Section 6.12.2	1	1	1
Methane	CH_4	$3.7x10^{-4\,\Sigma}$	12.0*	62	23	7
Nitrous oxide	N_2O	$3.1x10^{-3\,\Sigma}$	114*	275	296	156
Chlorofluorocarbons						
CFC-11	CCl_3F	0.25	45	6300	4600	1600
CFC-12	CCl_2F_2	0.32	100	10200	10600	5200
CFC-13	$CClF_3$	0.25	640 (c)	10000	14000	16300
CFC-113	CCl_2FCClF_2	0.30	85	6100	6000	2700
CFC-114	$CClF_2CClF_2$	0.31	300	7500	9800	8700
CFC-115	CF_3CClF_2	$0.18^{\dagger}$	1700	4900	7200	9900
Hydrochlorofluorocarbons						
HCFC-21	$CHCl_2F$	0.17	2.0 (d)	700	210	65
HCFC-22	$CHClF_2$	$0.20^{\S}$	11.9	4800	1700	540
HCFC-123	CF_3CHCl_2	0.20	1.4 (a)	390	120	36
HCFC-124	CF_3CHClF	0.22	6.1 (a)	2000	620	190
HCFC-141b	CH_3CCl_2F	0.14	9.3	2100	700	220
HCFC-142b	CH_3CClF_2	0.20	19	5200	2400	740
HCFC-225ca	$CF_3CF_2CHCl_2$	0.27	2.1 (a)	590	180	55
HCFC-225cb	$CClF_2CF_2CHClF$	0.32	6.2 (a)	2000	620	190
Hydrofluorocarbons						
HFC-23	CHF_3	$0.16^{\S}$	260	9400	12000	10000
HFC-32	CH_2F_2	$0.09^{\S}$	5.0	1800	550	170
HFC-41	CH_3F	0.02	2.6	330	97	30
HFC-125	CHF_2CF_3	$0.23^{\S}$	29	5900	3400	1100
HFC-134	CHF_2CHF_2	0.18	9.6	3200	1100	330
HFC-134a	CH_2FCF_3	$0.15^{\S}$	13.8	3300	1300	400
HFC-143	CHF_2CH_2F	0.13	3.4	1100	330	100
HFC-143a	CF_3CH_3	$0.13^{\S}$	52	5500	4300	1600
HFC-152	CH_2FCH_2F	0.09	0.5	140	43	13
HFC-152a	CH_3CHF_2	$0.09^{\S}$	1.4	410	120	37
HFC-161	CH_3CH_2F	0.03	0.3	40	12	4
HFC-227ea	CF_3CHFCF_3	0.30	33.0	5600	3500	1100
HFC-236cb	$CH_2FCF_2CF_3$	0.23	13.2	3300	1300	390
HFC-236ea	CHF_2CHFCF_3	0.30	10.0	3600	1200	390
HFC-236fa	$CF_3CH_2CF_3$	0.28	220	7500	9400	7100
HFC-245ca	$CH_2FCF_2CHF_2$	0.23	5.9	2100	640	200
HFC-245fa	$CHF_2CH_2CF_3$	$0.28^{\&}$	7.2	3000	950	300
HFC-365mfc	$CF_3CH_2CF_2CH_3$	0.21 (k)	9.9	2600	890	280
HFC-43-10mee	$CF_3CHFCHFCF_2CF_3$	0.40	15	3700	1500	470
Chlorocarbons						
CH_3CCl_3		0.06	4.8	450	140	42
CCl_4		$0.13^{\dagger\dagger}$	35	2700	1800	580
$CHCl_3$		$0.11^{\S}$	0.51 (a)	100	30	9
CH_3Cl		0.01	1.3 (b)	55	16	5
CH_2Cl_2		0.03	0.46 (a)	35	10	3

Gas		Radiative Efficiency ($Wm^{-2} ppb^{-1}$) (from (b) unless indicated)	Lifetime (years) (from Chapter 4 unless indicated)	Global Warming Potential Time horizon		
				20 years	100 years	500 years
Bromocarbons						
CH_3Br		0.01	0.7 (b)	16	5	1
CH_2Br_2		0.01	0.41 (i)	5	1	<<1
$CHBrF_2$		0.14	7.0 (i)	1500	470	150
Halon-1211	$CBrClF_2$	0.30	11	3600	1300	390
Halon-1301	$CBrF_3$	0.32	65	7900	6900	2700
Iodocarbons						
CF_3I		0.23	0.005 (a)	1	1	<<1
Fully fluorinated species						
SF_6		0.52	3200	15100	22200	32400
CF_4		0.08	50000	3900	5700	8900
C_2F_6		0.26[§]	10000	8000	11900	18000
C_3F_8		0.26	2600	5900	8600	12400
C_4F_{10}		0.33	2600	5900	8600	12400
c-C_4F_8		0.32[§]	3200	6800	10000	14500
C_5F_{12}		0.41	4100	6000	8900	13200
C_6F_{14}		0.49	3200	6100	9000	13200
Ethers and Halogenated Ethers						
CH_3OCH_3		0.02	0.015 (e)	1	1	<<1
$(CF_3)_2CFOCH_3$		0.31	3.4 (l)	1100	330	100
$(CF_3)CH_2OH$		0.18	0.5 (m)	190	57	18
$CF_3CF_2CH_2OH$		0.24	0.4 (m)	140	40	13
$(CF_3)_2CHOH$		0.28	1.8 (m)	640	190	59
HFE-125	CF_3OCHF_2	0.44	150	12900	14900	9200
HFE-134	CHF_2OCHF_2	0.45	26.2	10500	6100	2000
HFE-143a	CH_3OCF_3	0.27	4.4	2500	750	230
HCFE-235da2	$CF_3CHClOCHF_2$	0.38	2.6 (i)	1100	340	110
HFE-245cb2	$CF_3CF_2OCH_3$	0.32	4.3 (l)	1900	580	180
HFE-245fa2	$CF_3CH_2OCHF_2$	0.31	4.4 (i)	1900	570	180
HFE-254cb2	$CHF_2CF_2OCH_3$	0.28	0.22 (h)	99	30	9
HFE-347mcc3	$CF_3CF_2CF_2OCH_3$	0.34	4.5 (l)	1600	480	150
HFE-356pcf3	$CHF_2CF_2CH_2OCHF_2$	0.39	3.2 (n)	1500	430	130
HFE-374pc2	$CHF_2CF_2OCH_2CH_3$	0.25	5.0 (n)	1800	540	170
HFE-7100	$C_4F_9OCH_3$	0.31	5.0 (f)	1300	390	120
HFE-7200	$C_4F_9OC_2H_5$	0.30 [Ω]	0.77 (g)	190	55	17
H-Galden 1040x	$CHF_2OCF_2OC_2F_4OCHF_2$	1.37(j) [Ω]	6.3 [Ω]	5900	1800	560
HG-10	$CHF_2OCF_2OCHF_2$	0.66 [Ω]	12.1 [Ω]	7500	2700	850
HG-01	$CHF_2OCF_2CF_2OCHF_2$	0.87 [Ω]	6.2 [Ω]	4700	1500	450

* The values for CH_4 and N_2O are adjustment times including feedbacks of emission on lifetimes (see Chapter 4).
[Σ] From the formulas given in Table 6.2, with updated constants based on the IPCC (1990) expressions.

Note: For all gases destroyed by reaction with OH, updated lifetimes include scaling to CH_3CCl_3 lifetimes, as well as an estimate of the stratospheric destruction. See references below for rates along with Chapter 4 and WMO (1999).
(a) Taken from the SAR   (b) Taken from WMO (1999) (c) Taken from WMO (1995) (d) DeMore *et al.* (1997)
(e) Good *et al.* (1998)   (f) Wallington *et al.* (1997)   (g) Christensen *et al.* (1998) (h) Heathfield *et al.* (1998a)
(i) Christidis *et al.* (1997)   (j) Gierczak *et al.* (1996)   (k) Barry *et al.* (1997)   (l) Tokuhashi *et al.* (1999a)
(m) Tokuhashi *et al.* (1999b) (n) Tokuhashi *et al.* (2000)

[†] Myhre *et al.* (1998b)   [††] Jain *et al.* (2000)   [§] Highwood and Shine (2000)   [&] Ko *et al.* (1999).
[Ω] See Cavalli *et al.* (1998) and Myhre *et al.* (1999)

Table 6.8: *Direct Global Warming Potentials (mass basis) relative to carbon dioxide (for gases for whose lifetime has been determined only via indirect means, rather than laboratory measurements, or for whom there is uncertainty over the loss processes). Radiative efficiency is defined with respect to all sky.*

Gas		Radiative efficiency $(Wm^{-2} ppb^{-1})$ (from (b) unless indicated)	Estimated lifetime (years)	Global Warming Potential Time horizon		
				20 years	100 years	500 years
NF_3		0.13	740 (a)	7700	10800	13100
SF_5CF_3		0.57 (d)	>1000*	>12200	>17500	>22500
$c\text{-}C_3F_6$		0.42	>1000*	>11800	>16800	>21600
HFE-227ea	$CF_3CHFOCF_3$	0.40	11 (c)	4200	1500	460
HFE-236ea2	$CF_3CHFOCHF_2$	0.44	5.8 (c)	3100	960	300
HFE-236fa	$CF_3CH_2OCF_3$	0.34	3.7 (c)	1600	470	150
HFE-245fa1	$CHF_2CH_2OCF_3$	0.30	2.2 (c)	940	280	86
HFE-263fb2	$CF_3CH_2OCH_3$	0.20	0.1 (c)	37	11	3
HFE-329mcc2	$CF_3CF_2OCF_2CHF_2$	0.49	6.8 (c)	2800	890	280
HFE-338mcf2	$CF_3CF_2OCH_2CF_3$	0.43	4.3 (c)	1800	540	170
HFE-347mcf2	$CF_3CF_2OCH_2CHF_2$	0.41	2.8 (c)	1200	360	110
HFE-356mec3	$CF_3CHFCF_2OCH_3$	0.30	0.94 (c)	330	98	30
HFE-356pcc3	$CHF_2CF_2CF_2OCH_3$	0.33	0.93 (c)	360	110	33
HFE-356pcf2	$CHF_2CF_2OCH_2CHF_2$	0.37	2.0 (c)	860	260	80
HFE-365mcf3	$CF_3CF_2CH_2OCH_3$	0.27	0.11 (c)	38	11	4
$(CF_3)_2CHOCHF_2$		0.41	3.1 (c)	1200	370	110
$(CF_3)_2CHOCH_3$		0.30	0.25 (c)	88	26	8
$\text{-}(CF_2)_4CH(OH)\text{-}$		0.30	0.85 (c)	240	70	22

(a) Molina *et al.* (1995).
(b) WMO (1999).
(c) Imasu *et al.* (1995).
(d) Sturges *et al.* (2000).
* Estimated lower limit based upon perfluorinated structure.

along with the box-model estimate for the latter term alone from Daniel and Solomon (1998), which is based on the analytical formalism developed by Prather (1996). Table 6.9 shows that the 100-year GWP for CO is likely to be 1.0 to 3.0, while that for shorter time horizons is estimated at 2.8 to 10. These estimates are subject to large uncertainties, as discussed further in Chapter 4.

6.12.3.3 Halocarbons
In addition to their direct radiative forcing, chlorinated and brominated halocarbons can lead to a significant indirect forcing through their destruction of stratospheric O_3 (Section 6.4). By destroying stratospheric O_3, itself a greenhouse gas, halocarbons induce a negative indirect forcing that counteracts some or perhaps all (in certain cases) of their direct forcing. Furthermore, decreases in stratospheric O_3 act to increase the ultraviolet field of the troposphere and hence can increase OH and deplete those gases destroyed by reaction with the OH radical (particularly CH_4); this provides an additional negative forcing. Quantifying the magnitude of the negative indirect forcing is quite difficult for several reasons. As discussed in Section 6.4, the negative forcing

arising from the O_3 destruction is highly dependent on the altitude profile of the O_3 loss. The additional radiative effect due to enhanced tropospheric OH is similarly difficult to quantify (see e.g., WMO, 1999). While recognising these uncertainties, estimates have been made of the net radiative forcing due to particular halocarbons, which can then be used to determine net GWPs (including both direct and indirect effects). This was done by Daniel *et al.* (1995), where it was shown that if the enhanced tropospheric OH effect were ignored, and the negative forcing due to O_3 loss during the 1980s was −0.08 Wm^{-2}, the net GWPs for the bromocarbons were significantly negative, illustrating the impact of the negative forcing arising from the bromocarbon-induced ozone depletion. While the effect on the chlorocarbon GWPs was less pronounced, it was significant as well. Table 6.10 updates the results from Daniel *et al.*'s "constant-alpha" case A as in WMO (1999), where the effectiveness of bromine for O_3 loss relative to chlorine (called alpha) has been increased from 40 to 60. The updated radiative efficiency of CO_2 has also been included. An uncertainty in the 1980 to 1990 O_3 radiative forcing of −0.03 to −0.15 Wm^{-2} has been adopted based upon Section

Table 6.9: *Estimated indirect Global Warming Potentials for CO for time horizons of 20, 100, and 500 years.*

	Indirect Global Warming Potentials Time horizon		
	20 years	100 years	500 years
Daniel and Solomon (1998): box model considering CH$_4$ feedbacks only	2.8	1.0	0.3
Fuglestvedt *et al.* (1996): two-dimensional model including CH$_4$ feedbacks and tropospheric O$_3$ production by CO itself	10	3.0	1.0
Johnson and Derwent (1996): two-dimensional model including CH$_4$ feedbacks and tropospheric O$_3$ production by CO itself	—	2.1	—

Table 6.10: *Net Global Warming Potentials (mass basis) of selected halocarbons (updated from Daniel et al., 1995; based upon updated stratospheric O$_3$ forcing estimates, lifetimes, and radiative data from this report).*

Species	Time horizon = 2010 (20 years)			Time horizon = 2090 (100 years)		
	Direct	Min	Max	Direct	Min	Max
CFC-11	6300	100	5000	4600	−600	3600
CFC-12	10200	7100	9600	10600	7300	9900
CFC-113	6100	2400	5300	6000	2200	5200
HCFC-22	4800	4100	4700	1700	1400	1700
HCFC-123	390	100	330	120	20	100
HCFC-124	2000	1600	1900	620	480	590
HCFC-141b	2100	180	1700	700	−5	570
HCFC-142b	5200	4400	5100	2400	1900	2300
CHCl$_3$	450	−1800	10	140	−560	0
CCl$_4$	2700	−4700	1300	1800	−3900	660
CH$_3$Br	16	−8900	−1700	5	−2600	−500
Halon-1211	3600	−58000	−8600	1300	−24000	−3600
Halon-1301	7900	−79000	−9100	6900	−76000	−9300

6.4, and these correspond (respectively) to the maximum and minimum GWP estimates given in Table 6.10.

6.12.3.4 NO$_x$ and non-methane hydrocarbons

The short lifetimes and complex non-linear chemistries of NO$_x$ and NMHC make calculation of their indirect GWPs a challenging task subject to very large uncertainties (see Chapter 4). However, IPCC (l999) has probed in detail the issue of the relative differences in the impacts of NO$_x$ upon O$_3$ depending on where it is emitted (in particular, surface emissions versus those from aircraft). Higher altitude emissions have greater impacts both because of longer NO$_x$ residence times and more efficient tropospheric O$_3$ production, as well as enhanced radiative forcing sensitivity (see Section 6.5). Two recent two-dimensional model studies (Fuglestvedt *et al.*, l996; Johnson and Derwent, l996) have presented estimates of the GWPs for NO$_x$ emitted from aircraft. These studies suggest GWPs of the order of 450 for aircraft NO$_x$ emissions considering a 100-year time horizon, while those for surface emissions are likely to be much smaller, of the order of 5. While such numerical values are subject to very large quantitative uncertainties, they illustrate that the emissions of NO$_x$ from aircraft are characterised by far greater GWPs than those of surface sources, due mainly to the longer lifetime of the emitted NO$_x$ at higher altitudes.

6.13 Global Mean Radiative Forcings

6.13.1 Estimates

The global, annual mean radiative forcing estimates from 1750 to the present (late 1990s; about 2000) for the different agents are plotted in Figure 6.6, based on the discussions in the foregoing sections. As in the SAR, the height of the rectangular bar denotes a central or best estimate of the forcing, while the vertical line about the bar is an estimate of the uncertainty range, guided by the spread in the published results and physical understanding, and with no statistical connotation. The uncertainty range, as employed in this chapter, is not the product of systematic quantitative analyses of the various factors associated with the forcing, and thus lacks a rigorous statistical basis. The usage here is different from the manner "uncertainty range" is defined and addressed elsewhere in this document. The SAR had also stated a "confidence level" which represented a subjective judgement that the actual forcing would lie within the specified uncertainty range. In order to avoid the confusion over the use of the term "confidence level", we introduce in this assessment a "level of scientific understanding" (LOSU) that represents, again, a subjective judgement and expresses somewhat similar notions as in the SAR (refer also to IPCC, 1999). The LOSU index for each
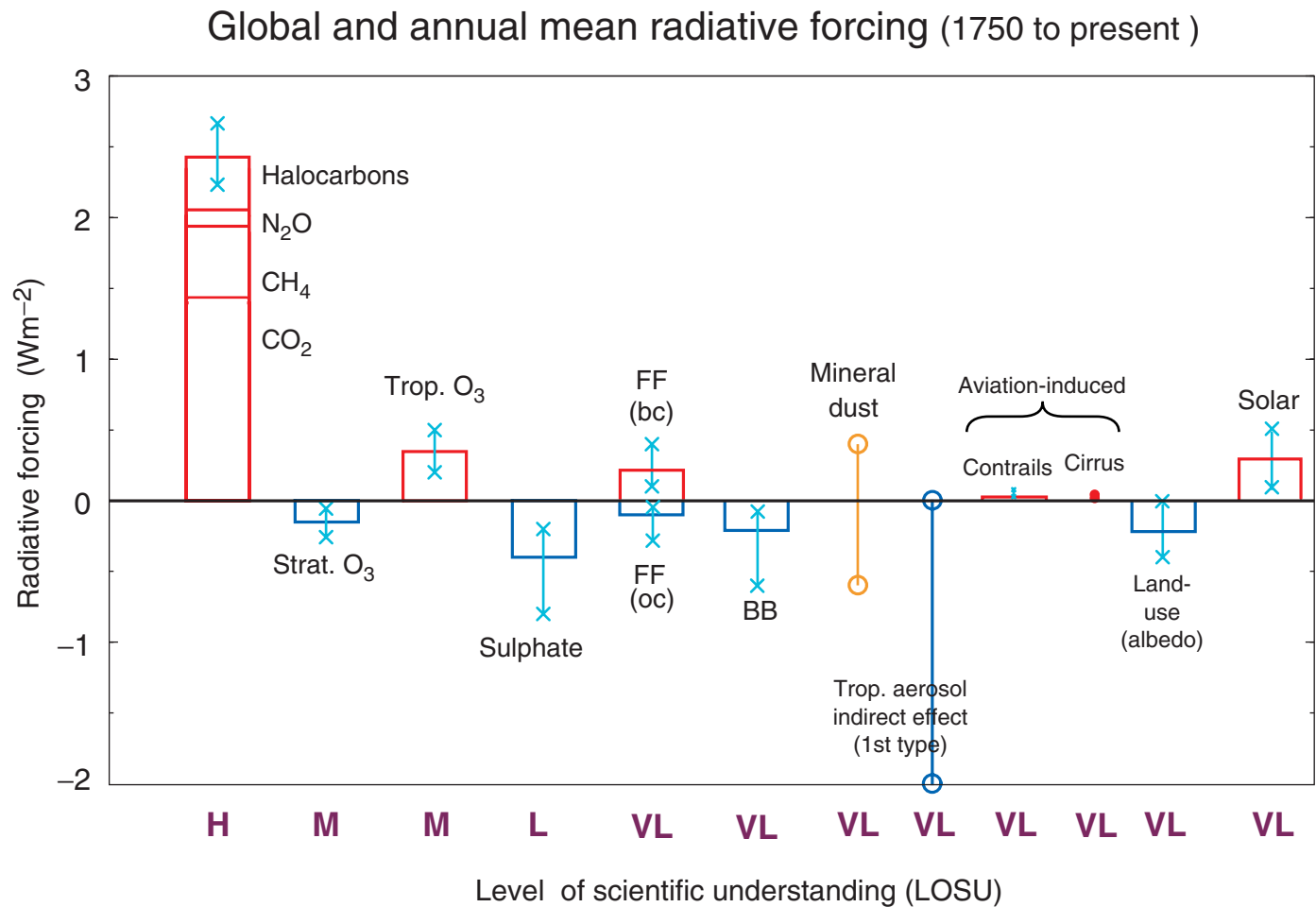
Global and annual mean radiative forcing (1750 to present)

Figure 6.6: Global, annual mean radiative forcings (Wm^{-2}) due to a number of agents for the period from pre-industrial (1750) to present (late 1990s; about 2000) (numerical values are also listed in Table 6.11). For detailed explanations see Section 6.13. The height of the rectangular bar denotes a central or best estimate value while its absence denotes no best estimate is possible. The vertical line about the rectangular bar with "×" delimiters indicates an estimate of the uncertainty range, guided by the spread in the published values of the forcing and physical understanding. A vertical line without a rectangular bar and with "o" delimiters denotes a forcing for which no central estimate can be given owing to large uncertainties. The uncertainty range specified here has no statistical basis and therefore differs from the use of the term elsewhere in this document. A "level of scientific understanding" (LOSU) index is accorded to each forcing, with H, M, L and VL denoting high, medium, low and very low levels, respectively. This represents our subjective judgement about the reliability of the forcing estimate, involving factors such as the assumptions necessary to evaluate the forcing, the degree of our knowledge of the physical/chemical mechanisms determining the forcing, and the uncertainties surrounding the quantitative estimate of the forcing (see Table 6.12). The well-mixed greenhouse gases are grouped together into a single rectangular bar with the individual mean contributions due to CO_2, CH_4, N_2O, and halocarbons (see Tables 6.1 and 6.11) shown; halocarbons refers to all halogen-containing compounds listed in Table 6.1. "FF" denotes fossil fuel burning while "BB" denotes biomass burning aerosol. Fossil fuel burning is separated into the "black carbon" (bc) and "organic carbon" (oc) components with its separate best estimate and range. The sign of the effects due to mineral dust is itself an uncertainty. The indirect forcing due to tropospheric aerosols is poorly understood. The same is true for the forcing due to aviation via their effects on contrails and cirrus clouds. Only the *first* type of indirect effect due to aerosols as applicable in the context of liquid clouds is considered here. The *second* type of effect is conceptually important but there exists very little confidence in the simulated quantitative estimates. The forcing associated with stratospheric aerosols from volcanic eruptions is highly variable over the period and is not considered for this plot (however, see Figure 6.8d). All the forcings shown have distinct spatial and seasonal features (Figure 6.7) such that the global, annual means appearing on this plot do not yield a complete picture of the radiative perturbation. They are only intended to give, in a relative sense, a first-order perspective on a global, annual mean scale, and cannot be readily employed to obtain the climate response to the total natural and/or anthropogenic forcings. As in the SAR, it is emphasised that the positive and negative global mean forcings cannot be added up and viewed a priori as providing offsets in terms of the complete global climate impact.

Table 6.11: *Numerical values of the global and annual mean forcings from 1850 to about the early 1990s as presented in the SAR, and from 1750 to present (about 2000) as presented in this report. The estimate for the well-mixed greenhouse gases is partitioned into the contributions from CO_2, CH_4, N_2O, and halocarbons. An approximate estimate of the Northern Hemisphere (NH) to Southern Hemisphere (SH) ratio is also given for the present report (see also Figure 6.6). The uncertainty about the central estimate (if applicable) is listed in square brackets. No uncertainty is estimated for the NH/SH ratio.*

	Global mean radiative forcing (Wm^{-2}) [Uncertainty]		NH/SH ratio
	SAR	**This Report**	**This Report**
Well-mixed greenhouse gases {Comprising CO_2, CH_4, N_2O, and halocarbons}	+2.45 [15%] {CO_2 (1.56); CH_4 (0.47); N_2O (0.14); Halocarbons (0.28)}	+2.43 [10%] {CO_2 (1.46); CH_4 (0.48); N_2O (0.15); Halocarbons (0.34)}	1
Stratospheric O_3	−0.10 [2X]	−0.15 [67%]	<1
Tropospheric O_3	+0.40 [50%]	+0.35 [43%]	>1
Direct sulphate aerosols	−0.40 [2X]	−0.40 [2X]	>>1
Direct biomass burning aerosols	−0.20 [3X]	−0.20 [3X]	<1
Direct FF aerosols (BC)	+0.10 [3X]	+0.20 [2X]	>>1
Direct FF aerosols (OC)	*	−0.10 [3X]	>>1
Direct mineral dust aerosols	*	−0.60 to +0.40	*
Indirect aerosol effect	0 to −1.5 {sulphate aerosols}	0 to −2.0 {1st effect only; all aerosols}	>1
Contrails	*	0.02 [~3.5 X]	>>1
Aviation-induced cirrus	*	0 to 0.04	*
Land-use (albedo)	*	−0.20 [100%]	>>1
Solar	+0.30 [67%]	+0.30 [67%]	1

* No estimate given.

forcing agent is based on an assessment of the nature of assumptions involved, the uncertainties prevailing about the processes that govern the forcing, and the resulting confidence in the numerical value of the estimate. The subjectivity reflected in the LOSU index is unavoidable and is necessitated by the lack of sufficient quantitative information on the uncertainties, especially for the non-well-mixed greenhouse gas forcing mechanisms. In the case of some forcings, this is in part due to a lack of enough investigations. Thus, the application of rigorous statistical methods to quantify the uncertainties of all of the forcing agents in a uniform manner is not possible at present.

The discussions below relate to the changes with respect to the SAR estimates. In many respects, there is a similarity between the estimates, range and understanding levels listed here, and those stated in the recent studies of Hansen *et al.* (1998) and Shine and Forster (1999). Table 6.11 compares the numerical values with the estimates in the SAR. Also, the Northern to Southern Hemisphere ratio is shown for the present estimates (see also Section 6.14). Table 6.12 summarises the principal aspects known regarding the forcings, along with a brief listing of the key uncertainties in the processes which, in turn, lead to uncertainties in and affect the reliability of the quantitative estimates.

The total forcing estimate for well-mixed greenhouse gases is slightly less now, by about 1% (see Section 6.3) compared to the estimate given in the SAR. The uncertainty range remains

quite small and these estimates retain a "high" LOSU. This forcing continues to enjoy the highest confidence amongst the different natural and anthropogenic forcings.

The estimate for stratospheric O_3 has increased in magnitude, owing mainly to the inclusion of observed ozone depletions through mid-1995 and beyond. It is an encouraging feature that several different model calculations yield similar estimates for the forcing. The uncertainty range remains similar to that given in the SAR. These arguments suggest an elevation of the confidence in the forcing estimate relative to the SAR. Accordingly, a "medium" LOSU is assigned here. A still higher elevation of the rank is precluded because the O_3 loss profile near tropopause continues to be an uncertainty that is significant and that has not been adequately resolved. Also, the global stratospheric temperature change calculations involved in the forcing determination are not quantitatively identical to the observed changes, which in turn, affects, the precision of the forcing estimate.

The estimate for tropospheric O_3 (0.35 ± 0.15 Wm^{-2}) is on firmer grounds now than in the SAR. Since that assessment, many different models have been employed to compute the forcing, including one analysis constrained by observations. These have resulted in a narrowing of the uncertainty range and increased the confidence with regards to the central estimate. The preceding argument strongly suggests an advancement of the confidence in this forcing estimate. Hence, a "medium" LOSU is

Table 6.12: *Summary of the known inputs (i.e., very good knowledge available), and major uncertainties (i.e., key limitations) that affect the quantitative estimates of the global and annual mean radiative forcing of climate change due to the agents listed in Figure 6.6. The summary forms a basis for assigning a level of scientific understanding (LOSU) rank to each agent (H=High, M=Medium, L=Low, and VL=Very low; see Section 6.13).*

	Known inputs	**Major uncertainties**	**Overall rank**
Well-mixed greenhouse gases	Concentrations; spectroscopy		H
Stratospheric O$_3$	Global observations of column change; observations of profiles information at many sites; spectroscopy; qualitative observational evidence of global stratospheric cooling	Change before 1970s; profile of change near tropopause; quantitative attribution of observed stratospheric temperature change	M
Tropospheric O$_3$	Surface observations from many sites since about 1960s; near-global data on present day column; limited local data on vertical distribution; spectroscopy	Emissions, chemistry and transport of precursors and O$_3$; profile near tropopause; lack of global data on pre-industrial levels	M
Sulphate aerosols (direct effect)	Pre-industrial and present source regions and strengths; chemical transformation and water uptake; deposition in some regions; observational evidence of aerosol presence	Transport and chemistry of precursors; aerosol microphysics; optical properties and vertical distribution; cloud distributions; lack of quantitative global observations of distributions and/or forcing	L
Other aerosols (direct effect)	Source regions; some observational evidence of aerosol presence	Pre-industrial and present source strengths; in-cloud chemistry and water uptake; aerosol microphysics; optical properties and vertical distributions; cloud distributions; lack of quantitative global data on forcing	VL
Aerosols (indirect; 1st type)	Evidence for phenomenon in ship tracks; measurement of variations in cloud droplet size from satellite and field observations	Quantification of aerosol-cloud interactions; model simulation of aerosol and cloud distributions; difficulty in evaluation from observations; lack of global measurements; optical properties of mixtures; pre-industrial aerosol concentration and properties	VL
Contrails and aviation-induced cirrus	Air traffic patterns; contrail formation; cirrus clouds presence	Ice microphysics and optics; geographical distributions; quantification of induced-cirrus cloudiness	VL
Land use (albedo)	Present day limited observations of deforestation	Human and natural effects on vegetation since 1750; lack of quantitative information, including separation of natural and anthropogenic changes	VL
Solar	Variations over last 20 years; information on Sun-like stars; proxy indicators of solar activity	Relation between proxies and total solar irradiance; induced changes in O$_3$; effects in troposphere; lack of quantitative information going back more than 20 years; cosmic rays and atmospheric feedbacks	VL

accorded for tropospheric O_3 forcing. Key uncertainties remain concerning the pre-industrial distributions, the effects of stratospheric-tropospheric exchange and the manner of its evolution over time, as well as the seasonal cycle in some regions of the globe.

As the LOSU rankings are subjective and reflect qualitative considerations, the fact that tropospheric and stratospheric O_3 have the same ranks does not imply that the degree of confidence in their respective estimates is identical. In fact, from the observational standpoint, stratospheric O_3 forcing, which has occurred only since 1970s and is better documented, is on relatively firmer ground. Nevertheless, both O_3 components are less certain relative to the well-mixed greenhouse gases, but more so compared with the agents discussed below.

The estimate for the direct sulphate aerosol forcing has also seen multiple model investigations since the SAR, resulting in more estimates being available for this assessment. It is striking that consideration of all of the estimates available since 1996 lead to the same best estimate (-0.4 Wm^{-2}) and uncertainty (-0.2 to -0.8 Wm^{-2}) range as in the previous assessment. As in the case of O_3, that could be a motivation for elevating the status of knowledge of this forcing to a higher confidence level. However, there remain critical areas of uncertainty concerning the modelling of the geographical distribution of sulphate aerosols, spatial cloud distributions, effects due to relative humidity etc. Hence, we retain a "low" LOSU for this forcing.

The SAR stated a radiative forcing of $+0.1$ Wm^{-2} for fossil fuel (FF) black carbon aerosols with a range $+0.03$ to $+0.3$ Wm^{-2}, and a "very low" level of confidence. For biomass burning (BB) aerosols, the SAR stated a radiative forcing of -0.2 Wm^{-2} with a range -0.07 to -0.6 Wm^{-2}, and a "very low" level of confidence. In the present assessment, the radiative forcing of the black carbon component from FF is estimated to be $+0.2$ Wm^{-2} with a range from $+0.1$ to $+0.4$ Wm^{-2} based on studies since the SAR. A "very low" LOSU is accorded in view of the differences in the estimates from the various models. The organic carbon component from FF is estimated to yield a forcing of -0.1 Wm^{-2} with a range from -0.03 to -0.30 Wm^{-2}; this has a "very low" LOSU. Note that extreme caution must be exercised in adding the uncertainties of the organic and black carbon components to get the uncertainty for FF as a whole. For BB aerosols, no attempt is made to separate into black and organic carbon components, in view of considerable uncertainties. The central estimate and range for BB aerosols remains the same as in the SAR; this has a "very low" LOSU in view of the several uncertainties in the calculations (Section 6.7).

Mineral dust is a new component in the current assessment. The studies on the "disturbed" soils suggest an anthropogenic influence, with a range from $+0.4$ to -0.6 Wm^{-2}. In general, the evaluation for dust aerosol is complicated by the fact that the short-wave consists of a significant reflection and absorption component, and the long-wave also exerts a substantial contribution by way of a trapping of the infrared radiation. Thus, the net radiative energy gained or lost by the system is the difference between non-negligible positive and negative radiative flux changes operating simultaneously. Because of this complexity, we refrain from giving a best estimate and accord this component a "very low" LOSU.

As explained in Section 6.8, the "indirect" forcing due to all tropospheric aerosols can be thought of as comprising two effects. Only the first type of effect as applicable in the context of liquid clouds is considered here. As in the SAR, no best estimate is given in view of the large uncertainties prevailing in this problem (Section 6.8). The range (0 to -2 Wm^{-2}) is based on published estimates and subjective assessment of the uncertainties. Although several model studies suggest a non-zero, negative value as the upper bound (about -0.3 Wm^{-2}), substantial gaps in the knowledge remain which affect the confidence in the model simulations of this forcing (e.g., uncertainties in aerosol and cloud processes and their representations in GCMs, the potentially incomplete knowledge of the radiative effect of black carbon in clouds, and the possibility that the forcings for individual aerosol types may not be additive), such that the possibility of a very small negative value cannot be excluded; thus zero is retained as an upper bound as in the SAR. In view of the large uncertainties in the processes and the quantification, a "very low" LOSU is assigned to this forcing. Inclusion of the second indirect effect (Chapter 5) is fraught with even more uncertainties and, despite being conceptually valid as an anthropogenic perturbation, raises the question of whether the model estimates to-date can be unambiguously characterised as an aerosol radiative forcing.

Aviation introduces two distinct types of perturbation (Section 6.8). Contrails produced by aircraft constitute an anthropogenic perturbation. This is estimated to contribute 0.02 Wm^{-2} with an uncertainty of a factor of 3 or 4 (IPCC, 1999); the uncertainty factor is assumed to be 3.5 in Figure 6.6. This has an extremely low level of confidence associated with it. Additionally, aviation-produced cirrus is estimated by IPCC (1999) to yield a forcing of 0 to 0.04 Wm^{-2}, but no central estimate or uncertainty range was estimated in that report. Both components have a "very low" LOSU.

Volcanic aerosols that represent a transient forcing of the climate system following an eruption are not plotted since they are episodic events and cannot be categorised as a century-scale secular forcing, unlike the others. However, they can have substantial impacts on interannual to decadal scale temperature changes and hence are important factors in the time evolution of the forcing (see Section 6.15). Some studies (Hansen *et al.*, 1998; Shine and Forster, 1999) have attempted to scale the volcanic forcings in a particular decade with respect to that in a quiescent decade.

Land-use change was dealt with in IPCC (1990) but was not considered in the SAR. However, recent studies (e.g., Hansen *et al.*, 1998) have raised the possibility of a negative forcing due to deforestation and the ensuing effects of snow-covered land albedo changes in mid-latitudes. There are not many studies on this subject and rigorous investigations are lacking such that this forcing has a "very low" LOSU, with the range in the estimate being 0 to -0.4 Wm^{-2} (central estimate: -0.2 Wm^{-2}). Note that the land-use forcing here is restricted to that due to albedo change.

Solar forcing remains the same as in the SAR, in terms of best estimate, the uncertainty range and the confidence level. Thus, the range is 0.1 to 0.5 Wm^{-2} with a best estimate of 0.3 Wm^{-2}, and with a "very low" LOSU.

6.13.2 Limitations

It is important that the global mean forcing estimates be interpreted in a proper manner. Recall that the utility of the forcing concept is to afford a first-order perspective into the relative climatic impacts (viz., global-mean surface temperature change) of the different forcings. As stated in Section 6.2, for many of the relevant forcings (e.g., well-mixed greenhouse gases, solar, certain aerosol and O_3 profile cases), model studies suggest a reasonable similarity of the climate sensitivity factor (Equation 6.1), such that a comparison of these forcings is meaningful for assessing their relative effects on the global mean surface temperature. However, as mentioned earlier, the climate sensitivity factor for some of the spatially inhomogeneous forcings has yet to be fully explored. For some of the forcings (e.g., involving some absorbing aerosol and O_3 profile cases; see Hansen *et al.*, 1997a), the climate sensitivity is markedly different than for, say, the well-mixed greenhouse gases, while, for other forcings (e.g., indirect aerosol effect), more comprehensive studies are needed before a generalisation can become possible.

It is also cautioned that it may be inappropriate to perform a sum of the forcings to derive a best estimate "total" radiative forcing. Such an operation has the limitation that there are differing degrees of reliability of the global mean estimates of the various forcings, which do not necessarily lend themselves to a well-justified quantitative manipulation. For some forcings, there is not even a central or best estimate given at present (e.g., indirect aerosol forcing), essentially due to the substantial uncertainties.

The ranges given for the various forcings in Figure 6.6, as already pointed out, do not have a statistical basis and are guided mostly by the estimates from published model studies. Performing mathematical manipulations using these ranges to obtain a "net uncertainty range" for the total forcing, therefore, lacks a rigorous basis. Adding to the complexity is the fact that each forcing has associated with it an assessment of the level of knowledge that is subjective in nature viz., LOSU (Table 6.12). The LOSU index is not a quantitative indicator and, at best, yields a qualitative sense about the reliability of the estimates, with the well-mixed greenhouse gases having the highest reliability, those with "medium" rank having lesser reliability, and with even less reliability for the "low" and "very low" rankings. To some extent, the relatively lower ranking of the non-well-mixed greenhouse gases (e.g., aerosols, O_3) is associated with the fact that the forcing estimates for these agents depend on model simulations of species' concentrations, in contrast to the well-mixed greenhouse gases whose global concentrations are well quantified.

In a general sense, the strategy and usefulness of combining global mean estimates of forcings that have different signs, spatial patterns, vertical structures, uncertainties, and LOSUs, and the resulting significance in the context of the global climate response are yet to be fully explored. For some combinations of forcing agents (e.g., well-mixed greenhouse gases and sulphate aerosol; see Section 6.2), it is apparent from model tests that the global mean responses to the individual forcings can be added to yield the total global mean response. Because linear additivity

tests have yet to be performed for the complete set of agents shown in Figure 6.6, it is not possible to state with absolute certainty that the additivity concept will necessarily hold for the entire set of forcings.

Figure 6.6 depicts the uncertainties and LOSUs only for the global mean estimates. No attempt is made here to extend these subjective characterisations to the spatial domains associated with each of the forcings (see Figure 6.7, and Table 6.11 for the Northern to Southern Hemisphere ratios). As in the SAR, we reiterate that, in view of the spatial character of several of the forcing agents, the global mean estimates do not necessarily describe the complete spatial (horizontal and vertical dimensions) and seasonal climate responses to a particular radiative perturbation. Nor do they yield quantitative information about changes in parameters other than the global mean surface temperature response.

One diagnostic constraint on the total global mean forcing since pre-industrial times is likely to be provided by comparisons of model-simulated (driven by the combination of forcings) and observed climate changes, including spatially-based detection-attribution analyses (Chapter 12). However, the *a posteriori* inference involves a number of crucial assumptions, including the uncertainties associated with the forcings, the representativeness of the climate models' sensitivity to the forcings, and the model's representation of the real world's "natural" variations.

Overall, the net forcing comprises of a large positive value due to well-mixed greenhouse gases, followed by a number of other agents that have smaller positive or negative values. Thus, relative to IPCC (1990) and over this past decade, there are now more forcing agents to be accounted for, each with a sizeable uncertainty that can affect the estimated climate response. In this regard, consideration of the "newer" forcing agents brings on an additional element of uncertainty in climate change analyses, over and above those concerning climate feedbacks and natural variability (IPCC, 1990). Both the spatial character of the forcing and doubts about the magnitudes (and, in some cases, even the sign) add to the complexity of the climate change problem. However, this does not necessarily imply that the uncertainty associated with the forcings is now of much greater importance than the issue of climate sensitivity of models.

6.14 The Geographical Distribution of the Radiative Forcings

While previous sections have concentrated upon estimates of the global annual mean of the radiative forcing of particular mechanisms, this section presents the geographical distribution of the present day radiative forcings. Although the exact spatial distribution of the radiative forcing may differ between studies, many of them show similar features that are highlighted in this section. With the exception of well-mixed greenhouse gases, different studies calculate different magnitudes of the radiative forcing. In these cases, the spatial distributions are discussed, not the absolute values of the radiative forcing. It should be stressed that the Figure 6.7 represents plausible examples of geographical distributions only – significant differences may occur in other studies. In addition to Figure 6.7, Table 6.11 lists Northern to Southern Hemisphere ratio for forcings.

6.14.1 Gaseous Species

An example of the radiative forcing due to the combined effects of present day concentrations of CO_2, CH_4, N_2O, CFC-11 and CFC-12 is shown in Figure 6.7a (see Shine and Forster, 1999, for further details). The zonal nature of the radiative forcing is apparent and is similar to the radiative forcing due to well-mixed greenhouse gases from Kiehl and Briegleb (1993) presented in IPCC (1994). The radiative forcing ranges from approximately $+1$ Wm^{-2} at the polar regions to $+3$ Wm^{-2} in the sub-tropics. The pattern of the radiative forcing is governed mainly by variations of surface temperature and water vapour and the occurrence of high level cloud (Section 6.3).

An example of the radiative forcing due to stratospheric ozone depletion is shown in Figure 6.7b which was calculated using zonal mean stratospheric ozone depletions from 1979 to 1994 (WMO, 1995) by Shine and Forster (1999). The zonal nature of the radiative forcing is apparent with strongest radiative forcings occurring in polar regions which are areas of maximum ozone depletion (Section 6.4). The gradient of the radiative forcing tends to enhance the zonal gradient of the radiative forcing due to gaseous species shown in Figure 6.7a.

An example of the radiative forcing due to modelled increases in tropospheric O_3 is shown in Figure 6.7c (Berntsen *et al.*, 1997; Shine and Forster, 1999). While the exact spatial distribution of the radiative forcing may differ in other studies, the general pattern showing a maximum radiative forcing over North Africa and the Middle East is common to many other studies (Section 6.5). However, observational evidence presented by Kiehl *et al.* (1999) suggests that this might be an artefact introduced by the chemical transport models. The radiative forcing is much less homogeneous than for well-mixed greenhouse gases, the maximum radiative forcing being due to the coincidence of a relatively large O_3 change, warm surface temperatures, high surface reflectance, and cloud-free conditions.

6.14.2 Aerosol Species

An example of the direct radiative forcing due to sulphate aerosol is shown in Figure 6.7d (Haywood *et al.*, 1997a). In common with many other studies (see Section 6.7), the direct radiative forcing is negative everywhere, and there are three main areas where the radiative forcing is strongest in the Northern Hemisphere corresponding to the main industrialised regions of North America, Europe, and Southeast Asia. In the Southern Hemisphere, two less strong regions are seen. The ratio of the radiative forcing in the Northern Hemisphere to the Southern Hemisphere has been reported by many studies and varies from 2 (Graf *et al.*, 1997) to approximately 7 (Myhre *et al.*, 1998c). Generally, the strongest sulphate direct radiative forcing occurs over land areas although the low surface reflectance means that areas of water close to heavily industrialised regions such as the Mediterranean Sea, the Black Sea and the Baltic Sea result in strong local radiative forcings. Due to the large areal extent of ocean regions, the contribution to the total annual mean radiative forcing from ocean regions is significant. The ratio of the annual mean radiative forcing over land to that over oceans varies from

approximately 1.3 (Kiehl *et al.*, 2000) to 3.4 (Boucher and Anderson, 1995) (see Table 6.4).

An example of the direct radiative forcing due to organic carbon and black carbon from biomass burning is shown in Figure 6.7e (Penner *et al.*, 1998b; Grant *et al.*, 1999). While the radiative forcing is generally negative, positive forcing occurs in areas with a very high surface reflectance such as desert regions in North Africa, and the snow fields of the Himalayas. This is because biomass burning aerosols contain black carbon and are partially absorbing. The dependency of the sign of the radiative forcing from partially absorbing aerosols upon the surface reflectance has been investigated by a number of recent studies (e.g., Chylek and Wong, 1995; Chylek *et al.*, 1995; Haywood and Shine, 1995; Hansen *et al.*, 1997a). The strongest negative radiative forcing is associated with regions of intense biomass burning activity namely, South America, Africa, and Southern Asia and Indonesia and differ from the regions where the sulphate radiative forcing is strongest (Figure 6.7d), being confined to approximately 30ºN to 30ºS.

An example of the direct radiative forcing due to organic and black carbon from fossil fuel burning is shown in Figure 6.7f (Penner *et al.*, 1998b; Grant *et al.*, 1999). In contrast to the direct radiative forcing from biomass burning (Figure 6.7e), the modelled direct radiative forcing is generally positive except over some oceanic regions near industrialised regions such as the Mediterranean Sea and Black Sea. This is because, on average, aerosols emitted from fossil fuels contain a higher black/organic carbon ratio than biomass aerosols (Penner *et al.*, 1998b; Grant *et al.*, 1999) and are thus more absorbing. Comparison of the radiative forcing due to sulphate aerosols reveals that the areas of strongest sulphate direct radiative forcing are offset to some degree by the radiative forcing due to fossil fuel emissions of black carbon as shown in calculations by Haywood *et al.* (1997a) and Myhre *et al.* (1998c). Additional regions of moderate positive radiative forcing are present over areas of high surface reflectance such as northern polar regions and the North African deserts.

An example of the direct radiative forcing due to anthropogenic emissions of mineral dust is shown in Figure 6.7g (Tegen *et al.*, 1996). Areas of strong positive forcing are shown over regions with high surface reflectance such as desert regions in Africa and over the snow surfaces of the Himalayas and areas of strong negative forcing are apparent over ocean areas close to mineral dust sources such as off the coasts of Arabia and North Africa. The exact switchover between areas of positive and negative radiative forcing are not well established owing to uncertainties in the modelled mineral aerosol optical properties and depends upon the assumed single scattering albedo (Miller and Tegen, 1998), the long-wave properties and altitude of the aerosol (Section 6.7.6).

An example of the "first" indirect radiative effect (i.e., changes in the cloud reflectivity only) due to anthropogenic industrial aerosols is shown in Figure 6.7h. The forcing is calculated diagnostically in a similar way to Jones and Slingo (1997), but is based on a more recent version of the Hadley Centre model (HadAM3; Pope *et al.*, 2000), uses updated sulphur emission scenarios from the SRES scenario for the year 2000 (Johns *et al.*, 2001) and also includes a simple parametrization of
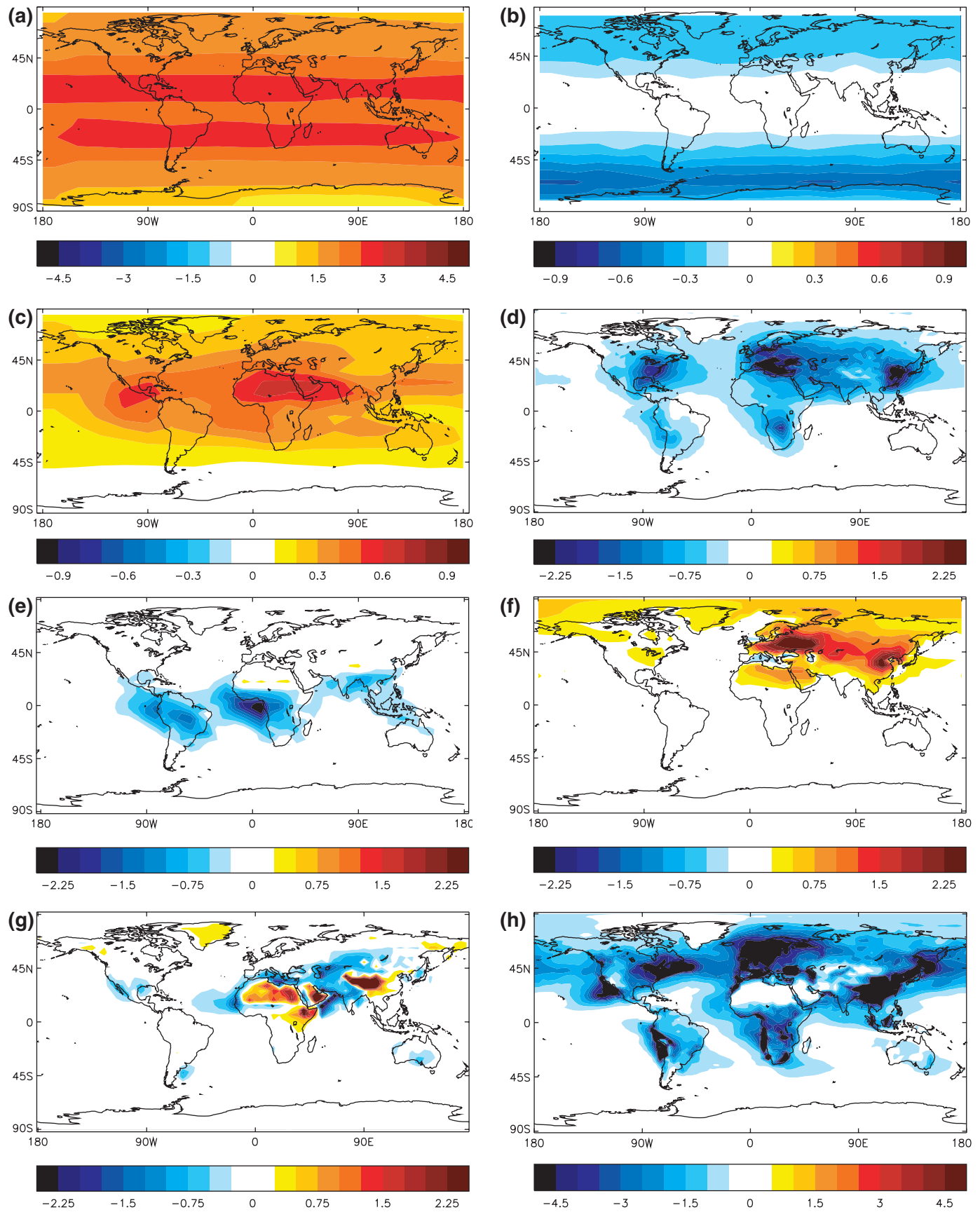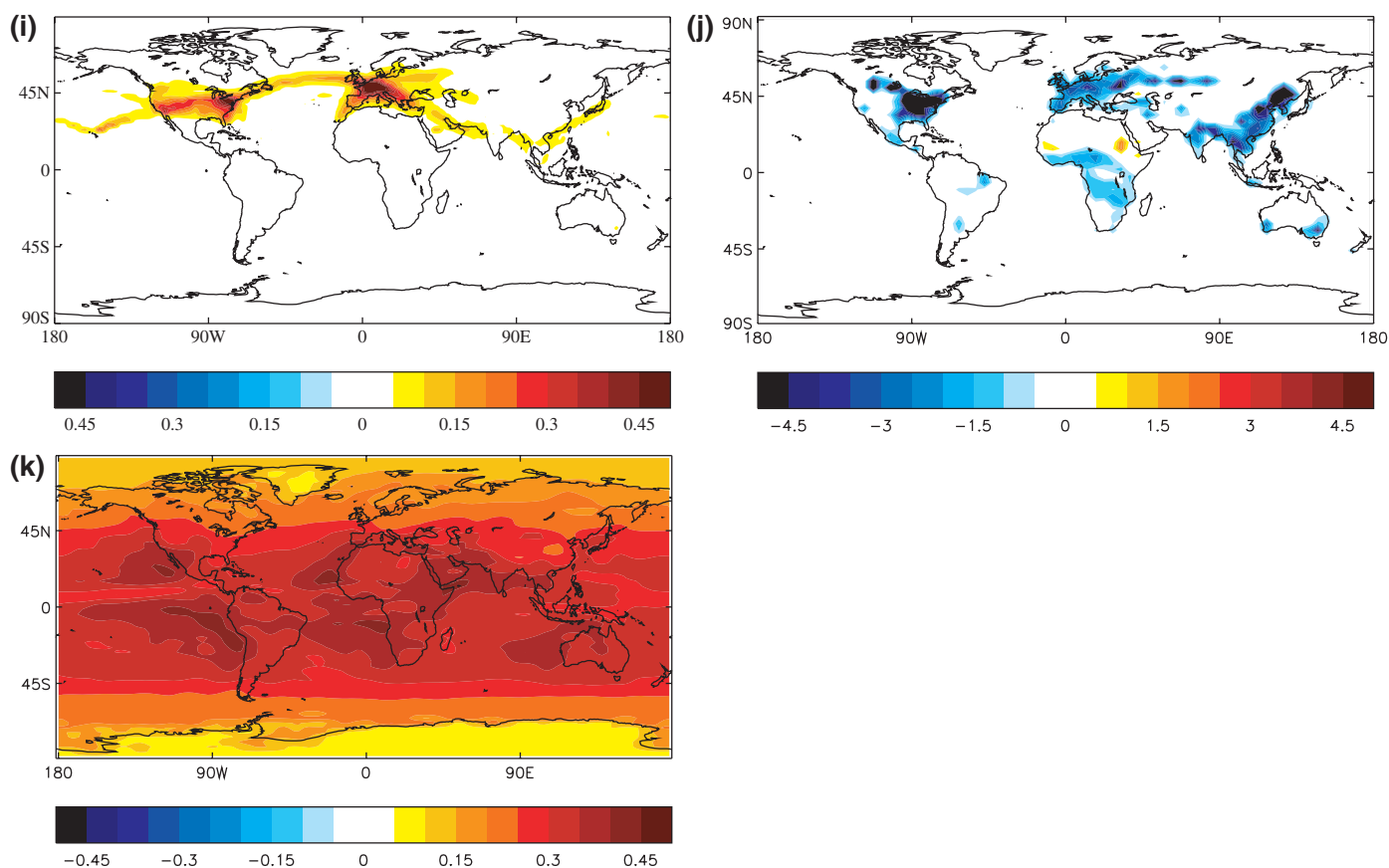
Figure 6.7: Examples of the geographical distribution of present-day annual-average radiative forcing (1750 to 2000) due to (a) well-mixed greenhouse gases including CO$_2$, CH$_4$, N$_2$O, CFC-11 and CFC-12 (Shine and Forster, 1999); (b) stratospheric ozone depletion over the period 1979 to 1994 given by WMO, 1995 (Shine and Forster, 1999); (c) increases in tropospheric O$_3$ (Berntsen *et al.*, 1997; Shine and Forster, 1999); (d) the direct effect of sulphate aerosol (Haywood *et al.*, 1997a); (e) the direct effect of organic carbon and black carbon from biomass burning (Penner *et al.*, 1998b; Grant *et al.*, 1999); (f) the direct effect of organic carbon and black carbon from fossil fuel burning (Penner *et al.*, 1998b; Grant *et al.*, 1999), (g) the direct effect of anthropogenic emissions of mineral dust (Tegen *et al.*, 1996); (h) the "first" indirect effect of sulphate aerosol calculated diagnostically in a similar way to Jones and Slingo (1997), but based on a more recent version of the Hadley Centre model (HadAM3; Pope *et al.*, 2000), using sulphur emission scenarios for year 2000 from the SRES scenario (Johns *et al.*, 2001) and including a simple parametrization of sea salt aerosol (Jones *et al.*, 1999); (i) contrails (Minnis *et al.*, 1999); (j) surface albedo change due to changes in land use (Hansen *et al.*, 1998), (k) solar variability (Haigh, 1996). Note that the scale differs for the various panels. Different modelling studies may show considerably different spatial patterns as described in the text. (Units: Wm^{-2})

sea salt aerosol (Jones *et al.*, 1999). The spatial distribution of the indirect radiative forcing is quite different from the direct radiative forcing with strong areas of forcing off the coasts of industrialised regions (note the change in scale of Figure 6.7h). There is a significant radiative forcing over land regions such as Europe and the Eastern coast of North America, and Southeast Asia. The spatial distribution of the indirect radiative forcing will depend critically upon the assumed spatial distribution of the background aerosol field and the applied anthropogenic perturbation and differs substantially between studies (see Section 6.8.5). It would have a very different spatial distribution if the effect of biomass burning aerosols were included. The "second" indirect effect whereby inclusion of aerosols influences the lifetime of clouds is not considered here due to the complications of necessarily including some cloud feedback processes in the estimates (Section 6.8.5), but may well resemble the spatial distribution of the "first" indirect effect.

6.14.3 Other Radiative Forcing Mechanisms

The spatial distribution of three other radiative forcing mechanisms are considered in this section: the radiative forcing due to contrails, land-use change, and solar variability. The radiative forcing due to other constituents such as nitrate aerosol and aviation-induced cirrus that are very difficult to quantify at present are not presented as geographic distributions of the radiative forcing are currently considered to be speculative.

An example of the present day radiative forcing due to the effect of contrails is shown in Figure 6.7i (Minnis *et al.*, 1999). The radiative forcing is very inhomogeneous, being confined to air-traffic corridors (IPCC, 1999). Future scenarios for aircraft emissions may shift the current geographical pattern of the radiative forcing as discussed in IPCC (1999).

An example of an estimate of the radiative forcing due to changes in land use is shown in Figure 6.7j (Hansen *et al.*, 1998).

The areas of strongest negative forcing occur at northern latitudes of the Northern Hemisphere due to the felling of forests which have a lower albedo when snow is present (see Section 6.13). Additional effects are due to the change in albedo between crop lands and naturally occurring vegetation. Examples where the radiative forcing is positive include areas where irrigation has enabled crop-growing on previously barren land.

An example of the present day radiative forcing due to solar variability is shown in Figure 6.7k. The solar radiative forcing was calculated by scaling the top of the atmosphere net solar radiation such that the global average is +0.3 Wm^{-2} (as deduced for global average radiative forcing since 1750, see Section 6.13.1). Thus it assumes a 0.125% increase in solar constant and no change in any other parameter (e.g., O_3, cloud). The cloud and radiation fields were calculated within a run of the UGAMP GCM (Haigh, 1996). The strongest radiative forcings exist where the surface reflectance is low (i.e., oceanic regions) and the insolation is highest (i.e., equatorial regions). The solar radiative forcing is also modulated by cloud amount, areas with low cloud amount showing the strongest radiative forcing. The solar radiative forcing is more inhomogeneous than the radiative forcing due to gaseous species (Section 6.14.1), but more homogeneous than the radiative forcing due to aerosol species (Section 6.14.2).

While the preceding sections have shown that the radiative forcing due to the different forcing mechanisms have very different spatial distributions, it is essential to note that the forcing/response relationship given in Section 6.2 relates global mean radiative forcings to global mean temperature response. Thus, it is not possible to simply map the geographical radiative forcing mechanisms by assuming a globally invariant climate sensitivity parameter to predict a geographic temperature response, due to the complex nature of the atmosphere-ocean system. Rather, the effects of spatial inhomogeneity in the distribution of the radiative forcing may lead to locally different responses in surface temperature (Section 6.2) indicating that the spatial distributions of the radiative forcing need to be accurately represented to improve regional estimates of surface temperature response and other physical parameters.

6.15 Time Evolution of Radiative Forcings

6.15.1 Past to Present

IPCC (1990) showed time evolution of the radiative forcing due to the well-mixed greenhouse gases. For the other radiative forcing mechanisms, the previous IPCC reports (IPCC, 1990; SAR) did not consider the evolution of the radiative forcing, and assessed mainly the radiative fluxes in the pre-industrial and present epochs. However, more recent studies have considered the time evolution of several forcing mechanisms (Hansen *et al.*, 1993; Wigley *et al.*, 1997; Myhre *et al.*, 2001). The information on the time evolution of the radiative forcing from pre-industrial times to present illustrates the differing importance of the various radiative forcing mechanisms over the various time periods, as well as the different start times of their perturbation of the radiative balance. It also gives useful information in the form of

inputs to climate models viz., as driving mechanisms to investigate potential causes of climate changes. Studies of the evolution of various anthropogenic as well as natural forcing mechanisms may then be used to explain potential causes of past climate change, e.g. since pre-industrial times (Chapter 12).

The knowledge of the various forcing mechanisms varies substantially (see Section 6.13) and, for some, the knowledge of their time evolution is more problematic than for others. For example, well-mixed greenhouse gas concentrations are observed very accurately from about 1950, with observations even further back in time, whereas data for most aerosol components are much more scarce and uncertain. Uncertainties in the evolution of many of the radiative forcing mechanisms shown in Figure 6.8 have not been assessed yet, and the presented time history should be regarded as an example of a possible evolution.

The forcing mechanisms, considered, where information on their time evolution is available, are plotted in Figure 6.8, with the present forcing corresponding to the best estimates given in Section 6.13. The time evolution differs considerably among the forcing mechanisms as different processes controlling the emissions and lifetimes are involved. Concentrations of the well-mixed greenhouse gases are taken from Chapters 3 and 4 and the simplified expressions for the radiative forcing in Table 6.2 (first row for CO_2) are used. The evolution of the radiative forcing due to tropospheric O_3 is taken from Berntsen *et al.* (2000). For the radiative forcing due to stratospheric O_3, information on the evolution is taken from the SAR and scaled to the present forcing of -0.15 Wm^{-2} (Section 6.4).

For sulphate, the time evolution for SO_2 emission (Schlesinger *et al.*, 1992) is used, updated with values after 1990 (Stern and Kaufmann, 1996). For black and organic carbon aerosols, the fossil fuel component is scaled to coal, diesel, and oil use and fossil fuel emission (IPCC, 1996b), respectively. Altered emission coefficients as a result of improved technology have not been taken into account and is a substantial uncertainty for the time evolution of the black carbon emission. The biomass component is scaled to the gross deforestation (see SAR). In addition to different forcing mechanisms of anthropogenic origin, two natural forcings have also been considered: solar irradiance variations and stratospheric aerosols of volcanic origin. The Lean *et al.* (1995) and Hoyt and Schatten (1993) estimates of direct solar forcing due to variation in total solar irradiance are shown. Differences between the solar irradiance constructions are due to use of different proxy parameters for the solar irradiance variations (Section 6.11). The optical depth of the stratospheric aerosols of volcanic origin is taken from Sato *et al.* (1993) and Robock and Free (1996). The data from Sato *et al.* (1993) (updated from www.giss.nasa.gov) are given for the period 1850 to 1998, whereas those from Robock and Free (1996) are for the period 1750 to 1988. In Robock and Free (1996) the optical depth is given for the Northern Hemisphere. The relationship between optical depth and radiative forcing from Lacis *et al.* (1992) is used. The stratospheric aerosols yield a very strong forcing immediately after major eruptions (Section 6.9); however, the lifetime of the stratospheric aerosols is only a few years. Therefore, the transient response due to the forcing by stratospheric aerosols
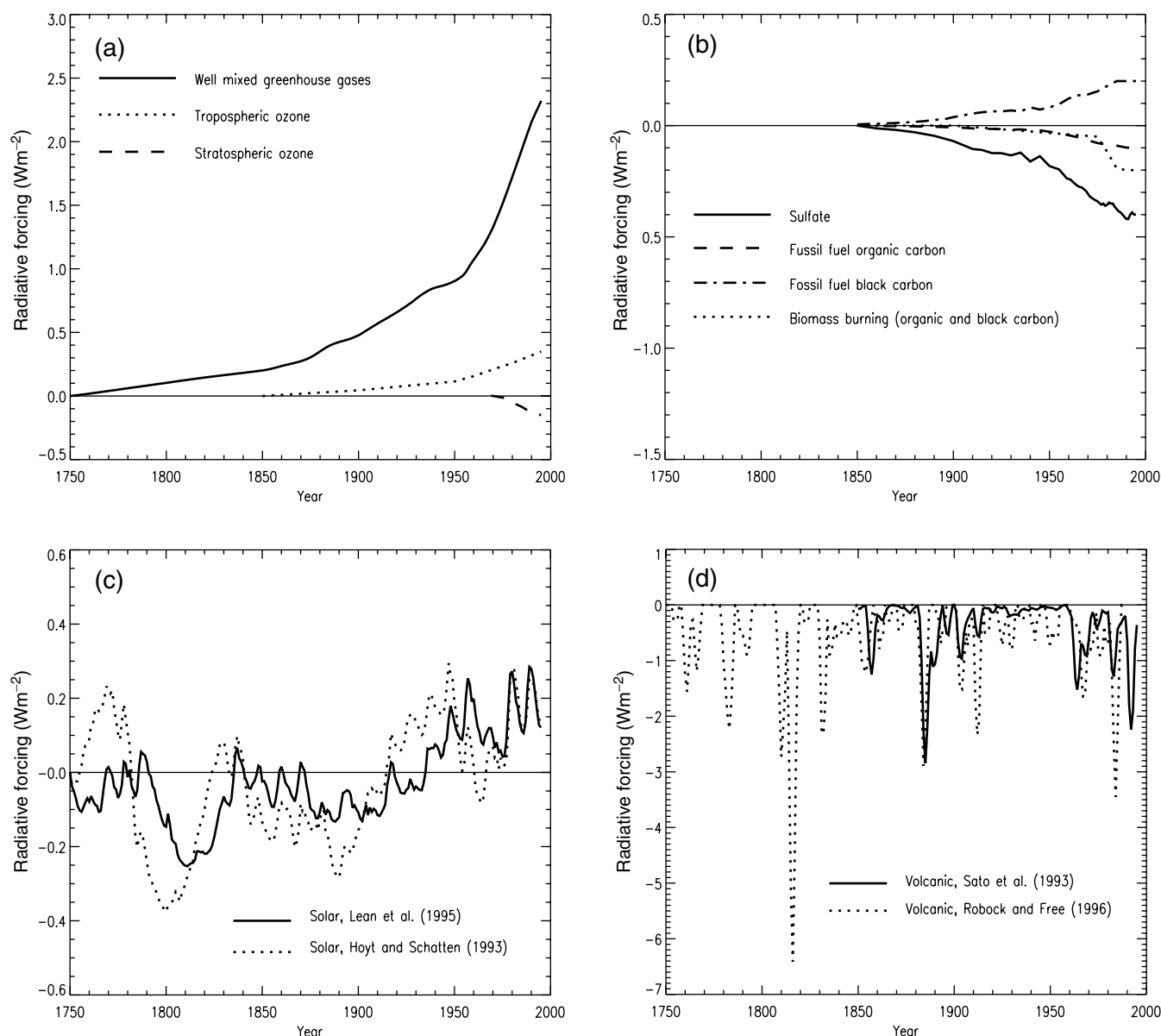
Figure 6.8: Time evolution of global mean radiative forcing from pre-industrial times (1750) to present. Annual mean radiative forcing values are shown, except for stratospheric aerosols of volcanic origin where a three-year running mean is used. Radiative forcings due to (a) well-mixed greenhouse gases, tropospheric O_3, and stratospheric O_3, (b) direct effect of sulphate aerosols, fossil fuel organic and black carbon aerosols, and biomass burning aerosols, (c) solar irradiance variations from Lean *et al.* (1995) and Hoyt and Schatten (1993), respectively, and (d) stratospheric aerosols of volcanic origin from Sato *et al.* (1993) (and updated with data from www.giss.nasa.gov) for the period 1850 to 1998 and from Robock and Free (1996) for the period 1750 to 1988 (for the Northern Hemisphere only). Note the change of scales in the different panels.

cannot readily be compared to that due to the more sustained or steadily increasing forcings.

The relative evolution of the strengths of the different forcing mechanisms presented above are seen to be very different. The forcing due to well-mixed greenhouse gases (consisting of the components listed in Table 6.11) is the dominant forcing mechanism over the century time period. For tropospheric O_3, the relative radiative forcing compared to the well-mixed greenhouse gases has slightly increased; it was 10% of the well-mixed greenhouse gas forcing in 1900 and is 15% at present. The stratospheric O_3 forcing is significant only over the last two

decades. The aerosols have short lifetimes compared with the well-mixed greenhouse gases, and their forcings at any given time depend on the current emissions. This is not the case for the well-mixed greenhouse gases for which both current and previous emissions are relevant. Table 6.13 shows five year averages for the radiative forcings denoted in Figure 6.8 over the period 1960 to 1995. For some of the forcing mechanisms a large increase in the radiative forcing (computed since pre-industrial times) is estimated to have occurred over the period 1960 to 1995. This is the case for the well-mixed greenhouse gases, tropospheric O_3, biomass burning aerosols and organic carbon

Table 6.13: *Radiative forcings (5-year averages) due to change in well-mixed greenhouse gases (WMGG), stratospheric O₃, tropospheric O₃, direct effect of sulphate aerosols, fossil fuel organic carbon aerosols (FF OC), fossil fuel black carbon aerosols (FF BC), aerosols from biomass burning (organic carbon and black carbon) (BB), stratospheric aerosols of volcanic origin, and changes in Total Solar Irradiance. All values are evaluated with respect to pre-industrial times (1750).*

Time period	WMGG	Strat O_3	Trop O_3	Sulphate	FF OC	FF BC	BB	Volcanic	Solar[a]	Solar[b]
1961 to 1965	1.14	0.00	0.17	−0.26	−0.05	0.14	−0.04	−1.00	0.11	−0.07
1966 to 1970	1.27	0.00	0.20	−0.29	−0.06	0.14	−0.04	−0.77	0.11	0.04
1971 to 1975	1.44	−0.01	0.22	−0.33	−0.07	0.15	−0.05	−0.28	0.06	0.03
1976 to 1980	1.64	−0.04	0.25	−0.35	−0.08	0.16	−0.09	−0.15	0.17	0.14
1981 to 1985	1.85	−0.07	0.28	−0.36	−0.09	0.19	−0.16	−0.88	0.17	0.20
1986 to 1990	2.07	−0.11	0.31	−0.40	−0.10	0.20	−0.20	−0.35	0.21	0.19
1991 to 1995	2.26	−0.14	0.34	−0.40	−0.10	0.20	−0.20	−1.42	0.18	0.18

[a] From Lean *et al.* (1995).
[b] From Hoyt and Schatten (1993).

aerosols from fossil fuel consumption, whereas, for sulphate aerosols and black carbon aerosols from fossil fuel consumption, a smaller increase is estimated.

As seen from Figure 6.8d the radiative forcing due to stratospheric aerosols of volcanic activity has very large year to year variations. The solar irradiance, according to the two reconstructions, generally increases and may have contributed in an important manner to the warming in the 20th century, particularly in the period from 1900 to 1950. Volcanic activity was particularly strong around 1900 and at different times since 1963. Table 6.13 shows a strong radiative forcing due to the temporal evolution of the stratospheric aerosols of volcanic origin during the period 1961 to 1965; however, the strongest forcing in the course of the past four decades has occurred over the period from 1991 to 1995. The temporal evolution of the stratospheric aerosol content together with the small solar irradiance variations during the last few (two to four) decades indicates that the natural forcing has been negative over the past two and possibly even the past four decades. In contrast, the positive forcing due to well-mixed greenhouse gases has increased rapidly over the past four decades.

6.15.2 SRES Scenarios

6.15.2.1 Well-mixed greenhouse gases

Emissions from the SRES scenarios (Nakićenović *et al.*, 2000) were used in Chapter 4 to simulate the concentrations of well-mixed greenhouse gases and O_3 in the atmosphere for the period 2000 to 2100. Here we compute the associated radiative forcing due to well-mixed greenhouse gases using the simplified expressions given in Table 6.2 (for CO_2, the expression in the first row of that Table is employed). The numbers displayed in Table 6.14 represent the radiative forcings in 2050 and 2100 with respect to the year 2000. For the gases relevant to radiative forcing only, the SRES scenarios give a wide range of radiative forcings for the various compounds. Note that the CO_2 forcing increases substantially in the future. All the SRES scenarios give positive radiative forcing values for the well-mixed greenhouse gases (except for the radiative forcing by CH_4 in the B1 scenario for 2100). The scenario for gases relevant to radiative forcing and ozone

depletion yields negative values of the radiative forcing, reflecting the reductions in atmospheric concentrations of ozone depleting gases due to emission control.

From Table 6.11, the radiative forcing due to CO_2 is at present slightly larger than 50% of the total greenhouse gas forcing (including tropospheric O_3). In 2050 and 2100 the SRES scenarios indicate a stronger dominance of CO_2 on the total greenhouse gas forcing (including tropospheric O_3), at about 70 to 80% of the total forcing. The SRES scenarios indicate that HFC-134a will give the largest radiative forcing amongst the HFCs.

6.15.2.2 Tropospheric ozone

The radiative forcings associated with future tropospheric O_3 increases are calculated on the basis of the O_3 changes calculated by Chapter 4 and presented in Appendix II, Table II.2.5 for the various SRES scenarios. The mean forcing per DU estimated from the various models and given in Table 6.3 (i.e., 0.042 Wm⁻²/DU) is used to derive these future forcings. Most scenarios lead to increases in the abundances of tropospheric O_3 and consequently to positive radiative forcings in 2050 and 2100. Scenarios A1fi, A2, and A2p provide the maximum tropospheric O_3 forcings reaching 0.89 Wm⁻² in 2100. Only scenario B1 predicts a decrease in tropospheric O_3 and a negative forcing of −0.16 Wm⁻² in 2100.

6.15.2.3 Aerosol direct effect

The direct radiative forcing due to anthropogenic sulphate, black carbon (BC), and organic carbon (OC) aerosols are assessed using the scenarios described in Chapter 5, Section 5.5.3 and the column burdens presented in Appendix II, Tables II.2.7, II.2.8 and II.2.9 respectively. Scenarios for mineral dust are not considered here, as there is no "best estimate" available (Sections 6.7.6 and 6.13). For each aerosol species, the ratio of the column burdens for the particular scenario to that of the year 2000 is multiplied by the "best estimate" of the present day radiative forcing. The year 2000 "best estimate" radiative forcing is then subtracted to give the radiative forcing for the period from the year 2000 to the date of the scenario. Estimates of the direct radiative forcing for each of the aerosol species are given in Table 6.15.

Table 6.14: *Future (2050 and 2100) radiative forcings due to gases that are relevant for radiative forcing only (based on SRES scenarios), and due to gases that are relevant for radiative forcing and ozone depletion (based on WMO (1999) scenarios). For some gases the results for the IS92a emission scenario, with updated model calculations, are also shown (see Chapter 4 for further details). The radiative forcings presented here are with respect to the year 2000. They may be added to the approximately present day (1998) total radiative forcing given in Table 6.1 to obtain the approximate radiative forcings with respect to pre-industrial times (1750).*

Gas	Radiative forcing (Wm^{-2}) 2050										
	A1b	A1t	A1fi	A2	B1	B2	A1p	A2p	B1p	B2p	IS92a
	Gases relevant to radiative forcing only										
CO$_2$	1.90	1.62	2.24	1.90	1.46	1.37	1.97	1.93	1.30	1.45	1.66
CH$_4$	0.22	0.25	0.30	0.27	0.04	0.20	0.31	0.26	0.09	0.24	0.25
N$_2$O	0.10	0.08	0.18	0.17	0.12	0.08	0.10	0.17	0.12	0.09	0.14
Tropospheric O$_3$	0.24	0.37	0.66	0.43	0.04	0.28	0.32	0.42	0.15	0.28	0.32
HFC-23	0.003	0.003	0.003	0.003	0.003	0.003	0.003	0.003	0.003	0.003	
HFC-125	0.013	0.013	0.013	0.008	0.008	0.008	0.013	0.007	0.008	0.009	0.020
HFC-32	0.001	0.001	0.001	0.001	0.001	0.001	0.001	0.001	0.001	0.001	
HFC-134a	0.079	0.078	0.076	0.043	0.042	0.048	0.111	0.054	0.057	0.070	0.079
HFC-143a	0.009	0.009	0.009	0.006	0.006	0.006	0.010	0.006	0.006	0.007	
HFC-152a	0.000	0.000	0.000	0.000	0.000	0.000	0.000	0.000	0.000	0.000	0.005
HFC-227ea	0.010	0.010	0.010	0.006	0.006	0.007	0.010	0.005	0.006	0.007	
HFC-245ca	0.017	0.017	0.016	0.008	0.009	0.010	0.017	0.008	0.009	0.011	
HFC-43-10mee	0.002	0.002	0.002	0.001	0.001	0.001	0.002	0.001	0.001	0.001	
CF$_4$	0.007	0.007	0.007	0.007	0.004	0.008	0.013	0.010	0.008	0.012	
C$_2$F$_6$	0.002	0.002	0.002	0.002	0.001	0.002	0.003	0.002	0.002	0.002	
C$_4$F$_{10}$	0.000	0.000	0.000	0.000	0.000	0.000	0.007	0.005	0.005	0.005	
SF$_6$	0.010	0.010	0.010	0.011	0.007	0.009	0.011	0.011	0.008	0.011	
	Gases relevant to radiative forcing and ozone depletion										
CFC-11	−0.04										
CFC-12	−0.06										
CFC-113	−0.01										
CFC-114	−0.002										
CFC-115	0.000										
CCl$_4$	−0.009										
CH$_3$CCl$_3$	−0.004										
HCFC-22	−0.020										
HCFC-141b	−0.001										
HCFC-142b	0.000										
HCFC-123	0.000										
Halon-1211	−0.001										
Halon-1301	0.000										

Gas	Radiative forcing (Wm^{-2}) 2100										
	A1b	A1t	A1fi	A2	B1	B2	A1p	A2p	B1p	B2p	IS92a
	Gases relevant to radiative forcing only										
CO$_2$	3.48	2.39	5.15	4.42	2.06	2.73	3.46	4.42	2.34	2.79	3.48
CH$_4$	0.08	0.14	0.51	0.59	−0.07	0.39	0.15	0.58	0.10	0.27	0.43
N$_2$O	0.16	0.11	0.40	0.36	0.17	0.14	0.13	0.36	0.21	0.12	0.25
Tropospheric O$_3$	0.15	0.11	0.89	0.87	−0.16	0.43	0.21	0.87	0.05	0.37	0.55
HFC-23	0.003	0.003	0.003	0.003	0.003	0.003	0.002	0.002	0.002	0.002	
HFC-125	0.031	0.032	0.031	0.025	0.013	0.023	0.030	0.023	0.013	0.023	
HFC-32	0.002	0.002	0.002	0.002	0.001	0.002	0.002	0.002	0.001	0.001	
HFC-134a	0.129	0.142	0.133	0.130	0.055	0.123	0.172	0.168	0.076	0.154	
HFC-143a	0.026	0.027	0.026	0.020	0.012	0.018	0.026	0.020	0.012	0.019	
HFC-152a	0.000	0.000	0.000	0.000	0.000	0.000	0.000	0.000	0.000	0.000	0.007
HFC-227ea	0.021	0.022	0.021	0.018	0.011	0.020	0.020	0.016	0.010	0.018	
HFC-245ca	0.021	0.023	0.022	0.024	0.009	0.024	0.020	0.023	0.009	0.020	
HFC-43-10mee	0.004	0.005	0.004	0.003	0.002	0.003	0.004	0.002	0.002	0.002	
CF$_4$	0.021	0.021	0.021	0.025	0.010	0.024	0.028	0.034	0.015	0.033	
C$_2$F$_6$	0.004	0.004	0.004	0.005	0.002	0.005	0.006	0.007	0.003	0.007	
C$_4$F$_{10}$	0.000	0.000	0.000	0.000	0.000	0.000	0.022	0.016	0.013	0.017	
SF$_6$	0.027	0.027	0.027	0.031	0.016	0.020	0.027	0.032	0.017	0.034	
	Gases relevant to radiative forcing and ozone depletion										
CFC-11	−0.06										
CFC-12	−0.10										
CFC-113	−0.02										
CFC-114	−0.003										
CFC-115	0.000										
CCl$_4$	−0.010										
CH$_3$CCl$_3$	−0.004										
HCFC-22	−0.030										
HCFC-141b	−0.001										
HCFC-142b	−0.002										
HCFC-123	0.000										
Halon-1211	−0.001										
Halon-1301	−0.001										

Table 6.15. *Direct aerosol radiative forcings (Wm^{-2}) estimated as an average of different models for the IPCC SRES scenarios described in Chapter 5. The burdens used in calculating the radiative forcings are given in Appendix II, Tables II.2.7, II.2.8 and II.2.9, the radiative forcings presented here are from the year 2000 to the date of the scenario. They may be added to the present day forcings given in Section 6.7 (–0.4 Wm^{-2} for sulphate aerosols, +0.4 Wm^{-2} assumed for BC aerosols (from fossil fuel and biomass burning), and –0.5 Wm^{-2} assumed for OC aerosols (from fossil fuel and biomass burning)) to obtain the radiative forcings from pre-industrial times.*

Aerosol	Radiative forcing (Wm^{-2}) 2050										
	A1b	A1t	A1fi	A2	B1	B2	A1p	A2p	B1p	B2p	IS92a
Sulphate	+0.03	+0.17	−0.07	−0.21	0.0	+0.08	+0.03	−0.21	+0.10	+0.07	−0.43
BC	+0.13	+0.35	+0.49	+0.21	−0.16	+0.17	+0.37	+0.21	−0.04	+0.12	+0.12
OC	−0.16	−0.43	−0.61	−0.27	+0.20	−0.21	−0.46	−0.27	+0.05	−0.15	−0.15
Aerosol	Radiative forcing (Wm^{-2}) 2100										
	A1b	A1t	A1fi	A2	B1	B2	A1p	A2p	B1p	B2p	IS92a
Sulphate	+0.24	+0.28	+0.17	+0.05	+0.25	+0.12	+0.24	+0.05	+0.23	+0.12	−0.39
BC	+0.30	+0.46	+0.65	+0.56	−0.20	+0.44	+0.55	+0.56	−0.03	+0.40	+0.26
OC	−0.38	−0.58	−0.82	−0.70	+0.25	−0.54	−0.69	−0.70	+0.04	−0.50	−0.33

The uncertainty associated with these estimates of the direct radiative forcing is necessarily higher than the estimates for the year 2000. This is because estimates for the year 2000 are constrained as best as possible to observations. Additionally, the simplified approach applied here does not account for changes in the spatial pattern of the global distribution of the aerosol species that may arise from changes in the geographic distribution of emissions. The uncertainty is therefore estimated as a factor of three for the radiative forcing by sulphate aerosols, and a factor of four for the radiative forcing by BC and OC aerosols.

For sulphate aerosols, only scenarios A1fi, A2, and A2p show a negative direct radiative forcing for the period 2000 to 2050, with all scenarios showing positive radiative forcings over the period 2000 to 2100. This contrasts with the IS92a scenario which predicted an increasingly negative radiative forcing due to the higher column burden of sulphate. For BC aerosols the majority of the scenarios show an increasingly positive direct radiative forcing in 2050 and 2100 (except for B1 and B1p). For OC aerosols, the opposite is true, with the majority of scenarios showing an increasingly negative direct radiative forcing in 2050 and 2100 (except for B1 and B1p). The direct aerosol radiative forcing evolution due to sulphate, black and organic carbon aerosols taken together varies in sign for the different scenarios. The magnitudes are much smaller than that for CO_2. As with the trace gases, there is considerable variation amongst the different scenarios.

6.15.2.4 Aerosol indirect effect

The indirect radiative forcing was calculated by the LLNL/Umich model (Chuang *et al*., 2000a), the GISS model (Koch *et al.*, 1999), and the Max Planck/Dalhousie (Lohmann *et al*., 1999a,b, 2000) model. The LLNL/Umich model uses the mechanistic formulation for the determination of droplet concentration described by Chuang *et al*. (1997) but has been updated to include interactive dust and sea salt. This model provides an estimate of the "first" indirect effect. The GISS model used an empirical formulation for relating droplet concentrations and aerosol concentrations and

also provides an estimate of the "first" indirect effect. The Max-Planck/Dalhousie model used the mechanistic formulation of Chuang *et al.* (1997) as described in Lohmann *et al.* (1999a,b, 2000) and includes both the "first" and "second" indirect effects. In addition, the Max-Planck/Dalhousie model used monthly averaged dust and sea salt fields from the LLNL/Umich model. Further details of the models are provided in Chapter 5. The indirect radiative forcing scenarios are summarised in Table 6.16, and represent the radiative forcing from the year 2000 due to sulphate and carbonaceous aerosols. Some simulations suggest that changes in the concentrations of natural aerosols due to changes in the climate could also contribute to a negative aerosol indirect effect (see Chapter 5).

As for the aerosol direct effect, the uncertainty associated with these estimates is higher than for the estimates for the present day. Considering the very low LOSU of the indirect aerosol effect and the fact that no best estimate was recommended for the present day (Sections 6.8 and 6.13), the numbers provided in Table 6.16 give only a rough indication of how the forcings could change between the present and the future (according to the SRES scenarios) in three different models. Relative to 2000, the change in the direct plus indirect aerosol radiative forcing is projected to be smaller in magnitude than that of CO_2.

Table 6.16: Indirect aerosol radiative forcing (Wm^{-2}) estimated by different models for the IPCC SRES scenarios described in Chapter 5. The sulphate burdens in each case are given in Chapter 5, Table 5.14. These estimates are from the average difference in cloud forcing between two simulations. The numbers represent the radiative forcing from 2000. No numbers are given for the year 2000 as no best estimate of the radiative forcing is suggested in Section 6.8.

	LLNL/Umich	GISS	Max Planck/ Dalhousie
A2 2030	−0.24	−0.29	−0.05
A2 2100	−0.47	−0.36	−0.32
B1 2100	+0.10		

Appendix 6.1 Elements of Radiative Forcing Concept

The principal elements of the radiative forcing concept are summarised below.

(A) The concept was developed first in the context of the one-dimensional radiative-convective models that investigated the equilibrated global, annual mean surface temperature responses to radiative perturbations caused by changes in the concentrations of radiatively active species (Manabe and Wetherald, 1967; Ramanathan and Coakley, 1978; WMO, 1986). Over the past decade, the concept has been extended to cover different spatial dimensions and seasonal time-scales (IPCC, 1992, 1994).

(B) In the one-dimensional radiative-convective model framework, the surface and troposphere are closely coupled, behaving as a single thermodynamic system under the joint control of radiative and convective processes, with a specified lapse rate determining the thermal structure. The stratospheric state is determined by the radiative equilibrium condition. The stratosphere and troposphere irradiances are together constrained by the requirement that the top of the atmosphere net total irradiance (i.e., radiative energy absorbed minus that emitted by the Earth's entire climate system) must be zero at equilibrium. In applying the forcing concept to arbitrary spatial and seasonal time-scales, as opposed to the global annual mean, it has been assumed (WMO, 1992; SAR) that the stratosphere is in radiative-dynamical (rather than radiative) equilibrium (see (D) below).

(C) The stratosphere is a *fast response* system which, in response to an imposed radiative perturbation, comes into equilibrium on a time-scale (about a few months) that is much more rapid than the surface-troposphere system (typically decades) (Hansen *et al.*, 1997a; Shine and Forster, 1999). The latter is a *slow response* system owing principally to the thermal inertia of the oceans.

(D) When a perturbation is applied (such as increases in well-mixed greenhouse gases), there is an *instantaneous* change in irradiances that is manifest in general as a radiative imbalance (forcing) at the surface, tropopause and the top of the atmosphere. The rapid thermal re-equilibration of the stratosphere leads to an alteration of the radiative imbalance imposed on the surface-troposphere system (WMO, 1992), thereby yielding an *adjusted* forcing (SAR). The surface and troposphere, operating in a *slow response* mode, are still in a process of adjustment while the stratosphere has already reached its new equilibrium state. The SAR points out the clear distinction existing between the *instantaneous* and *adjusted* forcings.

For the arbitrary space and time mean stratosphere, there arises the need to evaluate the radiative flux changes with the stratosphere in a radiative-dynamical equilibrium. A classical method to determine this is the "Fixed Dynamical Heating" (FDH; WMO, 1995) in which it is assumed that the dynamical heating rate in the stratosphere is unchanged and that the stratosphere comes to a new thermal equilibrium in response to the perturbation through adjustments in the temperature profile, such that a new radiative-dynamical equilibrium is attained (*radiative response*; see Ramanathan and Dickinson (1979) and Fels *et al.* (1980)). The resulting adjustment process in the stratosphere makes an additional contribution to the forcing of the surface-troposphere system. When the stratosphere has adjusted to a new radiative-dynamical equilibrium with resultant changes to its thermal state, the change in flux at the tropopause and at the top of the atmosphere become identical. It is important that the stratosphere be in radiative-dynamical equilibrium and, as shown by Hansen *et al.* (1997a), it is the *adjusted* rather than the *instantaneous* forcing that is a more relevant indicator of the surface temperature response. The adjustment of stratosphere is crucial for some of the forcings, but not for all of them (Shine and Forster, 1999). In the case of some radiative perturbations, the stratosphere is hardly perturbed and the instantaneous and adjusted radiative flux changes thus tend to be similar (SAR). In other cases, there is only a small (20% or less) influence due to the stratospheric adjustment process. However, for the case of ozone depletion in the lower stratosphere, the effect of a stratospheric adjustment could even yield a change in the sign of the forcing.

(E) As a direct consequence of the above, the forcing definition most appropriate for the response of the surface-troposphere system to a radiative perturbation is the net (down minus up) radiative (solar plus long-wave) change defined at the tropopause after the stratosphere has come to a new thermal equilibrium state. Thus, the level at which the tropopause is assumed in the models is an important aspect for the quantitative determination of the forcing (Forster *et al.*, 1997), as is the model vertical resolution used to resolve the vicinity of the tropopause region (Shine *et al.*, 1995). The classical radiative-convective model definition of the tropopause considers it as a boundary between a region where radiative-convective equilibrium prevails (i.e., troposphere) and a region that is in radiative (or radiative-dynamical, i.e., stratosphere) equilibrium. Such a distinction could be ambiguous in the case of the three-dimensional GCMs or the real world. However, radiative forcing appears to be relatively robust to changes in the definition of the tropopause in a GCM (Christiansen, 1999).

(F) A major motivation for the radiative forcing concept is the ease of climate change analysis when radiative forcing, feedback, and climate response are distinguished from one another. Such a separation is possible in the modelling framework where forcing and feedback can be evaluated separately e.g., for the case of CO_2 doubling effects (see Dickinson, 1982; Dickinson and Cicerone, 1986; Cess and Potter, 1988; Cess *et al.*, 1993). The consideration of forcing, feedback and response as three distinct entities in the modelling framework (see also Charlson, 2000) while originating from the one-dimensional radiative/convective models, has made the transition to GCM studies of climate (Hansen *et al.*, 1981; Wetherald and Manabe, 1988; Chen and Ramaswamy, 1996a).

(G) A critical aspect of the separability mentioned in (F) is holding the surface and troposphere state fixed in the evaluation

of the radiative forcing. For example, in the case of a change in the concentration of a radiatively active species, the term "state" implies that all parameters are held at the unperturbed values with only the concerned species' concentration being changed. Thus, in the strictest sense, temperature in the troposphere, water vapour and clouds in the entire atmosphere, and circulation, are held fixed in the computation of the irradiance changes at the tropopause, with only the stratosphere adjusted to a new thermal equilibrium state via the radiative response. In contrast to this prescription for calculating the forcing, the resulting changes in the meteorological and climatic parameters (e.g., tropospheric temperature and water vapour) constitute responses to the imposed perturbation (WMO, 1986; Charlson, 2000). In the IPCC context, the change in a radiative agent's characteristic has involved anthropogenic (e.g., CO_2) and natural (e.g., aerosols after a volcanic eruption) perturbations.

It is important to emphasise that changes in water vapour in the troposphere are viewed as a feedback variable rather than a forcing agent. However, in the case of the second indirect aerosol forcing, the separation is less distinct. Anthropogenic emissions (e.g., aircraft, fossil fuel) or precursors to water vapour are negligible. The same is true for changes in water vapour in the stratosphere, except in the instance that the oxidation of CH_4 provides an input. Changes in the condensed liquid and solid phases of water (i.e., clouds) are also considered as part of the climate feedback. The strict requirement of no feedbacks in the surface and troposphere demands that no secondary effects such as changes in troposphere motions or its thermodynamic state, or dynamically-induced changes in water substance in the surface and atmosphere, be included in the evaluation of the net irradiance change at the tropopause. (Note: the second indirect effect of aerosols consists of microphysically-induced changes in the water substance.)

(H) The foregoing governing factors reflect the fundamental recognition that, in response to an externally imposed radiative forcing, there is a shift in the equilibrium state of the climate system. This forcing of the climate change in the IPCC parlance is to be distinguished from *forcing* definitions initiated for other purposes, e.g., cloud forcing (Ramanathan *et al.*, 1989), sea surface temperature related forcing during ENSO periods, etc.

References

Abbas, M.A. and J. Latham, 1969: The electrofreezing of supercooled water drops. *J. Met. Soc. Japan*, **47**, 65-74.

Ackerman, S.A. and H. Chung, 1992: Radiative effects of airborne dust on regional energy budgets at the top of the atmosphere. *J. Appl. Meteor.*, **31**, 223-233.

Ackerman, A.S., O.B. Toon, D.E. Stevens, A.J. Heymsfield, V. Ramanathan, and E.J. Welton, 2000: Reduction of tropical cloudiness by soot. *Science*, **288**, 1042-1047.

Adams, P.J., J.H. Seinfeld, D.M. Koch, L Mickley, and D. Jacob, 2001: General circulation model assessment of direct radiative forcing by the sulfate-nitrate-ammonium-water inorganic aerosol system. *J. Geophys. Res.*, **106**, 1097-1111.

Albrecht, B.A., 1989: Aerosols, cloud microphysics, and fractional cloudiness. *Science*, **245**, 1227-1230.

Allen, D., K. Pickering, G. Stenchikov, A. Thompson, and Y. Kondo, 2000: A three-dimensional total odd nitrogen (NOy) simulation during SONEX using a stretched-grid chemical transport model. *J. Geophys. Res.*, **105**, 3851-3876.

Andronova, N.G., E.V. Rozanov, F. Yang. M.E. Schlesinger, and G.L. Stenchikov, 1999: Radiative forcing by volcanic aerosols from 1850 through 1994. *J. Geophys. Res.*, **104**, 16807-16826.

Arnold, N.F. and T.R. Robinson, 1998: Solar cycle changes to planetary wave propagation and their influence on the middle atmosphere circulation. *Annal. Geophys.*, **16**, 69-76.

Baliunas, S. and R. Jastrow, 1990: Evidence for long-term brightness changes of solar-type stars. *Nature*, **348**, 520-523.

Ballard, J., R.J. Knight, D.A. Newnham, J. Vander Auwera, M. Herman, G. Di Lonardo, G. Masciarelli, F.M. Nicolaisen, J.A. Beukes, L.K. Christensen, R. McPheat, G. Duxbury, R. Freckleton, and K.P. Shine, 2000: An intercomparison of laboratory measurements of absorption cross-sections and integrated absorption intensities for HCFC-22. *J. Quant. Spectrosc. Radiat. Transfer.*, **66**, 109-128.

Barry, J., G. Locke, D. Scollard, H. Sidebottom, J. Treacy, C. Clerbaux, R. Colin, and J. Franklin, 1997: 1,1,1,3,3,-pentafluorobutane (HFC-365mfc): Atmospheric degradation and contribution to radiative forcing. *Int. J. Chem. Kinet.*, **29**, 607-617.

Beer, J., S.T. Baumgartner, B. Dittrich-Hannen, J. Hauenstein, P. Kubik, C. Lukasczyk, W. Mende, R. Stellmacher, and M. Suter, 1994: Solar variability traced by cosmogenic isotopes. In: The Sun as a Variable Star [Pap, J.M., C. Fröhlich, H.S. Hudson, and S.K. Solanki (eds.)]. CUP 291-300.

Bekki, S., K.S. Law, and J.A. Pyle, 1994: Effect of ozone depletion on atmospheric CH_4 and CO concentrations. *Nature*, **371**, 595-597.

Berger, A., C. Tricot, H. Gallée, and M.F. Loutre, 1993: Water vapor, CO_2 and insolation over the last glacial-interglacial cycles. *Phil. Trans. Roy. Soc. London. B,* **341**, 253-261.

Berntsen, T.K. and I.S.A. Isaksen, 1999: Effects of lightning and convection on changes in tropospheric ozone due to NO_x emissions from aircraft. *Tellus*, **51B**, 766-788.

Berntsen, T., I.S.A. Isaksen, W.-C. Wang, and X-Z. Liang, 1996: Impacts of increased anthropogenic emissions in Asia on tropospheric ozone and climate. *Tellus*, **48B**, 13-32.

Berntsen, T.K., I.S.A. Isaksen, G. Myhre, J.S. Fuglestvedt, F. Stordal, T. A. Larsen, R.S. Freckleton, and K.P. Shine, 1997: Effects of anthropogenic emissions on tropospheric ozone and its radiative forcing. *J. Geophys. Res.*, **102**, 28101-28126.

Berntsen, T.K., G. Myhre, F. Stordal, and I.S.A. Isaksen, 2000: Time evolution of tropospheric ozone and its radiative forcing. *J. Geophys. Res.*, **105**, 8915-8930.

Betts, R., 2001: Biogeophysical impacts of land use on present-day climate: near-surface temperature and radiative forcing. *Atmos. Sci. Lett.*, doi:10.1006/asle.2000.0023.

Bintanja, R., J.P.F. Fortuin, and H. Kelder, 1997: Simulation of the

meridionally and seasonally varying climate response caused by changes in ozone concentration. *J. Climate*, **10**, 1288-1311.

Boucher, O., 1995: GCM estimate of the indirect aerosol forcing using satellite-retrieved cloud effective droplet radii. *J. Climate*, **8**, 1403-1409.

Boucher, O., 1999: Aircraft can increase cirrus cloudiness. *Nature*, **397**, 30-31.

Boucher, O. and H. Rodhe, 1994: The sulfate-CCN-cloud albedo effect: A sensitivity study. Report CM-83, Department of Meteorology, Stockholm University, 20 pp.

Boucher, O. and T.L. Anderson, 1995: GCM assessment of the sensitivity of direct climate forcing by anthropogenic sulfate aerosols to aerosol size and chemistry. *J. Geophys. Res*., **100**, 26117-26134.

Boucher, O. and U. Lohmann, 1995: The sulfate-CCN-cloud albedo effect: A sensitivity study using two general circulation models. *Tellus*, **47B**, 281-300.

Boucher, O. and D. Tanré, 2000: Estimation of the aerosol perturbation to the Earth's radiative budget over oceans using POLDER satellite aerosol retrievals. *Geophys. Res. Lett*., **27**, 1103-1106.

Boucher, O., H. Le Treut, and M.B. Baker, 1995: Precipitation and radiation modelling in a GCM: Introduction of cloud microphysics. *J. Geophys. Res*., **100**, 16395-16414.

Boucher, O., S.E. Schwartz, T.P. Ackerman, T.L. Anderson, B. Bergstrom, B. Bonnel, P. Chylek, A. Dahlback, Y. Fouquart, Q. Fu, R.N. Halthore, J.M. Haywood, T. Iversen, S. Kato, S. Kinne, A. Kirkevåg, K.R. Knapp, A. Lacis, I. Laszlo, M.I. Mishchenko, S. Nemesure, V. Ramaswamy, D.L. Roberts, P. Russell, M.E. Schlesinger, G.L. Stephens, R. Wagener, M. Wang, J. Wong, and F. Yang, 1998: Intercomparison of models representing direct shortwave radiative forcing by sulfate aerosols. *J. Geophys. Res*., **103**, 16979-16998.

Brasseur, G.P., J.T. Kiehl, J.-F. Muller, T. Schneider, C. Granier, X.X. Tie, and D. Hauglustaine, 1998: Past and future changes in global tropospheric ozone: impact on radiative forcing. *Geophys. Res. Lett*., **25,** 3807-3810.

Brueckner, G.E., K.L. Edlow, L.E. Floyd, J.L. Lean, and M.E. VanHoosier, 1993: The Solar Ultraviolet Spectral Irradiance Monitor (SUSIM) experiment on board the Upper Atmosphere Research Satellite (UARS). *J. Geophys. Res*., **98**, 10695-10711.

Brühl, C., 1993: The impact of the future scenarios for methane and other chemically active gases on the GWP of methane. *Chemosphere*, **26**, 731-738.

Capaldo, K., J.J. Corbett, P. Kasibhatla, P. Fischbeck, and S.N. Pandis, 1999: Effects of ship emissions on sulphur cycling and radiative climate forcing over the ocean. *Nature*, **400**, 743-746.

Cavalli, F., M. Glasius, S. Hjorth, B. Rindone, and N. R. Jensen, 1998: Atmospheric lifetimes, infrared spectra, and degradation products of a series of hydrofluoroethers. *Atmos. Env.*, **32**, 3767-3773.

Cebula, R. P., M.T. DeLand, and E. Hilsenrath, 1998: NOAA 11 Solar Backscattered Ultraviolet, model 2 (SBUV/2) instrument solar spectral irradiance measurements in 1989-1994. 1. Observations and long-term calibration. *J. Geophys. Res*., **103**, 16235-16249.

Cess, R.D. and G.L. Potter, 1988: A methodology for understanding and intercomparing atmospheric climate feedback processes in GCMs. *J. Geophys. Res*., **93**, 8305-8314.

Cess, R.D., M.-H. Zhang, G.L. Potter, H.W. Barker, R.A. Colman, D.A. Dazlich, A.D. Del Genio, M. Esch, J.R. Fraser, V. Galin, W.L. Gates, J.J. Hack, W.J. Ingram, J.T. Kiehl, A.A. Lacis, H. Le Treut, Z.-X. Li, X.Z. Liang, J.-F. Mahfouf, B.J. McAvaney, K.P. Meleshko, J.-J. Morcrette, D.A. Randall, E. Roeckner, J.-F. Royer, A.P. Sokolov, P.V. Sporyshev, K.E. Taylor, W.-C. Wang, and R.T. Wetherald, 1993: Uncertainties in CO_2 radiative forcing in atmospheric general circulation models. *Science*, **262**, 1252-1255.

Chalita, S., D.A. Hauglustaine, H. Le Treut, and J.-F. Müller, 1996: Radiative forcing due to increased tropospheric ozone concentra-tions. *Atmos. Env.*, **30**, 1641-1646.

Chandra, S., J.R. Ziemke, W. Min, and W.G. Read, 1998: Effects of 1997-1998 El Niño on tropospheric ozone and water vapor. *Geophys. Res. Lett*., **25**, 3867-3870.

Chandra, S., J.R. Ziemke, and R.W. Stewart, 1999: An 11-year solar cycle in tropospheric ozone from TOMS measurements. *Geophys. Res. Lett*., **26**, 185-188.

Charlson, R.J., 2000: The coupling of biogeochemical cycles and climate: Forcings, feedbacks and responses. In "Earth System Sciences: from Biogeochemical Cycles to Global Change", Academic Press.

Charlson, R.J., S.E. Schwartz, J.M. Hales, R.D. Cess, J.A. Coakley, J.E. Hansen, and D.J. Hofmann, 1992: Climate forcing by anthropogenic aerosols. *Science*, **255**, 423-430.

Charlson, R.J., T.L. Anderson, and H. Rodhe, 1999: Direct climate forcing by anthropogenic aerosols: quantifying the link between sulfate and radiation. *Contrib. Atmos. Phys.*, **72**, 79-94.

Chazette, P., C. Clerbaux, and G. Mégie, 1998: Direct estimate of methane radiative forcing by use of nadir spectral radiances. *Applied Optics*, **37**, 3113-3120.

Chen, C-T. and V. Ramaswamy, 1996a: Sensitivity of simulated global climate to perturbations in low cloud microphysical properties. I. Globally uniform perturbations. *J. Climate*, **9**, 1385-1402.

Chen, C-T. and V. Ramaswamy, 1996b: Sensitivity of simulated global climate to perturbations in low cloud microphysical properties. II. Spatially localized perturbations. *J. Climate*, **9**, 2788-2801.

Chin, M. and D.J. Jacob, 1996: Anthropogenic and natural contributions to tropospheric sulfate: a global model analysis. *J. Geophys. Res*., **101**, 18691-18699.

Christiansen, B., 1999: Radiative forcing and climate sensitivity: The ozone experience. *Quart. J. R. Meteorol. Soc*., **125**, 3011-3035.

Christensen, L.K., J. Sehested, O.J. Nielsen, M. Bilde, T.J. Wallington, A. Guschin, L.T. Molina, and M.J. Molina, 1998: Atmospheric chemistry of HFE-7200 ($C_4F_9OC_2H_5$): Reaction with OH radicals, fate of $C_4F_9OCH_2CH_2O$ and C_4F_9OCHO CH_3 radicals. *J. Phys. Chem*. A, **102**, 4839-4845.

Christidis, N., M.D. Hurley, S. Pinnock, K.P. Shine, and T.J. Wallington, 1997: Radiative forcing of climate change by CFC-11 and possible CFC replacements. *J. Geophys. Res*., **102**, 19597-19609.

Christopher, S.A., D.V., Kliche, J. Chou, and R.M. Welch, 1996: First estimates of the radiative forcing of aerosols generated from biomass burning using satellite data. *J. Geophys. Res*., **101**, 21265-21273.

Chuang, C.C., J.E. Penner, K.E. Taylor, and J.J. Walton, 1994: Climate effects of anthropogenic sulfate: Simulations from a coupled chemistry/climate model. In: Preprints of the Conference on Atmospheric Chemistry, Nashville, Tennessee, January 1994. American Meteorological Society, Boston, USA, pp. 170-174.

Chuang, C.C., J.E. Penner, K.E. Taylor, A.S. Grossman, and J.J. Walton, 1997: An assessment of the radiative effects of anthropogenic sulfate. *J. Geophys. Res*., **102**, 3761-3778.

Chuang, C.C., J.E. Penner, and Y. Zhang, 2000a: Simulations of aerosol indirect effect for IPCC emissions scenarios. In: Proceedings of the 11th Symposium on Global Change Studies, January 9-14, 2000, Long Beach, California. American Meteorological Society, Boston, USA, pp. 320-323.

Chuang, C.C., J.E. Penner, J.M. Prospero, K.E. Grant and G.H. Rau, 2000b: Effects of anthropogenic aerosols on cloud susceptibility: a sensitivity study of radiative forcing to aerosol characteristics and global concentration. Lawrence Livermore National Laboratory Internal Report, No. UCRL-JC-139097 Rev. 1., Lawrence Livermore National Laboratory, CA, USA.

Chylek, P. and J. Wong, 1995: Effect of absorbing aerosols on the global radiation budget. *Geophys. Res. Lett*., **22**, 929-931.

Chylek, P., G. Videen, and D. Ngo, 1995: Effect of black carbon on the optical properties and climate forcing of sulfate aerosols. *J. Geophys.*

Res., **100**, 16325-16332.

Chylek, P., C.M. Banic, B. Johnson, P.A. Damiano, G.A. Isaac, W.R. Leaitch, P.S.K. Liu, F.S. Boudala, B. Winter, and D. Ngo, 1996a: Black carbon: Atmospheric concentrations and cloud water content measurements over southern Nova Scotia. *J. Geophys. Res.*, **101**, 29105-29110.

Chylek, P., G.B. Lesins, G. Videen, J.G.D. Wong, R.G. Pinnick, D. Ngo, and J.D. Klett, 1996b: Black carbon and absorption of solar radiation by clouds. *J. Geophys. Res.*, **101**, 23365-23371.

Claquin, T., M. Schulz, Y. Balkanski, and O. Boucher, 1998: Uncertainties in assessing radiative forcing by mineral dust. *Tellus*, **50B**, 491-505.

Cooke, W.F. and J.J.N. Wilson, 1996: A global black carbon model. *J. Geophys. Res.*, **101**, 19395-19409.

Cooke, W.F., C. Liousse, H. Cachier, and J. Feichter, 1999: Construction of a 1°x1° fossil-fuel emission dataset for carbonaceous aerosol and implementation and radiative impact in the ECHAM-4 model. *J. Geophys. Res.*, **104**, 22137-22162.

Cox, S.J., W.-C. Wang, and S.E. Schwartz, 1995: Climate response to forcings by sulfate aerosols and greenhouse gases. *Geophys. Res. Lett.*, **18**, 2509-2512.

Crommelynk, D., A. Fichot, R.B. Lee III, and J. Romero, 1995: First realisation of the space absolute radiometric reference (SARR) during the ATLAS 2 flight period. *Adv. Spac. Res.*, **16**, 17-23.

Daniel, J.S. and S. Solomon, 1998. On the climate forcing of carbon monoxide. *J. Geophys. Res.*, **103**, 13249-13260.

Daniel, J.S., S. Solomon, and D. Albritton, 1995: On the evaluation of halocarbon radiative forcing and global warming potentials. *J. Geophys. Res.*, **100**, 1271-1285.

DeLand, M.T. and R.P. Cebula, 1998: NOAA 11 Solar Backscattered Ultraviolet, model 2 (SBUV/2) instrument solar spectral irradiance measurements in 1989-1994. 2. Results, validation, and comparisons. *J. Geophys. Res.*, **103**, 16251-16273.

Delobbe, L. and H. Gallée, 1998: Simulation of marine stratocumulus: Effect of precipitation parameterization and sensitivity to droplet number concentration. *Boundary-Layer Meteorol.*, **89**, 75-107.

DeMore, W.B., S.P. Sander, D.M. Golden, R.F. Hampson, M.J. Kurylo, C.J. Howard, A.R. Ravishankara, C.E. Kolb, and M.J. Molina, 1997: Chemical kinetics and photochemical data for use in stratospheric modeling, Evaluation Number **12**, JPL Publ. 97-4, Jet Propulsion Laboratory, Pasadena, Calif.

Dentener, F.J., G.R. Carmichael, Y. Zhang, J. Lelieveld, and P. Crutzen, 1996: Role of mineral aerosol as a reactive surface in the global troposphere. *J. Geophys. Res.*, **101**, 22869-22889.

Dickinson, R.E., 1982: In: Carbon Dioxide Review [Clark, W.C. (ed.)]. Clarendon, New York, NY, USA, pp. 101-133.

Dickinson, R.E., and R.J. Cicerone, 1986: Future global warming from atmospheric trace gases. *Nature*, **319**, 109-115.

van Dorland, R., F.J. Dentener, and J. Lelieveld, 1997: Radiative forcing due to tropospheric ozone and sulfate aerosols. *J. Geophys. Res.*, **102**, 28079-28100.

Emmons, L.K., M.A. Carroll, D.A. Hauglustaine, G.P. Brasseur, C. Atherton, J. Penner, S. Sillman, H. Levy, F. Rohrer, W.M.F. Wauben, P.F.J. Van Velthoven, Y. Wang, D. Jacob, P. Bakwin, R. Dickerson, B. Doddridge, C. Gerbig, R. Honrath, G. Hübler, D. Jaffe, Y. Kondo, J.W. Munger, A. Torres, and A. Volz-Thomas, 1997: Climatologies of NO$_x$ and NOy: a comparison of data and models. *Atmos. Env.*, **31**, 1851-1904.

Evans, W.F.J. and E. Puckrin, 1995: An observation of the greenhouse radiation associated with carbon monoxide. *Geophys. Res. Lett.*, **22**, 925-928.

Evans, W.F.J. and E. Puckrin, 1999: A comparison of GCM models with experimental measurements of surface radiative forcing by greenhouse gases. 10th Symposium on Global Change Studies, American Meteorological Society, pp. 378-381, 10-15 January 1999,

Dallas, Texas.

Evans, S.J., R. Toumi, J.E. Harries, M.P. Chipperfield, and J.M. Russell III, 1998: Trends in stratospheric humidities and the sensitivity of ozone to these trends. *J. Geophys. Res.*, **103**, 8715-8725.

Fahey, D.W., U. Schumann, S. Ackerman, P. Artaxo, O. Boucher, M.Y. Danilin, B. Kärcher, P. Minnis, T. Nakajima, and O.B. Toon, 1999: Aviation-produced aerosols and cloudiness. In: Intergovernmental Panel on Climate Change Special Report on Aviation and the Global Atmosphere [Penner, J.E., D.H. Lister, D.J. Griggs, D.J. Dokken, and M. McFarland (eds.)]. Cambridge University Press, Cambridge, United Kingdom and New York, NY, USA, pp. 65-120.

Farrar, P.D., 2000: Are cosmic rays influencing oceanic cloud coverage – Or is it only El Niño? *Clim. Change*, **47**, 7-15.

Feichter, J., U. Lohmann, and I. Schult, 1997: The atmospheric sulfur cycle in ECHAM-4 and its impact on the shortwave radiation. *Clim. Dyn.*, **13,** 235-246.

Fels, S.B., J.D. Mahlman, M.D. Schwarzkopf, and R.W. Sinclair, 1980: Stratospheric sensitivity to perturbations in ozone and carbon dioxide: Radiative and dynamical response. *J. Atmos. Sci.*, **37**, 2265-2297.

Fishman, J., 1991: The global consequences of increasing tropospheric ozone concentrations. *Chemosphere*, **22**, 685-695.

Fishman, J. and V.G. Brackett, 1997: The climatological distribution of tropospheric ozone derived from satellite measurements using version 7 Total Ozone Mapping Spectrometer and Stratospheric Aerosol and Gas Experiment data sets. *J. Geophys. Res.*, **102**, 19275-19278.

Fleming, E.L., S. Chandra, C.H. Jackman, D.B. Considine, and A.R. Douglass, 1995: The middle atmosphere response to short and long term UV variations: An analysis of observations and 2D model results. *J. Atmos. Terr. Phys.*, **57**, 333-365.

Floyd, L.E., P.A. Reiser, P.C. Crane, L.C. Herring, D.K. Prinz, and G.E. Brueckner, 1998: Solar cycle 22 UV spectral irradiance variability: Current measurements by SUSIM UARS. *Solar Phys.*, **177**, 79-87.

Forster, P.M. de F., 1999: Radiative forcing due to stratospheric ozone changes 1979-1997, using updated trend estimates, *J. Geophys. Res.*, **104**, 24,395-24,399.

Forster, P. M. de F. and K.P. Shine, 1999: Stratospheric water vapour changes as a possible contributor to observed stratospheric cooling, *Geophys. Res. Lett.*, **26**, 3309-3312.

Forster, P.M. de F. and K.P. Shine, 1997: Radiative forcing and temperature trends from stratospheric ozone changes. *J. Geophys. Res.*, **102**, 10841-10857.

Forster, P.M. de F., R.S. Freckleton, and K.P. Shine, 1997: On aspects of the concept of radiative forcing. *Clim. Dyn.*, **13**, 547-560.

Forster, P.M. de F., M. Blackburn, R. Glover, and K.P. Shine, 2001: An examination of climate sensitivity for idealized climate change experiments in an intermediate general circulation model. *Clim. Dyn.*, **16**, 833-849.

Fortuin, J.P.F. and H. Kelder, 1996: Possible links between ozone and temperature profiles. *Geophys. Res. Lett.*, **23**, 1517-1520.

Fowler, L.D., D.A. Randall, and S.A. Rutledge, 1996: Liquid and ice cloud microphysics in the CSU general circulation model. Part I: Model description and simulated microphysical processes. *J. Climate*, **9**, 489-529.

Freckleton, R.S., S. Pinnock, and K.P. Shine, 1996: Radiative forcing of halocarbons: A comparison of line-by-line and narrow-band models using CF$_4$ as an example. *J. Quant. Spectrosc. Radiat. Transfer*, **55**, 763-769.

Freckleton, R.S., E.J. Highwood, K.P. Shine, O. Wild, K.S. Law, and M.G. Sanderson, 1998: Greenhouse gas radiative forcing: Effects of averaging and inhomogeneities in trace gas distribution. *Q. J. R. Meteorol. Soc.*, **124**, 2099-2127.

Fröhlich, C. and J. Lean, 1998: The Sun's total irradiance: Cycles, trends and related climate change uncertainties since 1976. *Geophys. Res.*

Lett., **25**, 4377-4380.

Fuglestvedt, J.S., J.E. Jonson, and I.S.A. Isaksen, 1994: Effects of reduction in stratospheric ozone on tropospheric chemistry through changes in photolysis rates. *Tellus*, **46B**, 172-192.

Fuglestvedt, J.S., J.E. Jonson, W.-C. Wang, and I.S.A. Isaksen, 1995: Response in tropospheric chemistry to changes in UV fluxes, temperatures and water vapor densities. In: Atmospheric Ozone as a Climate Gas [Wang, W.-C. and I.S.A. Isaksen (eds.)]. NATO Series I 32, Springer-Verlag, Berlin, Germany, pp. 143-162.

Fuglestvedt, J.S., I.S.A. Isaksen, and W.-C. Wang, 1996: Estimates of indirect global warming potentials for CH_4, CO, and NO_x. *Clim. Change*, **34**, 405-437.

Fuglestvedt, J.S., T.K. Berntsen, I.S.A. Isaksen, H. Mao, X.-Z. Liang, and W.-C. Wang, 1999: Climate forcing of nitrogen oxides through changes in tropospheric ozone and methane: global 3D model studies. *Atmos. Env.*, **33**, 961-977.

Fuglestvedt, J. S., T. K. Berntsen, O. Godal, and T. Skodvin, 2000: Climate implications of GWP-based reductions in greenhouse gas emissions. *Geophys. Res. Lett*., **27**, 409-412.

Ghan, S. and R. Easter, 1998: Comments: A limited-area-model case study of the effects of sub-grid scale variations in relative humidity and cloud upon the direct radiative forcing of sulfate aerosol. *Geophys. Res. Lett*., **25**, 1039-1040.

Ghan, S.J., G. Guzman, and H. Abdul-Razzak, 1998: Competition between sea salt and sulfate particles as cloud condensation nuclei. *J. Atmos. Sci*., **55**, 3340-3347.

Ghan, S.J., R.C. Easter, E. Chapman, H. Abdul-Razzak, Y. Zhang, R. Leung, N. Laulainen, R. Saylor, and R. Zaveri, 2001a: A physically-based estimate of radiative forcing by anthropogenic sulfate aerosol. *J. Geophys. Res.*, in press.

Ghan, S., R. Easter, J. Hudson, and F.-M. Bréon, 2001b: Evaluation of aerosol indirect radiative forcing in MIRAGE. *J. Geophys. Res.*, in press.

Gierczak, T., R.K. Talukdar, J.B. Burdkholder, R.W. Portmann, J.S. Daniel, S. Solomon, and A.R. Ravishankara, 1996: Atmospheric fate and greenhouse warming potentials of HFC-236fa and HFC-236ea. *J. Geophys. Res*., **101**, 12905-12911.

Gierens, K. and M. Ponater, 1999: Comment on "Variation of cosmic ray flux and global cloud coverage - a missing link in solar-climate relationships" by H. Svensmark and E. Friis-Christensen. *J. Atmos. Solar-Terrest. Phys.*, **61**, 795-797.

Good, D.A., J.S. Francisco, A.K. Jain, D.J. Wuebbles, 1998: Lifetimes and global warming potentials for dimethyl ether and for fluorinated ethers: CH_3OCF_3 (E143a), CHF_2OCHF_2 (E134), CHF_2OCF_3 (E125). *J. Geophys. Res*., **103**, 28181-28186.

Graf, H.-F., J. Feichter, and B. Langmann, 1997: Volcanic sulfur emissions: Estimates of source strength and its contribution to the global sulfate distribution. *J. Geophys. Res*., **102**, 10727-10738.

Granier, C., J.-F. Müller, S. Madronich, and G. P. Brasseur, 1996: Possible causes for the 1990-1993 decrease in global tropospheric CO abundances: a three-dimensional sensitivity study. *Atmos. Env.*, **30**, 1673-1682.

Grant, K.E., C.C. Chuang, A.S. Grossman, and J.E. Penner: 1999: Modeling the spectral optical properties of ammonium sulfate and biomass aerosols: Parameterization of relative humidity effects and model results. *Atmos. Env.*, **33**, 2603-2620.

Grossman, A.S., K.E. Grant, W.E. Blass, and D.J. Wuebbles, 1997: Radiative forcing calculations for CH_3Cl and CH_3Br. *J. Geophys. Res.*, **102**, 13651-13656.

Gupta, M., L., R.J. Cicerone, and S. Elliott, 1998: Perturbation to global tropospheric oxidizing capacity due to latitudinal redistribution of surface sources of NO_x, CH_4, and CO. *Geophys. Res. Lett*., **25**, 3931-3934.

Haigh, J.D., 1994: The role of stratospheric ozone in modulating the solar radiative forcing of climate. *Nature*, **370**, 544-546.

Haigh, J.D., 1996: The impact of solar variability on climate. *Science*, **272**, 981-984.

Haigh, J.D., 1999: A GCM study of climate change in response to the 11-year solar cycle. *Quart. J. Roy. Meteorol. Soc.*, **125**, 871-892.

Han, Q., W.B. Rossow, and A.A. Lacis, 1994: Near-global survey of effective droplet radii in liquid water clouds using ISCCP data. *J. Climate*, **7**, 465-497.

Han, Q., W.B. Rossow, J. Chou, and R.M. Welch, 1998: Global survey of the relationships of cloud albedo and liquid water path with droplet size using ISCCP. *J. Climate*, **7**, 1516-1528.

Hansen, J., D. Johnson, A. Lacis, S. Lebedeff, P. Lee, D. Rind, and G. Russell, 1981: Climate impact of increasing atmospheric carbon dioxide. *Science*, **213**, 957-966.

Hansen, J., A. Lacis, D. Rind, G. Russell, P. Stone, I. Fung, R. Ruedy, and J. Lerner, 1984: Climate sensitivity: analysis of feedback mechanisms, in Climate Processes and Climate Sensitivity Geophys. Monogr. Ser., New York, **29**, pp. 130-163.

Hansen, J., I. Fung, A. Lacis, D. Rind, S. Lebedeff, R. Ruedy, G. Russell, and P. Stone, 1988: Global climate changes as forecast by Goddard Institute for Space Studies 3-dimensional model. *J. Geophys. Res.*, **93**, 9341-9364.

Hansen, J., A. Lacis, R. Ruedy, M. Sato, and H. Wilson, 1993: How sensitive is the world's climate? *National Geographic Research and Exploration*, **9**, 142-158.

Hansen, J.E., M. Sato, and R. Ruedy, 1995: Long-term changes of the diurnal temperature cycle: implications about mechanisms of global climate change. *Atmos. Res.*, **37**, 175-209.

Hansen, J., M. Sato, and R. Ruedy, 1997a: Radiative forcing and climate response. *J. Geophys. Res.*, **102**, 6831-6864.

Hansen, J., M. Sato, A. Lacis, and R. Ruedy, 1997b: The missing climate forcing. *Phil. Trans. R. Soc. London B*, **352**, 231-240.

Hansen, J., M. Sato, A. Lacis, R. Ruedy, I. Tegen, and E. Matthews, 1998: Climate forcings in the Industrial Era. *Proc. Natl. Acad. Sci.*, **95**, 12753-12758.

Harris, N., R. Hudson, and C. Philips (eds.), 1998: Assessment of Trends in the Vertical Distribution of Ozone. WMO Ozone Research and Monitoring Project report number **43**, SPARC report number **1**, SPARC Office, Verrières le Buisson, France.

Harrison, R.G. and K.P. Shine, 1999: A review of recent studies of the influence of solar changes on the Earth's climate. Hadley Centre Technical Note **6**, available from: Hadley Centre for Climate Prediction and Research, The Met Office, London Road, Bracknell, Berks, RG12 2SY, UK.

Hauglustaine, D.A. and C. Granier, 1995: Radiative forcing by tropospheric ozone changes due to increased emissions of CH_4, CO and NO_x. In: Atmospheric Ozone as a Climate Gas [Wang, W.-C. and I. Isaksen (eds.)]. NATO-ASI Series, Springer-Verlag, Berlin, Germany, pp. 189-203.

Hauglustaine, D.A., C. Granier, and G.P. Brasseur, 1994: Impact of increased methane emissions on the atmospheric composition and related radiative forcing on the climate system. In: Non CO_2 Greenhouse Gases [van Ham, J. *et al.* (eds.)]. Kluwer Academic Publishers, pp. 253-259.

Hauglustaine, D. A., G. P. Brasseur, S. Walters, P. J. Rasch, J.-F. Muller, L. K. Emmons, and M. A. Carroll, J., 1998: MOZART, a global chemical transport model for ozone and related chemical tracers. Part 2: Model results and evaluation. *J. Geophys. Res.*, **103**, 28291-28335.

Hauglustaine, D.A., G.P. Brasseur, and J.S. Levine, 1999: A sensitivity simulation of tropospheric ozone changes due to the l997 Indonesian fire emissions. *Geophys. Res. Lett*, **26**, 3305-3308.

Hauglustaine, D.A., L.K. Emmons, M. Newchurch, G.P. Brasseur, T. Takao, K. Matsubara, J. Johnson, B. Ridley, J. Stith, and J. Dye, 2001: On the role of lightning NO_x in the formation of tropospheric ozone plumes: a global model perspective. *J. Atmos. Chem.*, **38**, 277-294.

Haywood, J.M. and K.P. Shine, 1995: The effect of anthropogenic sulfate and soot on the clear sky planetary radiation budget. *Geophys. Res. Lett.*, **22**, 603-606.

Haywood, J.M. and K.P. Shine, 1997: Multi-spectral calculations of the radiative forcing of tropospheric sulphate and soot aerosols using a column model. *Quart. J. R. Met. Soc.*, **123**, 1907-1930.

Haywood, J.M. and V. Ramaswamy, 1998: Global sensitivity studies of the direct radiative forcing due to anthropogenic sulfate and black carbon aerosols. *J. Geophys. Res.*, **103**, 6043-6058.

Haywood, J.M. and Boucher, O., 2000: Estimates of the direct and indirect radiative forcing due to tropospheric aerosols: a review. *Revs. Geophys.*, **38**, 513-543.

Haywood, J.M., D.L. Roberts, A. Slingo, J.M. Edwards, and K.P. Shine, 1997a: General circulation model calculations of the direct radiative forcing by anthropogenic sulphate and fossil-fuel soot aerosol. *J. Clim.*, **10**, 1562-1577.

Haywood, J.M., V. Ramaswamy, and L.J. Donner, 1997b: A limited-area-model case study of the effects of sub-grid scale variations in relative humidity and cloud upon the direct radiative forcing of sulfate aerosol. *Geophys. Res. Lett.*, **24**, 143-146.

Haywood, J., R. Stouffer, R. Wetherald, S. Manabe, and V. Ramaswamy, 1997c: Transient response of a coupled model to estimated changes in greenhouse gas and sulfate concentrations. *Geophys. Res. Lett.*, **24**, 1335-1338.

Haywood, J.M., M.D. Schwarzkopf, and V. Ramaswamy, 1998a: Estimates of radiative forcing due to modeled increases in tropospheric ozone. *J. Geophys. Res.*, **103**, 16999-17007.

Haywood, J.M., V. Ramaswamy, and L.J. Donner, 1998b: Reply: A limited-area-model case study of the effects of sub-grid scale variations in relative humidity and cloud upon the direct radiative forcing of sulfate aerosol. *Geophys. Res. Lett.*, **25**, 1041.

Haywood, J.M., V. Ramaswamy, and B.J. Soden, 1999: Tropospheric aerosol climate forcing in clear-sky satellite observations over the oceans. *Science*, **283**, 1299-1303.

Heathfield, A.E., C. Anastasi, P. Pagsberg, and A. McCulloch, 1998a: Atmospheric lifetimes of selected fluorinated ether compounds. *Atmos. Env.*, **32**, 711-717.

Heathfield, A.E., C. Anastasi, A. McCulloch, and F.M. Nicolaisen, 1998b: Integrated infrared absorption coefficients of several partially fluorinated ether compounds: CF_3OCF_2H, CF_2HOCF_2H, $CH_3OCF_2CF_2H$, CH_3OCF_2CFClH, $CH_3CH_2OCF_2CF_2H$, $CF_3CH_2OCF_2CF_2H$, and $CH_2{=}CHCH_2OCF_2CF_2H$. *Atmos. Env.*, **32**, 2825-2833.

Hegg, D.A., 1994: The cloud condensation nucleus-sulfate mass relationship and cloud albedo. *J. Geophys. Res.*, **99**, 25903-25907.

Heintzenberg, J. and M. Wendisch, 1996: On the sensitivity of cloud albedo to the partitioning of particulate absorbers in cloudy air. *Contrib. Atmos. Phys.*, **69**, 491-499.

Henderson-Sellers, A., 1995: Human effects on climate through the large-scale impacts of land-use change. In: Future Climates of the World: A Modeling Perspective. World Survey of Climatology, Vol. 16, Elsevier, Amsterdam.

Hewitt, C.D. and J.F.B. Mitchell, 1997: Radiative forcing and response of a GCM to ice age boundary conditions: cloud feedback and climate sensitivity. *Clim. Dyn.*, **13**, 821-834.

Highwood, E.J. and K.P. Shine, 2000: Radiative forcing and global warming potentials of 11 halogenated compounds. *J. Quant. Spectrosc. Radiat. Transf.*, **66**, 169-183.

Highwood, E.J., K.P. Shine, M.D. Hurley, and T.L. Wallington, 1999: Estimation of direct radiative forcing due to non-methane hydrocarbons. *Atmos. Env.*, **33**, 759-767.

Hobbs, P.V., J.S. Reid, R.A. Kotchenruther, R.J. Ferek, and R. Weiss, 1997: Direct radiative forcing by smoke from biomass burning. *Science*, **275**, 1776-1778.

von Hoyningen-Huene, W., K. Wenzel, and S. Schienbein, 1999: Radiative properties of desert dust and its effect on radiative balance. *J. Aerosol Sci.*, **30**, 489-502.

Hoyt, D.V. and K.H. Schatten, 1993: A discussion of plausible solar irradiance variations, 1700-1992. *J. Geophys. Res.*, **98**, 18895-18906.

Hoyt, D.V. and K.H. Schatten, 1998: Group sunspot numbers: A new solar activity reconstruction. *Solar Phys.*, **181**, 491-512.

Hudson, R.D. and A.M. Thompson, 1998: Tropical tropospheric ozone from total ozone mapping spectrometer by a modified residual method. *J. Geophys. Res.*, **103**, 22129-22145.

Huntrieser, H., H. Schlager, C. Feigl, and H. Höller, 1998: Transport and production of NO_x in electrified thunderstorms: Survey of previous studies and new observations at midlatitudes. *J. Geophys. Res.*, **103**, 28247-28264.

Iacobellis, S.F., R. Frouin, and R.C.J. Somerville, 1999: Direct climate forcing by biomass-burning aerosols: impact of correlations between controlling variables. *J. Geophys. Res.*, **104**, 12031-12045.

Imasu, R., A. Suga, and T. Matsuno, 1995: Radiative effects and halocarbon global warming potentials of replacement compounds for chlorofluorocarbons. *J. Meteorol. Soc. Japan.*, **73**, 1123-1136.

IPCC, 1990: Climate Change 1990: The Intergovernmental Panel on Climate Change Scientific Assessment [Houghton, J.T., B.A. Callander, and S.K. Varney (eds)]. Cambridge University Press, Cambridge, United Kingdom and New York, NY, USA.

IPCC, 1992: Climate Change 1992: The Supplementary Report to the Intergovernmental Panel on Climate Change Scientific Assessment [Houghton, J.T., B.A. Callander, and S.K. Varney (eds.)]. Cambridge University Press, Cambridge, United Kingdom and New York, NY, USA, 100 pp.

IPCC, 1994: Climate Change 1994: Radiative Forcing of Climate Change and an Evaluation of the IPCC IS92 Emission Scenarios [Houghton, J.T., L.G. Meira Filho, J. Bruce, H. Lee, B.A. Callander, E.F. Haites, N. Harris, and K. Maskell (eds.)]. Cambridge University Press, Cambridge, United Kingdom and New York, NY, USA.

IPCC, 1996a: Climate Change 1995: The Science of Climate Change. Contribution of Working Group I to the Second Assessment Report of the Intergovernmental Panel on Climate Change [Houghton, J.T., L.G. Meira Filho, B.A. Callander, N. Harris, A. Kattenberg, and K. Maskell (eds.)]. Cambridge University Press, Cambridge, United Kingdom and New York, NY, USA, 572 pp.

IPCC, 1996b, Climate change 1995: Impacts, Adaptations and Mitigation of Climate Change: Scientific-Technical Analyses. Contribution of Working Group II to the Second Assessment Report of the Intergovernmental Panel on Climate Change [Watson, R.T., M.C. Zinyowera, and R.H. Moss (eds.)]. Cambridge University Press, Cambridge, United Kingdom and New York, NY, USA, 880 pp.

IPCC, 1999: Intergovernmental Panel on Climate Change Special Report on Aviation and the Global Atmosphere [Penner, J.E., D.H. Lister, D.J. Griggs, D.J. Dokken, and M. McFarland (eds.)]. Cambridge University Press, Cambridge, United Kingdom and New York, NY, USA, 373 pp.

Iversen, T., A. Kirkevåg, J.E. Kristjansson, and Ø. Seland, 2000: Climate effects of sulphate and black carbon estimated in a global climate model. In: Air pollution and its Application XIV [Gryning S.E. and F.A. Schiermeier (eds.)], Kluwer/Plenum, in press.

Jacobson, M.Z., 2000: A physically-based treatment of elemental carbon optics: Implications for global direct forcing of aerosols. *Geophys. Res. Lett.*, **27**, 217-220.

Jacobson, M.Z., 2001: Global direct radiative forcing due to multicomponent anthropogenic and natural aerosols. *J. Geophys. Res.*, **106**, 1551-1568.

Jacquinet-Husson, N., E. Arie, J. Ballard, A. Barbe, G. Bjoraker, B. Bonnet, L.R. Brown, C. Camy-Peyret, J.P. Champion, A. Chédin, A. Chursin, C. Clerbaux, G. Duxbury, J.-M. Flaud, N. Fourrie, A. Fayt, G. Graner, R. Gamache, A. Goldman, V. Golovko, G. Guelachvili,

J.M. Hartmann, J.C. Hilico, J. Hillman, G. Lefevre, E. Lellouch, S.N. Mikhailenko, O.V. Naumenko, V. Nemtchinov, D.A. Newnham, A. Nikitin, J. Orphal, A. Perrin, D. C. Reuter, C.P. Rinsland, L. Rosenmann, L.S. Rothman, N.A. Scott, J. Selby, L.N. Sinitsa, J.M. Sirota, A.M. Smith, K.M. Smith, V.G. Tyuterev, R.H. Tipping, S. Urban, P. Varanasi, and M. Weber, 1999: The 1997 spectroscopic GEISA databank. *J. Quant. Spectrosc. Radiat. Transfer*, **62**, 205-254.

Jain, A.K., B.P. Briegleb, K. Minschwaner, and D.J. Wuebbles, 2000: Radiative forcings and global warming potentials of 39 greenhouse gases. *J. Geophys. Res.*, **105**, 20773-20790.

Jensen, E.J. and O.B. Toon, 1997: The potential impact of soot from aircraft exhaust on cirrus clouds. *Geophys. Res. Lett.*, **24**, 249-252.

Johns, T.C., J.M. Gregory, W.J. Ingram, C.E. Johnson, A. Jones, J.A. Lowe, J.F.B. Mitchell, D.L. Roberts, D.M.H. Sexton, D.S. Stevenson, S.F.B. Tett, and M.J. Woodage, 2001: Anthropogenic climate change for 1860 to 2100 simulated with the HadCM3 model under updated emissions scenarios. Hadley Centre Technical Note **22**, Hadley Centre, Met Office, Bracknell, Berks, UK.

Johnson, C.E. and R.G. Derwent, 1996: Relative radiative forcing consequences of global emissions of hydrocarbons, carbon monoxide, and NO_x from human activities estimated with a zonally-averaged two-dimensional model. *Clim. Change*, **34**, 439-462.

Jones, A. and A. Slingo, 1996: Predicting cloud-droplet effective radius and indirect sulphate aerosol forcing using a general circulation model. *Q. J. R. Meteorol. Soc.*, **122**, 1573-1595.

Jones, A. and A. Slingo, 1997: Climate model studies of sulphate aerosols and clouds. *Phil. Trans. R. Soc. London B*, **352**, 221-229.

Jones, A., D.L. Roberts, and A. Slingo, 1994: A climate model study of the indirect radiative forcing by anthropogenic sulphate aerosols. *Nature*, **370**, 450-453.

Jones, A., D.L. Roberts, and M.J. Woodage, 1999: The indirect effects of anthropogenic sulphate aerosol simulated using a climate model with an interactive sulphur cycle. Hadley Centre Technical Note no. **14**, 38 pp., available from: Hadley Centre for Climate Prediction and Research, The Met Office, London Road, Bracknell, Berks, RG12 2SY, UK.

Joos, F., M. Bruno, R. Fink, T.F. Stocker, U. Siegenthaler, C. Le Quéré, and J.L. Sarmiento, 1996: An efficient and accurate representation of complex oceanic and biospheric models of anthropogenic carbon uptake. *Tellus*, **48B**, 397-417.

Jørgensen, T.S. and A.W. Hansen, 2000: Comment on "Variation of cosmic ray flux and global cloud coverage - a missing link in solar-climate relationships" by H. Svensmark and E. Friis-Christensen. *J. Atmos. Solar-Terrest. Phys.*, **62**, 73-77.

Karl, T.R., P.D. Jones, R.W. Knight, G. Kukla, N. Plummer, V. Razuvayev, K.P. Gallo, J. Lindseay, R.J. Charlson, and T.C. Peterson, 1993: A new perspective on recent global warming: Asymmetric trends of daily maximum and minimum temperature. *Bull. Am. Meteorol. Soc.*, **74**, 1007-1023.

Kasibhatla, P., W.L. Chameides, and J. St. John, 1997: A three-dimensional global model investigation of the seasonal variation in the atmospheric burden of anthropogenic sulfate aerosols. *J. Geophys. Res.*, **102**, 3737-3759.

Kattenberg, A., F. Giorgi, H. Grassl, G.A. Meehl, J.F.B. Mitchell, R.J. Stouffer, T. Tokioka, A.J. Weaver, and T.M.L. Wigley, 1996: Climate Models – Projections of Future Climate. In: Climate Change 1995: The Science of Climate Change. The Contribution of Working Group I to the Second Assessment Report of the International Panel on Climate Change [Houghton, J.T., L.G. Meira Filho, B.A. Callender, N. Harris, A. Kattenberg, and K. Maskell (eds.)]. Cambridge University Press, Cambridge, United Kingdom and New York, NY, USA, pp. 285-357.

Kaufman, Y.J. and T. Nakajima, 1993: Effect of Amazon smoke on cloud microphysics and albedo - Analysis from satellite imagery. J. Appl. Meteorol., **32**, 729-744.

Kaufman, Y.J. and R.S. Fraser, 1997: Control of the effect of smoke particles on clouds and climate by water vapor. *Science*, **277**, 1636-1639.

Kaufman, Y.J., D. Tanré, A. Karnieli, and L.A. Remer, 2001: Absorption of sunlight by dust as inferred from satellite and ground-based remote sensing. *Geophys. Res. Lett.*, **28**, 1479-1482.

Kernthaler, S.C., R. Toumi, and J.D. Haigh, 1999: Some doubts concerning a link between cosmic ray fluxes and global cloudiness. *Geophys. Res. Lett.*, **26**, 863-866.

Kiehl, J.T. and B.P. Briegleb, 1993: The relative roles of sulfate aerosols and greenhouse gases in climate forcing. *Science* **260**, 311-314.

Kiehl, J.T. and H. Rodhe, 1995: Modelling geographical and seasonal forcing due to aerosols. In: Aerosol Forcing of Climate [Charlson, R.J. and J. Heintzenberg (eds.)]. J. Wiley and Sons Ltd, pp. 281-296.

Kiehl, J. T., T. L. Schneider, R. W. Portmann, and S. Solomon, 1999: Climate forcing due to tropospheric and stratospheric ozone. *J. Geophys. Res.*, **104**, 31239-31254.

Kiehl, J.T., T.L. Schneider, P.J. Rasch, M.C. Barth, and J. Wong, 2000: Radiative forcing due to sulfate aerosols from simulations with the National Center for Atmospheric Research Community Climate Model, Version 3. *J. Geophys. Res.*, **105**, 1441-1457.

Kleinman, L.I., 1994: Low and high NO_x tropospheric photochemistry. *J. Geophys. Res.*, **99**, 16831-16838.

Klonecki, A. and H. Levy II, 1997: Tropospheric chemical ozone tendencies in $CO-CH_4-NOy-H_2O$ system: Their sensitivities to variations in environmental parameters and their application to global chemistry transport model study. *J. Geophys. Res.*, **102**, 21221-21237.

Ko, M., R.-L. Shia, N.-D. Sze, H. Magid, and R.G. Bray, 1999: Atmospheric lifetime and global warming potential of HFC-245fa. *J. Geophys. Res.*, **104**, 8173-8181.

Koch, D., D. Jacob, I. Tegen, D. Rind, and M. Chin, 1999: Tropospheric sulfur simulation and sulfate direct radiative forcing in the Goddard Institute for Space Studies general circulation model. *J. Geophys. Res.*, **104**, 23799-23822.

Kodera, K., 1995: On the origin and nature of the interannual variability of the winter stratospheric circulation in the northern hemisphere. *J. Geophys. Res.*, **100**, 14077-14087.

Kogan, Z.N., Y.L. Kogan, and D.K. Lilly, 1996: Evaluation of sulfate aerosols indirect effect in marine stratocumulus clouds using observation-derived cloud climatology. *Geophys. Res. Lett.*, **23**, 1937-1940.

Kogan, Z.N., Y.L. Kogan, and D.K. Lilly, 1997: Cloud factor and seasonality of the indirect effect of anthropogenic sulfate aerosols. *J. Geophys. Res.*, **102**, 25927-25939.

Kondratyev, K.Y., 1999: Climatic Effects of Aerosols and Clouds. Springer-Verlag, Berlin, 264 pp.

Kristjánsson, J.E. and J. Kristiansen, 2000: Is there a cosmic ray signal in recent variations in global cloudiness and cloud radiative forcing? *J. Geophys. Res.*, **105**, 11851-11863.

Kristensson, A., J.-F. Gayet, J. Ström, and F. Auriol, 2000: In situ observations of a reduction in effective crystal diameter in cirrus clouds near flight corridors. *Geophys. Res. Lett.*, **27**, 681-684.

Krol, M., P.J. van Leeuwen, and J. Lelieveld, 1998: Global OH trend inferred from methylchloroform measurements. *J. Geophys. Res.*, **103**, 10697-10711.

Kuang, Z., Y. Jiang, and Y.L. Yung, 1998: Cloud optical thickness variations during 1983-1991: Solar cycle or ENSO? *Geophys. Res. Lett.*, **25**, 1415-1417.

Kulmala, M., A. Laaksonen, P. Korhonen, T. Vesala, and T. Ahonen, 1993: The effect of atmospheric nitric acid vapor on cloud condensation nucleus activation. *J. Geophys. Res.*, **98**, 22949-22958.

Kulmala, M., P. Korhonen, A. Laaksonen, and T. Vesala, 1995: Changes in cloud properties due to NO_x emissions. *Geophys. Res. Lett.*, **22**, 239-242.

Kulmala, M., A. Toivonen, T. Mattila, and P. Korhonen, 1998: Variations

of cloud droplet concentrations and the optical properties of clouds due to changing hygroscopicity: A model study. *J. Geophys. Res.*, **103**, 16183-16195.

Laaksonen, A., J. Hienola, M. Kulmala, and F. Arnold, 1997: Supercooled cirrus cloud formation modified by nitric acid pollution of the upper troposphere. *Geophys. Res. Lett.*, **24**, 3009-3012.

Labitzke, K. and H. van Loon, 1997: The signal of the 11-year sunspot cycle in the upper troposphere-lower stratosphere. *Space Sci. Rev.*, **80**, 393-410.

Lacis, A., J. Hansen, and M. Sato, 1992: Climate forcing by stratospheric aerosols. *Geophys. Res. Lett.*, **19**, 1607-1610.

Lacis, A.A., D.J. Wuebbles, and J.A. Logan, 1990: Radiative forcing by changes in the vertical distribution of ozone. *J. Geophys. Res.*, **95**, 9971-9981.

Lamarque, J.-F., G.P. Brasseur, P.G. Hess, and J.-F. Muller, 1996: Three-dimensional study of the relative contributions of the different nitrogen sources in the troposphere. *J. Geophys. Res.*, **101**, 22955-22968.

Langner, J. and H. Rodhe, 1991: A global three-dimensional model of the tropospheric sulfur cycle. *J. Atmos. Chem.*, **13**, 225-263.

Larkin, A., J.D. Haigh, and S. Djavidnia, 2000: The effect of solar UV irradiance variations on the Earth's atmosphere. *Space Science Reviews*, **94**, 199-214.

Lashof, D.A. and D.R. Ahuja, 1990: Relative contributions of greenhouse gas emissions to global warming. *Nature*, **344**, 529-531.

Lean, J. and D. Rind, 1998: Climate forcing by changing solar radiation. *J. Clim.*, **11**, 3069-3094.

Lean, J., A. Skumanitch, and O. White, 1992: Estimating the Sun's radiative output during the Maunder Minimum. *Geophys. Res. Lett.*, **19**, 1591-1594.

Lean, J., J. Beer and R.S. Bradley, 1995: Reconstruction of solar irradiance since 1610: Implications for climate change. *Geophys. Res. Lett.*, **22**, 3195-3198.

Lean, J.L., G.J. Rottman, H.L. Kyle, T.N. Woods, J.R. Hickey, and L.C. Puga, 1997: Detection and parameterization of variations in solar mid- and near-ultraviolet radiation (200-400 nm). *J. Geophys. Res.*, **102**, 29939-29956.

Lelieveld, J. and P.J. Crutzen, 1992: Indirect chemical effects of methane on climate warming. *Nature*, **355**, 339-342.

Lelieveld, J. and P.J. Crutzen, 1994: Role of deep cloud convection in the ozone budget of the troposphere. *Science*, **264**, 1759-1761.

Lelieveld, J. and F. Dentener, 2000: What controls tropospheric ozone? *J. Geophys. Res.*, **105**, 3531-3551.

Lelieveld, J., P.J. Crutzen, and C. Brühl, 1993: Climate effects of atmospheric methane. *Chemosphere*, **26**, 739-768.

Lelieveld, J., P. Crutzen, and F.J. Dentener, 1998: Changing concentration, lifetime and climate forcing of atmospheric methane. *Tellus*, **50B**, 128-150.

Le Treut, H., M. Forichon, O. Boucher, and Z-X. Li, 1998: Sulfate aerosol, indirect effect and CO_2 greenhouse forcing: Equilibrium response of the LMD GCM and associated cloud feedbacks. *J. Climate*, **11**, 1673-1684.

Levin, Z., E. Ganor, and V. Gladstein, 1996: The effects of desert particles coated with sulfate on rain formation in the Eastern Mediterranean. *J. Appl. Meteor.*, **35**, 1511-1523.

Levy, II, H., W.J. Moxim, and P.S. Kasibhatla, 1996: A global three-dimensional time-dependent lightning source of tropospheric NO_x. *J. Geophys. Res.*, **101**, 22911-22922.

Li, Z., Z. Tao, V. Naik, D.A. Good, J. Hansen, G.-R. Jeong, J.S. Francisco, A.K. Jain, and D.J. Wuebbles, 2000: Global warming potential assessment for $CF_3OCF=CF_2$. *J. Geophys. Res.*, **105**, 4019-4029.

Liao, H. and J.H. Seinfeld, 1998: Effect of clouds on direct radiative forcing of climate. *J. Geophys. Res.*, **103**, 3781-3788.

Lindberg, J.D., J.B. Gillespie, and B.D. Hinds, 1976: Measurements of the refractive indices of atmospheric particulate matter from a variety of geographic locations. In: Proceedings of the International Symposium on Radiation in the Atmosphere, Garmisch-Partenkirchen [Bolle, H.J., (ed.)]. Science Press, New York.

Liousse, C., J.E. Penner, C.C. Chuang, J.J. Walton, and H. Eddleman, 1996. A global three dimensional model study of carbonaceous aerosols. *J. Geophys. Res.*, **101**, 19411-19432.

Lockwood, M. and R. Stamper, 1999: Long-term drift of the coronal source magnetic flux and the total solar irradiance. *Geophys. Res. Lett.*, **26**, 2461-2464.

Lohmann, U. and J. Feichter, 1997: Impact of sulfate aerosols on albedo and lifetime of clouds: A sensitivity study with the ECHAM4 GCM. *J. Geophys. Res.*, **102**, 13685-13700.

Lohmann, U., J. Feichter, C.C. Chuang, and J.E. Penner, 1999a: Prediction of the number of cloud droplets in the ECHAM GCM. *J. Geophys. Res.*, **104**, 9169-9198.

Lohmann, U., J. Feichter, C.C. Chuang, and J.E. Penner, 1999b: Correction. *J. Geophys. Res.*, **104**, 24557-24563.

Lohmann, U., J. Feichter, J. Penner, and R. Leaitch, 2000: Indirect effect of sulfate and carbonaceous aerosols: A mechanistic treatment. *J. Geophys. Res.*, **105**, 12193-12206.

Ma, J. and M. van Weele, 2000: Effects of stratospheric ozone depletion on the net production of ozone in polluted rural areas. *Chemosphere-Global Change Science*, **2**, 23-37.

Madronich, S. and C. Granier, 1994: Tropospheric chemistry changes due to increased UV-B radiation. In: Stratospheric Ozone Depletion/UV-B Radiation in the Biosphere [Biggs, R.H. and M.E.B. Joyner (eds.)]. NATO ASI Series, Springer-Verlag, Berlin, Germany.

Manabe, S. and R. Wetherald, 1967: Thermal equilibrium of the atmosphere with a given distribution of relative humidity. *J. Atmos. Sci.*, **24**, 241-259.

Manabe, S. and R. Wetherald, 1980: On the distribution of climate change resulting from an increase in CO_2 content of the atmosphere. *J. Atmos. Sci.*, **37**, 99-118.

Manabe, S. and A.J. Broccoli, 1985: The influence of continental ice sheets on the climate of an ice age. *J. Geophys. Res.*, **90**, 2167-2190.

Marenco, A., H. Gouget, P. Nédélec, J.P. Pagés, and F. Karcher, 1994: Evidence of a long-term increase in tropospheric ozone from Pic du Midi data series: Consequences: positive radiative forcing. *J. Geophys. Res.*, **99**, 16617-16632.

McCormack, J.P. and L.L. Hood, 1996: Apparent solar cycle variations of upper stratospheric ozone and temperature: Latitude and seasonal dependencies. *J. Geophys. Res.*, **101**, 20933-20944.

Meerkötter, R., U. Schumann, D.R. Doelling, P. Minnis, T. Nakajima, and Y. Tsushima, 1999: Radiative forcing by contrails. *Ann. Geophys.*, **17**, 1080-1094.

Mendoza, B., 1997: Estimates of Maunder Minimum solar irradiance and Ca II H and K fluxes using rotation rates and diameters. *Astrophys. J.*, **483**, 523-526.

Mickley, L.J., P.P. Murti, D.J. Jacob, J.A. Logan, D.M. Koch, and D. Rind, 1999: Radiative forcing from tropospheric ozone calculated with a unified chemistry-climate model. *J. Geophys. Res.*, **104**, 30153-30172.

Miller, R. and I. Tegen, 1998: Climate response to soil dust aerosols. *J. Clim.*, **11**, 3247-3267.

Miller, R. and I. Tegen, 1999: Radiative forcing of a tropical direct circulation by soil dust aerosols. *J. Atmos. Sci*, **56**, 2403-2433.

Minnis, P., U. Schumann, D.R. Doelling, K.M. Gierens, and D.W. Fahey, 1999: Global distribution of contrail radiative forcing. *Geophys. Res. Lett.*, **26**, 1853-1856.

Minschwaner, K., R.W. Carver, B.P. Briegleb, and A.E. Roche, 1998: Infrared radiative forcing and atmospheric lifetimes of trace species based on observations from UARS. *J. Geophys. Res.*, **103**, 23243-23253.

Mishchenko, M.I., L.D. Travis, R.A. Kahn, and R.A. West, 1997:

Modeling phase functions for dustlike tropospheric aerosols using a shape mixture of randomly orientated polydisperse spheroids. *J. Geophys. Res.*, **102**, 16831-16847.

Mitchell, J.F.B. and T.C. Johns, 1997: On modification of global warming by sulfate aerosols. *J. Clim.*, **10**, 245-267.

Molina, L.T., P.J. Wooldridge, and M.J. Molina, 1995: Atmospheric reactions and ultraviolet and infrared absorptivities of nitrogen trifluoride. *Geophys. Res. Lett.*, **22**, 1873-1876.

Murphy, D.M., J.R Anderson, P.K. Quinn, L.M. McInnes, M. Posfai, D.S. Thomson, and P.R. Buseck, 1998: Influence of sea-salt on aerosol radiative properties in the Southern Ocean marine boundary layer. *Nature*, **392**, 62-65.

Myhre, G. and F. Stordal, 1997: Role of spatial and temporal variations in the computation of radiative forcing and GWP. *J. Geophys. Res.*, **102**, 11181-11200.

Myhre, G., E.J. Highwood, K.P. Shine, and F. Stordal, 1998b: New estimates of radiative forcing due to well mixed greenhouse gases. *Geophys. Res. Lett.*, **25**, 2715-2718.

Myhre, G., F. Stordal, B. Rognerud, and I.S.A. Isaksen, 1998a: Radiative forcing due to stratospheric ozone. In: Atmospheric Ozone: Proceedings of the XVIII Quadrennial Ozone Symposium [Bojkov, R.D. and G. Visconti (eds.)]. L'Aquila, Italy, Parco Scientifico e Technologico d'Abruzzo, pp. 813-816.

Myhre, G., F. Stordal, K. Restad, and I. Isaksen, 1998c: Estimates of the direct radiative forcing due to sulfate and soot aerosols. *Tellus*, **50B**, 463-477.

Myhre, G., C.J. Nielsen, D.L. Powell, and F. Stordal, 1999: Infrared absorption cross section, radiative forcing, and GWP of four hydrofluoro(poly)ethers. *Atmos. Env.*, **33**, 4447-4458.

Myhre, G., S. Karlsdóttir, I.S.A. Isaksen, and F. Stordal, 2000: Radiative forcing due to changes in tropospheric ozone in the period 1980 to 1996. *J. Geophys. Res.*, **105**, 28935-28942.

Myhre, G, A. Myhre, and F. Stordal, 2001: Historical evolution of radiative forcing of climate. *Atmos. Env.*, **35**, 2361-2373.

Naik, V., A. Jain, K.O. Patten, and D.J. Wuebbles, 2000: Consistent sets of atmospheric lifetimes and radiative forcings on climate for CFC replacements: HCFCs and HFCs. *J. Geophys. Res.*, **105**, 6903-6914.

Nakićenović, N., J. Alcamo, G. Davis, B. de Vries, J. Fenhann, S. Gaffin, K. Gregory, A. Grübler, T.Y. Jung, T. Kram, E.L. La Rovere, L. Michaelis, S. Mori, T. Morita, W. Pepper, H. Pitcher, L. Price, K. Raihi, A. Roehrl, H.-H. Rogner, A. Sankovski, M. Schlesinger, P. Shukla, S. Smith, R. Swart, S. van Rooijen, N. Victor, and Z. Dadi, 2000: IPCC Special Report on Emissions Scenarios, Cambridge University Press, Cambridge, United Kingdom and New York, NY, USA, **599** pp.

Nedoluha, G.E., R. Bevilacqua, R.M. Gomez, D.E. Siskind, B. Hicks, J. Russell, and B.J. Connor, 1998: Increases in middle atmospheric water vapor as observed by the Halogen Occultation Experiment and the ground-based Water Vapor Millimeter-wave Spectrometer from 1991 to 1997. *J. Geophys. Res.*, **103**, 3531-3543.

Nemesure, S., R. Wagener, and S.E. Schwartz, 1995: Direct shortwave forcing of climate by anthropogenic sulfate aerosol: sensitivity to particle size, composition, and relative humidity. *J. Geophys. Res.*, **100**, 26105-26116.

Nesme-Ribes, E., E.N. Ferreira, R. Sadourny, H. Le Treut, and Z.X. Li, 1993: Solar dynamics and its impact on solar irradiance and the terrestrial climate. *J. Geophys. Res.*, **98**, 18923-18935.

Novakov, T. and J.E. Penner, 1993: Large contribution of organic aerosols to cloud-condensation-nuclei concentrations. *Nature*, **365**, 823-826.

Novakov, T. and C.E. Corrigan, 1996: Cloud condensation nucleus activity of the organic component of biomass smoke particles. *Geophys. Res. Lett.*, **23**, 2141-2144.

O'Dowd, D., J.A. Lowe, and M.H. Smith, 1999: Coupling sea-salt and sulphate interactions and its impact on cloud droplet concentration

predictions. *Geophys. Res. Lett.*, **26**, 1311-1314.

Oltmans, S.J. and D.J. Hofmann, 1995: Increase in lower-stratospheric water vapour at a mid-latitude Northern hemisphere site from 1981 to 1994. *Nature*, **374**, 146-149.

Oltmans, S.J., A.S. Lefohn, H.E. Sheel, J.M. Harris, H. Levy, I.E. Galbally, E.-G. Brunke, C.P. Meyer, J.A. Lathrop, B.J. Johnson, D.S. Shadwick, E. Cuevas, F.J. Schmidlin, D.W. Tarasick, H. Claude, J.B. Kerr, O. Uchino, and V. Mohnen, 1998: Trends of ozone in the troposphere. *Geophys. Res. Lett.*, **25**, 139-142.

Pan, W., M.A. Tatang, G.J. McRae, and R.G. Prinn, 1997: Uncertainty analysis of the direct radiative forcing by anthropogenic sulfate aerosols. *J. Geophys. Res.*, **102**, 21915-21924.

Papasavva, S., S. Tai, K.H. Illinger, and J.E. Kenny, 1997: Infrared radiative forcing of CFC substitutes and their atmospheric reaction products. *J. Geophys. Res.*, **102**, 13643-13650.

Penner, J.E., R.E. Dickinson, and C.A. O'Neill, 1992: Effects of aerosol from biomass burning on the global radiation budget. *Science*, **256**, 1432-1434.

Penner, J.E, R.J. Charlson, J.M. Hales, N.S. Laulainen, R. Leifer, T. Novakov, J. Ogren, L.F. Radke, S.E. Schwartz, and L. Travis, 1994: Quantifying and minimising uncertainty of climate forcing by anthropogenic aerosols. *Bull. Am. Meterol. Soc.*, **75**, 375-400.

Penner, J.E., C.C. Chuang, and C. Liousse, 1996: The contribution of carbonaceous aerosols to climate change. In: Nucleation and Atmospheric Aerosols [Kulmala, M. and P.E. Wagner (eds.)]. Elsevier Science, pp. 759-769.

Penner, J.E., T.M. Wigley, P. Jaumann, B.D. Santer, and K.E. Taylor, 1997: Anthropogenic aerosols and climate change: A method for calibrating forcing. In: Assessing Climate Change: Results from the Model Evaluation Consortium for Climate Assessment [Howe, W. and A. Henderson-Sellers (eds.)]. Gordon and Breach Publishers, Sydney, Australia, pp. 91-111.

Penner, J.E., D.J. Bergmann, J. Walton, D. Kinnison, M.J. Prather, D. Rotman, C. Price, K. Pickering, and S.L. Baughcum, 1998a: An evaluation of upper tropospheric NO_x in two models. *J. Geophys. Res.*, **103**, 22097-22113.

Penner, J. E., C.C. Chuang, and K. Grant, 1998b: Climate forcing by carbonaceous and sulfate aerosols. *Clim. Dyn.*, **14**, 839-851.

Petit, J.R., 1990. Paleoclimatological and chronological implications of the Vostok core dust record. *Nature*, **343**, 56-58.

Pham, M., J.F. Muller, G. Brasseur, C. Granier, and G. Mégie, 1995: A three-dimensional study of the tropospheric sulfur cycle. *J. Geophys. Res.*, **100**, 26061-26092.

Pilinis, C., S.N. Pandis, and J.H. Seinfeld, 1995: Sensitivity of direct climate forcing by atmospheric aerosols to aerosol size and composition. *J. Geophys. Res.*, **100**, 18739-18754.

Pincus, R. and M. Baker, 1994: Precipitation, solar absorption, and albedo susceptibility in marine boundary layer clouds. *Nature*, **372**, 250-252.

Pinnock, S. and K.P. Shine, 1998: The effects of changes in HITRAN and uncertainties in the spectroscopy on infrared irradiance calculations. *J. Atmos. Sci.*, **55**, 1950-1964.

Pinnock, S., M.D. Hurley, K.P. Shine, T.J. Wallington, and T.J. Smyth, 1995: Radiative forcing of climate by hydrochlorofluorocarbons and hydrofluorocarbons. *J. Geophys. Res.*, **100**, 23277-23238.

Platnick, S. and S. Twomey, 1994: Determining the susceptibility of cloud albedo to changes in droplet concentration with the Advanced Very High Resolution Radiometer. *J. Appl. Meteorol.*, **33**, 334-347.

Pope, V.D., M.L. Gallani, P.R. Rowntree, and R.A. Stratton, 2000: The impact of new physical parametrizations in the Hadley Centre climate model: HadAM3. *Clim. Dyn.*, **16**, 123-146.

Portmann, R.W., S. Solomon, J. Fishman, J.R. Olson, J.T. Kiehl, and B. Briegleb, 1997: Radiative forcing of the Earth-climate system due to tropical tropospheric ozone production. *J. Geophys. Res.*, **102**, 9409-9417.

Prather, M. J., 1994: Lifetimes and eigenstates in atmospheric chemistry. *Geophys. Res. Lett.*, **21**, 801-804.

Prather, M. J., 1996: Times scales in atmospheric chemistry: theory, GWPs for CH_4 and CO, and runaway growth. *Geophys. Res. Lett.*, **23**, 2597-2600.

Pruppacher, H.R., 1973: Electrofreezing of supercooled water. *Pure Appl. Geophys.*, **104**, 623-634.

Pruppacher, H.R. and J.D. Klett, 1997: Microphysics of clouds and precipitation. 2nd Ed., Kluwer.

Ramanathan, V., 1981: The role of ocean-atmosphere interactions in the CO_2-climate problem. *J. Atmos. Sci.*, **38**, 918-930.

Ramanathan, V. and J. Coakley, 1978: Climate modeling through radiative-convective models. *Rev. Geophys. Space Phys.*, **16**, 465-490.

Ramanathan, V. and R. Dickinson, 1979: The role of stratospheric ozone in the zonal and seasonal radiative energy balance of the earth-troposphere system. *J. Atmos. Sci.*, **36**, 1084-1104.

Ramanathan, V., R. Cicerone, H. Singh, and J. Kiehl, 1985: Trace gas trends and their potential role in climate change. *J. Geophys. Res.*, **90**, 5547-5566.

Ramanathan,V., L. Callis, R. Cess, J. Hansen, I. Isaksen, W. Kuhn, A. Lacis, F. Luther, J. Mahlman, R. Reck, and M. Schlesinger, 1987: Climate-chemical interactions and effects of changing atmospheric trace gases. *Rev. Geophys.*, **25**, 1441-1482.

Ramanathan, V., R.D. Cess, E.F. Harrison, P. Minnis, B. Barkstrom, E. Ahmed, and D. Hartmann, 1989: Cloud radiative forcing and climate: Results from the Earth Radiation Budget Experiment. *Science*, **243**, 57-63.

Ramaswamy, V. and C.-T. Chen, 1997a: Linear additivity of climate response for combined albedo and greenhouse perturbations. *Geophys. Res. Lett.*, **24**, 567-570.

Ramaswamy, V. and C.-T. Chen, 1997b: Climate forcing-response relationships for greenhouse and shortwave radiative perturbations. *Geophys. Res. Lett.*, **24**, 667-670.

Randel, W. J., F. Wu, J. R. Russell III, and J. Waters, 1999: Space-time patterns of trends in stratospheric constituents derived from UARS measurements. *J. Geophys. Res.*, **104**, 3711-3727.

Reid, G., 1997: Solar forcing of global climate change since the mid-17th century. *Clim. Change*, **37**, 391-405.

Reilly, J., R. Prinn, J. Harnisch, J. Fitzmaurice, H. Jacoby, D. Kicklighter, J. Mellilo, P. Stone, A. Sokolov, and C. Wang, 1999: Multi-gas assessment of the Kyoto Protocol. *Nature*, **401**, 549-554.

Remer, L.A., Y.J. Kaufman, D. Tanré, Z. Levin, and D.A. Chu, 1999: Principles in remote sensing of aerosol from MODIS over land and ocean, Proceedings of the ALPS99 International Conference, 18-22 January 1999, Méribel, France, pp. WK1/O/05/1-4.

Restad, K., I. Isaksen, and T.K. Berntsen, 1998: Global distribution of sulfate in the troposphere: A 3-dimensional model. *Atmos Env.*, **32**, 3593-3609.

Rind, D. and N.K. Balachandran, 1995: Modelling the effects of UV variability and the QBO on the troposphere-stratosphere system. Part II: The troposphere. *J. Clim.*, **8**, 2080-2095.

Rind, D., D. Peteet, and G. Kukla, 1989: Can Milankovitch orbital variations initiate the growth of ice sheets in a GCM? *J. Geophys. Res.*, **94**, 12851-12871.

Robock, A. and M.P. Free, 1995: Ice cores as an index of global volcanism from 1850 to the present. *J. Geophys. Res.*, **100**, 11549-11567.

Robock, A. and M.P. Free, 1996: The volcanic record in ice cores for the past 2000 years. In: Climatic Variations and Forcing Mechanisms of the Last 2000 Years [Jones, P., R. Bradley, and J. Jouzel (eds.)]. Springer-Verlag, Berlin, Germany, pp. 533-546.

Rodhe, H. and P.J. Crutzen, 1995: Climate and CCN. *Nature*, **375**, 111.

Rodhe, H., R.J. Charlson, and T.L. Anderson, 2000: Avoiding circular logic in climate modeling. *Clim. Change*, **44**, 419-422.

Roeckner, E., T. Siebert, and J. Feichter, 1994: Climatic response to anthropogenic sulfate forcing simulated with a general circulation model. In: Aerosol Forcing of Climate [Charlson, R. and J. Heintzenberg (eds.)]. John Wiley and Sons, pp. 349-362.

Roehl, C.M., D. Boglu, C. Brühl, and G.K. Moortgat, 1995: Infrared band intensities and global warming potentials of CF_4, C_2F_6, C_3F_8, C_4F_{10}, C_5F_{12}, and C_6F_{14}. *Geophys. Res. Lett.*, **22**, 815-818.

Roelofs, G.-J., J. Lelieveld, and R. van Dorland, 1997: A three dimensional chemistry/general circulation model simulation of anthropogenically derived ozone in the troposphere and its radiative climate forcing. *J. Geophys. Res.*, **102**, 23389-23401.

Roelofs, G.-J., J. Lelieveld, and L. Ganzeveld, 1998: Simulation of global sulfate distribution and the influence on effective cloud drop radii with a coupled photochemistry-sulfur cycle model. *Tellus*, **50B**, 224-242.

Ross, J.L., P.V. Hobbs, and B. Holben, 1998: Radiative characteristics of regional hazes dominated by smoke from biomass burning in Brazil: Closure tests and direct radiative forcing. *J. Geophys. Res.*, **103**, 31925-31941.

Rothman, L.S., R.R. Gamache, R.H. Tipping, C.P. Rinsland, M.A.H. Smith, D.C. Benner, V.M. Devi, J.-M. Flaud, C. Camy-Peyret, A. Perrin, A. Goldman, S.T. Massie, L.R. Brown, and R.A. Toth, 1992: The HITRAN molecular database: Editions of 1991 and 1992. *J. Quant. Spectrosc. Radiat. Transf.*, **48**, 469-507.

Rothman, L.S., C.P. Rinsland, A. Goldman, S.T. Massie, D.P. Edwards, J.-M. Flaud, A. Perrin, C. Camy-Peyret, V. Dana, J.-Y. Mandin, J. Schroeder, A. McCann, R.R. Gamache, R.B. Wattson, K. Yoshino, K.V. Chance, K.W. Jucks, L.R. Brown, V. Nemtchinov, and P. Varanasi, 1998: The HITRAN molecular spectroscopic database and HAWKS (HITRAN atmospheric workstation): 1996 edition. *J. Quant. Spectrosc. Radiat. Transfer*, **60**, 665-710.

Rotstayn, L.D., 1999: Indirect forcing by anthropogenic aerosols: A GCM calculation of the effective-radius and cloud lifetime effects. *J. Geophys. Res.*, **104**, 9369-9380.

Rotstayn, L.D., 2000: On the "tuning" of autoconversion parameterizations in climate models. *J. Geophys. Res.*, **105**, 15495-15507.

Rotstayn, L.D. and J.E. Penner, 2001: Indirect aerosol forcing, quasi-forcing, and climate response. *J. Climate*, in press.

Rottman, G.J, T.N. Woods, and T.P. Sparn, 1993: Solar Stellar Irradiance Comparison Experiment: Instrument design and operation. *J. Geophys. Res.*, **98**, 10667-10678.

Rowntree, P., 1998: Global average climate forcing and temperature response since 1750. *Int. J. Climatol.*, **18**, 355-377.

SAR, see IPCC, 1996a.

Sato, M., J. Hansen, M.P. McCormick, and J.B. Pollack, 1993: Stratospheric aerosol optical depths, 1850-1990. *J. Geophys. Res.*, **98**, 22987-22994.

Sausen, R., K. Gierens, M. Ponater, and U. Schumann, 1998: A diagnostic study of the global distribution of contrails: Part I: Present day climate. *Theor. Appl. Climatol.*, **61**, 127-141.

Schlesinger, M.E., X. Jiang, and R.J. Charlson, 1992: Implication of anthropogenic atmospheric sulphate for the sensitivity of the climate system. In: Climate Change and Energy Policy: Proceedings of the International Conference on Global Climate Change: Its Mitigation through Improved Production and Use of Energy [Rosen, L. and R. Glasser (eds.)]. Amer. Inst. Phys., New York, NY, USA, pp. 75-108.

Shi, G., 1992: Radiative forcing and greenhouse effect due to the atmospheric trace gases. Science in China (Series B), **35**, 217-229.

Shindell, D., D. Rind, N. Balachandran, J. Lean, and P. Lonergan, 1999: Solar cycle variability, ozone, and climate. *Science*, **284**, 305-308.

Shine, K.P. and P.M. de F. Forster, 1999: The effects of human activity on radiative forcing of climate change: a review of recent developments. *Global and Planetary Change*, **20**, 205-225.

Shine, K.P., B.P. Briegleb, A. Grossman, D. Hauglustaine, H. Mao, V. Ramaswamy, M.D. Schwarzkopf, R. van Dorland, and W-C. Wang,

1995: Radiative forcing due to changes in ozone: a comparison of different codes. In Atmospheric Ozone as a Climate Gas, NATO ASI Series, Springer-Verlag, Berlin, **32**, 373-396.

Shine, K.P., Y. Fouquart, V. Ramaswamy, S. Solomon, and J. Srinivasan, 1996: Radiative Forcing of Climate Change, Chapter 2.4. In: Climate Change 1995: The Science of Climate Change. Contribution of Working Group I to the Second Assessment Report of the Intergovernmental Panel on Climate Change [Houghton, J.T., L.G. Meira Filho, B.A. Callender, N. Harris, A. Kattenberg, and K. Maskell (eds.)]. Cambridge University Press, Cambridge, United Kingdom and New York, NY, USA, pp. 108-118.

Shine, K.P., R.S. Freckleton, and P.M. de F. Forster, 1998: Comment on "Climate forcing by stratospheric ozone depletion calculated from observed temperature trends" by Zhong *et al*. *Geophys. Res. Lett*., **25**, 663-664.

Shira, K., M.D. Hurley, K.P. Shine, and T.J. Wallington, 2001: Updated radiative forcing estimates of sixty-five halocarbons and non-methane hydrocarbons. *J. Geophys. Res*., in press.

Siegenthaler, U. and F. Joos, 1992: Use of a simple model for studying oceanic tracer distributions and the global carbon cycle. *Tellus*, **44B**, 186-207.

Sinha, A. and R. Toumi, 1996: A comparison of climate forcings due to chlorofluorocarbons and carbon monoxide. *Geophys. Res. Lett*., **23**, 65-68.

Sinha, A. and J.E. Harries, 1997: Possible change in climate parameters with zero net radiative forcing. *Geophys. Res. Lett*., **24**, 2355-2358.

Sinha, A. and R. Toumi, 1997: Tropospheric ozone, lightning and climate change. *J. Geophys. Res*., **102**, 10667-10672.

Skodvin, T. and J.S. Fuglestvedt, 1997: A comprehensive approach to climate change: Political and scientific considerations. *Ambio*, **26**, 351-358.

Smith, S.J. and T.M.L. Wigley, 2000a: Global warming potentials, 1, Climatic implications of emissions reductions. *Clim. Change*, **44**, 445-457.

Smith, S.J. and T.M.L. Wigley, 2000b: Global warming potentials, 2, Accuracy. *Clim. Change*, **44**, 459-469.

Smith, W.L., S. Ackerman, H. Revercomb, H. Huang, D.H. DeSlover, W. Feltz, L. Gumley and A. Collard, 1998: Infrared spectral absorption of nearly invisible cirrus clouds. *Geophys. Res. Lett*., **25**, 1137-1140.

Sokolik, I.N. and O.B. Toon, 1996: Direct radiative forcing by anthropogenic airborne mineral aerosols. *Nature*, **381**, 681-683.

Sokolik, I.N., A. Andronova, and T.C. Johnson, 1993: Complex refractive index of atmospheric dust aerosols. *Atmos. Env.*, **27A**, 2495-2502.

Sokolik, I.N., O.B. Toon, and R.W. Bergstrom, 1998: Modeling the direct radiative characteristics of airborne mineral aerosols at infrared wavelengths. *J. Geophys. Res*., **103**, 8813-8826.

Solanki, S. K. and M. Fligge, 1998: Solar irradiance since 1874 revisited. *Geophys. Res. Lett*., **25**, 341-344.

Solomon, S. and J.S. Daniel, 1996: Impact of the Montreal Protocol and its Amendments on the rate of change of global radiative forcing. *Clim. Change*, **32**, 7-17.

Solomon, S., R.W. Portmann, R.R. Garcia, L.W. Thomason, L.R. Poole, and M.P. McCormick, 1996: The role of aerosol variations in anthropogenic ozone depletion at northern midlatitudes. *J. Geophys. Res*., **101**, 6713-6727.

Solomon, S., R.W. Portmann, R.W. Sanders, J.S. Daniel, W. Madsen, B. Bartram, and E.G. Dutton, 1999: On the rôle of nitrogen dioxide in the absorption of solar radiation. *J. Geophys. Res*., **104**, 12047-12058.

Soon, W.H., E.S. Posmentier, and S.L. Baliunas, 1996: Inference of solar irradiance variability from terrestrial temperature changes, 1880-1993: An astrophysical application of the Sun-climate connection. *Astrophys. J.*, **472**, 891-982.

Stenchikov, G., I. Kirchner, A. Robock, H.-F. Graf, J.C. Antuna, R.G. Grainger, A. Lambert, and L. Thomason, 1998: Radiative forcing

from the 1991 Mount Pinatubo volcanic eruption. *J. Geophys. Res*., **103**, 13837-13857.

Stern, D.I. and R.K. Kaufmann, 1996: Estimates of global anthropogenic sulfate emissions 1860-1993, Center for Energy and Environmental Studies, Working Papers Series, Number 9602, Boston University.

Stevens, M.J. and G.R. North, 1996: Detection of the climate response to the solar cycle. *J. Atmos. Sci*., **53**, 2594-2608.

Stevenson, D.S., C.E. Johnson, W.J. Collins, R.G. Derwent, K.P. Shine, and J.M. Edwards, 1998: Evolution of tropospheric ozone radiative forcing. *Geophys. Res. Lett*., **25**, 3819-3822.

Ström, J. and S. Ohlsson, 1998: In situ measurements of enhanced crystal number densities in cirrus clouds caused by aircraft exhaust. *J. Geophys. Res*., **103**, 11355-11361.

Stuiver, M. and P.J. Reimer, 1993: Extended ^{14}C data base and revised CALIB 3.0 ^{14}C age calibration program. *Radiocarbon*, **35**, 215-230.

Sturges, W.T., T.J. Wallington, M.D. Hurley, K.P. Shine, K. Sihra, A. Engel, D.E. Oram, S.A. Penkett, R. Mulvaney, and C.A.M. Brenninkmeijer, 2000: A potent greenhouse gas identified in the atmosphere: SF_5CF_3. *Science*, **289**, 611-613.

Svensmark, H., 1998: Influence of cosmic rays on Earth's climate. *Phys. Rev. Lett.*, **81**, 5027-5030.

Svensmark, H. and E. Friis-Christensen, 1997: Variation of cosmic ray flux and global cloud coverage - A missing link in solar-climate relationships. *J. Atmos. Solar Terrest. Phys*., **59**, 1225-1232.

Taylor, J.P. and A. McHaffie, 1994: Measurements of cloud susceptibility. *J. Atmos. Sci*., **51**, 1298-1306.

Taylor, K.E. and J.E. Penner, 1994: Response of the climate system to atmospheric aerosols and greenhouse gases. *Nature*, **369**, 734-737.

Tegen, I. and I. Fung, 1995: Contribution to the atmospheric mineral aerosol load from land surface modification. *J. Geophys. Res*., **100**, 18707-18726.

Tegen, I. and A. Lacis, 1996: Modeling of particle size distribution and its influence on the radiative properties of mineral dust. *J. Geophys, Res*., **101**, 19237-19244.

Tegen, I., A. Lacis, and I. Fung, 1996: The influence of mineral aerosols from disturbed soils on climate forcing. *Nature*, **380**, 419-422.

Tegen, I., P. Hollrigl, M. Chin, I. Fung, D. Jacob, and J.E. Penner, 1997: Contribution of different aerosol species to the global aerosol extinction optical thickness: Estimates from model results. *J. Geophys. Res*., **102**, 23895-23915.

ten Brink, H.M., C. Kruisz, G.P.A. Kos, and A. Berner, 1997: Composition/size of the light-scattering aerosol in the Netherlands. *Atmos. Env.*, **31**, 3955-3962.

Tinsley, B.A., 1996: Correlations of atmospheric dynamics with solar wind-induced changes of air-earth current density into cloud top. *J. Geophys. Res*., **101**, 29701-29714.

Tokuhashi, K, A. Takahashi, M. Kaise, S. Kondo, A. Sekiya, S. Yamashita, and H. Ito, 1999a: Rate constants for the reactions of OH radicals with $CH_3OCF_2CF_3$, $CH_3OCF_2CF_2CF_3$, and $CH_3OCF(CF_3)_2$, *International Journal of Chemical Kinetics*, **31**, 846-853.

Tokuhashi, K., H. Nagai, A. Takahashi, M. Kaise, S. Kondo, A. Sekiya, M. Takahashi, Y. Gotoh, and A. Suga, 1999b: Measurement of the OH reaction rate constants for CF_3CH_2OH, $CF_3CF_2CH_2OH$, and $CF_3CH(OH)CF_3$, *J. Phys. Chem.* A, **103**, 2664-2672.

Tokuhashi, K., A. Takahashi, M. Kaise, S. Kondo, A. Sekiya, S. Yamashita, and H. Ito, 2000: Rate constants for the reactions of OH radicals with $CH_3OCF_2CHF_2$, $CHF_2OCH_2CF_2CHF_2$, $CHF_2OCH_2CF_2CF_3$, and $CF_3CH_2OCF_2CHF_2$ over the temperature range 250-430K, *J. Phys. Chem*. A, **104**, 1165-1170.

Toumi, R., S. Bekki, and K. Law, 1994: Indirect influence of ozone depletion on climate forcing by clouds. *Nature*, **372**, 348-351.

Toumi, R., S. Bekki, and K. Law, 1995: Response to Climate and CCN by Rodhe and Crutzen. *Nature*, **375**, 111.

Toumi, R., J.D. Haigh, and K. Law, 1996: A tropospheric ozone-lightning climate feedback. *Geophys. Res. Lett*., **23**, 1037-1040.

Twomey, S., 1974: Pollution and the planetary albedo. *Atmos. Env.*, **8**, 1251-1256.

Twohy, C.H., A.D. Clarke, S.G. Warren, L.F. Radke, and R.J. Charlson, 1989: Light-absorbing material extracted from cloud droplets and its effect on cloud albedo. *J. Geophys. Res.*, **94**, 8623-8631.

Van Dop, H. and M. Krol, 1996: Changing trends in tropospheric methane and carbon monoxide: a sensitivity analysis of the OH-radical. *J. Atmos. Chem.*, **25**, 271-288.

Veefkind, J.P., J.C.H. van der Hage, H.M. ten Brink, 1996: Nephelometer derived and directly measured aerosol optical depth of the atmospheric boundary layer. *Atmos. Res.*, **41**, 217-228.

Wallington, T.J., W.F. Schneider, J. Sehested, M. Bilde, J. Platz, O.J. Nielsen, L.K. Christensen, M.J. Molina, L.T. Molina, and P.W. Wooldridge, 1997: Atmospheric chemistry of HFE-7100 ($C_4F_9OCH_3$): Reaction with OH radicals, UV spectra, and kinetic data for $C_4F_9OCH_2$ and $C_4F_9OCH_2O_2$ radicals and the atmospheric fate of $C_4F_9OCH_2O$ radicals. *J. Phys. Chem.* A., **101**, 8264-8274.

Wang, H.J., D.M. Cunnold, and X. Bao, 1996: A critical analysis of stratospheric aerosol and gas experiment ozone trends. *J. Geophys. Res.*, **101**, 12495-12514.

Wang, W.-C., J.P. Pinto, and Y.L. Yung, 1980: Climatic effects due to halogenated compounds in the Earth's atmosphere. *J. Atmos. Sci.*, **37**, 333-338.

Wang, W.-C., M. Dudek, X-Z. Liang, and J. Kiehl, 1991: Inadequacy of effective CO_2 as a proxy in simulating the greenhouse effect of other radiatively active gases. *Nature*, **350**, 573-577.

Wang, W.-C., M. Dudek, and X-Z. Liang, 1992: Inadequacy of effective CO_2 as a proxy in assessing the regional climate change due to other radiatively active gases. *Geophys. Res. Lett.*, **19**, 1375-1378.

Wang, Y. and D.J. Jacob, 1998: Anthropogenic forcing on tropospheric ozone and OH since preindustrial times. *J. Geophys. Res.*, **103**, 31123-31135.

Wang, Y., A. W. DeSilva, G. C. Goldenbaum, and R. R. Dickerson, 1998: Nitric oxide production by simulated lightning: dependence on current, energy, and pressure, *J. Geophys. Res.*, **103**, 19,149-19,159, 1998.

Warren, S.G., C.J. Hahn, J. London, R.M. Chervin, and R.L. Jenne, 1988: Global distribution of total cloud cover and cloud type amounts over the ocean. NCAR Technical Note TN-317 + STR, Boulder, CO, 42 pp. + 170 maps.

Wetherald, R. and S. Manabe, 1988: Cloud feedback processes in a general circulation model. *J. Atmos. Sci.*, **45**, 1397-1415.

White, O.R., A. Skumanich, J. Lean, W.C. Livingston, and S. Keil, 1992: The sun in a non-cycling state. *Public. Astron. Soc. Pacif.*, **104**, 1139-1143.

Wigley, T.M.L., P.D. Jones, and S.C.B. Raper, 1997: The observed global warming record: What does it tell us? *Proc. Natl. Acad. Sci.* USA, **94**, 8314-8320.

Willson, R.C., 1997: Total solar irradiance trend during solar cycles 21 and 22. *Science*, **277**, 1963-1965.

WMO, 1986: Atmospheric Ozone: 1985, Global Ozone Research and Monitoring Project, World Meteorological Organization, Report No. **16**, Chapter 15, Geneva, Switzerland.

WMO, 1992: Scientific Assessment of Ozone Depletion: 1991, Global Ozone Research and Monitoring Project, World Meteorological Organization, Report No. **25**, Geneva, Switzerland.

WMO, 1995: Scientific Assessment of Ozone Depletion: 1994, Global Ozone Research and Monitoring Project, World Meteorological Organization, Report No. **37**, Geneva, Switzerland.

WMO, 1999: Scientific Assessment of Ozone Depletion: 1998, Global Ozone Research and Monitoring Project, World Meteorological Organization, Report No. **44**, Geneva, Switzerland.

Wuebbles, D.J. and J.M. Calm, 1997: An environmental rationale for retention of endangered chemicals. *Science*, **278**, 1090-1091.

Wuebbles, D.J., C.F. Wei, and K.O. Patten, 1998: Effects on stratospheric ozone and temperature during the Maunder Minimum. *Geophys. Res. Lett.*, **25**, 523-526.

Wyser, K. and J. Ström, 1998: A possible change in cloud radiative forcing due to aircraft exhaust. *Geophys. Res. Lett.*, **25**, 1673-1676.

Zhong, W., R. Toumi, and J.D. Haigh, 1996: Climate forcing by stratospheric ozone depletion calculated from observed temperature trends. *Geophys. Res. Lett.*, **23**, 3183-3186.

Zhong, W., R. Toumi, and J.D. Haigh 1998: Reply to comment on "Climate forcing by stratospheric ozone depletion calculated from observed temperature trends" by K.P. Shine, R.S. Freckleton, and P.M. de F. Forster. *Geophys. Res. Lett.*, **25**, 665.